


Spring 2013

Intrinsic mode function synchronization measures for the anticipation of seizures in epilepsy

Daniel William Moller

Follow this and additional works at: <https://digitalcommons.latech.edu/dissertations>

 Part of the [Nanoscience and Nanotechnology Commons](#), and the [Other Biomedical Engineering and Bioengineering Commons](#)

**INTRINSIC MODE FUNCTION SYNCHRONIZATION MEASURES
FOR THE ANTICIPATION OF SEIZURES
IN EPILEPSY**

by

Daniel William Mollér, B.S.E., M.S.

A Dissertation Presented in Partial Fulfillment
of the Requirements for the Degree
Doctor of Philosophy

COLLEGE OF ENGINEERING AND SCIENCE
LOUISIANA TECH UNIVERSITY

May 2013

UMI Number: 3573606

All rights reserved

INFORMATION TO ALL USERS

The quality of this reproduction is dependent upon the quality of the copy submitted.

In the unlikely event that the author did not send a complete manuscript and there are missing pages, these will be noted. Also, if material had to be removed, a note will indicate the deletion.

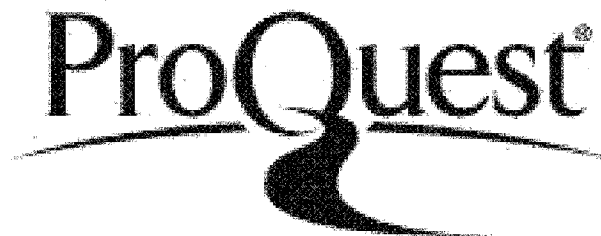


UMI 3573606

Published by ProQuest LLC 2013. Copyright in the Dissertation held by the Author.

Microform Edition © ProQuest LLC.

All rights reserved. This work is protected against unauthorized copying under Title 17, United States Code.



ProQuest LLC
789 East Eisenhower Parkway
P.O. Box 1346
Ann Arbor, MI 48106-1346

LOUISIANA TECH UNIVERSITY

THE GRADUATE SCHOOL

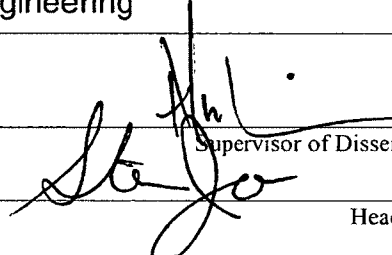
March 22, 2013

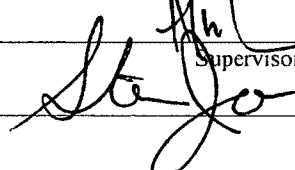
Date

We hereby recommend that the dissertation prepared under our supervision
by Daniel William Moller, M.S.

entitled Intrinsic Mode Function Synchronization Measures for the Anticipation of
Seizures in Epilepsy

be accepted in partial fulfillment of the requirements for the Degree of
Doctor of Philosophy in Biomedical Engineering

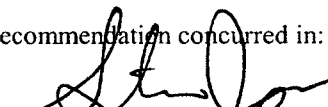


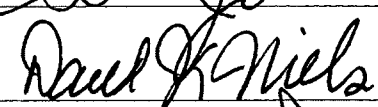
Supervisor of Dissertation Research


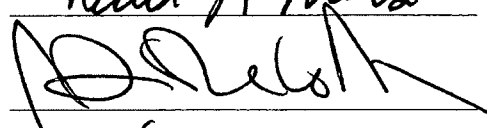
Head of Department

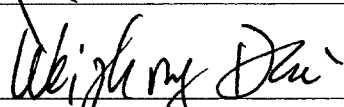
Department

Recommendation concurred in:










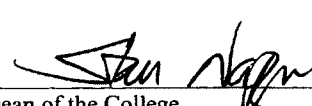
Advisory Committee

Approved: 

Director of Graduate Studies

Approved: 

Dean of the Graduate School



Dean of the College

ABSTRACT

Epileptic seizures affect as many as 50 million people and often occur without warning or apparent provocation. We explore the applicability of noise-assisted Ensemble Empirical Mode Decomposition (EEMD) for patient-specific seizure anticipation synchronization measures as applied to the EEMD intrinsic mode function (IMF) output. Intracranial EEG data were obtained from pre-surgical monitoring at the Epilepsy Center of the University Hospital of Freiburg. Data from twenty patients were analyzed. For each recorded channel, non-overlapping time windows were submitted to the EEMD algorithm, producing twelve levels of IMFs. IMF synchronization measures (mean and maximum coherence, mean and maximum cross-correlation, correlation coefficient and synchronized phase-locking value) for channel pairs were computed and smoothed with a 20-point moving average, producing IMF- x data. Statistical distributions of IMF- x synchronization data were determined for three hours of interictal training data. Three hours of interictal validation data were used to determine the smallest zero-false-positive threshold (multiples of 0.5 standard deviations of IMF- x data) for each channel pair and IMF level. These patient-, IMF level-, and channel pair-specific IMF- x thresholds were compared against periictal (60 minutes preictal with 15 minutes ictal/postictal) IMF- x data for each seizure. Our study shows that while not all channel pairs are able to detect every ictal event, low IMF levels containing frequency components greater than ~ 1 Hz can discriminate

between interictal and periictal activities. The anticipation window for channel pairs detecting all ictal events frequently ranged from 30 to 53 minutes prior to clinical manifestation. We propose an anticipation optimality index for a joint indicator of sensitivity and earliest anticipation times useful for selection of relevant channel pairs and IMF levels. Generalization of the analyzed synchronization measures may be appropriate for some patients, while other patients may require preferential selection of these measures. For the majority of patients, the electrode pairing type holds some relevance to performance assessment values. A strong indication of IMF-level dependence of anticipation performance data was shown, suggesting seizure dynamics in the patient-specific scenario manifest within certain frequency bandwidths. The patients with a hippocampal seizure origin show better sensitivity with our algorithm than patients with neocortical seizure origin.

APPROVAL FOR SCHOLARLY DISSEMINATION

The author grants to the Prescott Memorial Library of Louisiana Tech University the right to reproduce, by appropriate methods, upon request, any or all portions of this Dissertation. It is understood that "proper request" consists of the agreement, on the part of the requesting party, that said reproduction is for his personal use and that subsequent reproduction will not occur without written approval of the author of this Dissertation. Further, any portions of the Dissertation used in books, papers, and other works must be appropriately referenced to this Dissertation.

Finally, the author of this Dissertation reserves the right to publish freely, in the literature, at any time, any or all portions of this Dissertation.

Author David W. Moller

Date 22 MARCH 2013

DEDICATION

For my loving and patient family, I am thankful for your continued reminder of the truly important things in life. My immediate and extended family have made this effort possible with their encouragement and support. Thank you for embracing with me this non-traditional path that I have undertaken.

For my incredible wife Denise, you have been a patient counselor, a source of strength, a motivator, a family logistician, and a superb mother to our three boys. You are my best friend and a true partner in life. I love you.

TABLE OF CONTENTS

ABSTRACT	iii
DEDICATION	vi
LIST OF TABLES.....	xi
LIST OF FIGURES.....	xii
ACKNOWLEDGMENTS	xxiv
PREFACE	xxvii
CHAPTER 1 INTRODUCTION	1
1.1 Epilepsy	1
1.2 Interventional Therapies and Their Side Effects	2
1.3 General Nomenclature in Epileptic Seizures	5
1.4 Timing of Seizure Identification	7
1.5 Purpose of Early Seizure Identification.....	9
1.6 Similarity and Synchronization as a Preictal Measure.....	10
1.7 Scope of the Research	11
1.7.1 Hypothesis.....	12
1.8 Organization of Work Presented	13
CHAPTER 2 BACKGROUND.....	14
2.1 Existence of a Preictal State.....	14
2.1.1 Testing Null Hypotheses.....	17

2.1.2	Duration of the Presumed Preictal Period	18
2.1.3	Long-Duration Preictal Periods.....	19
2.2	Role of Hypersynchrony in Seizure Anticipation.....	20
2.3	Bivariate Measures of Synchronization	21
2.3.1	Contraindications for the Use of Bivariate Synchronization Measures	24
2.3.2	Predisposition of Synchronization Measures.....	25
2.4	Empirical Mode Decomposition in Seizure Anticipation.....	26
CHAPTER 3 METHODS.....		27
3.1	Computational Platform and Software	27
3.2	Intracranial Electroencephalogram Data Set	27
3.3	Data Preparation, Partitioning, and Preprocessing	32
3.4	Data Decomposition.....	33
3.4.1	Empirical Mode Decomposition.....	33
3.4.2	The EMD Sifting Process.....	34
3.4.3	Ensemble Empirical Mode Decomposition.....	37
3.4.4	EEMD Computation Time Limitations	40
3.5	Measures of Synchronization.....	40
3.5.1	Coherence	42
3.5.2	Cross-Correlation.....	44
3.5.3	Correlation Coefficient.....	44

3.5.4	Synchronized Phase-Locking Value	45
3.6	Measure Data Smoothing.....	45
3.7	Threshold Analyses.....	48
3.7.1	Statistical Training, Validation, and Testing.....	48
3.7.2	Performance Assessment.....	51
CHAPTER 4	RESULTS.....	52
4.1	Selection of Critical Intrinsic Mode Functions.....	52
4.2	Statistical Threshold of Synchronization Measures.....	56
4.3	Channel Pair Connectivity Maps.....	58
4.3.1	Ratio of IMF- x Data Above Threshold.....	62
4.4	Anticipation Optimality Index.....	67
4.5	Generalization Based on Focal Origin.....	72
4.6	Patient-Specific Generalizations.....	74
4.6.1	IMF- x Measure.....	74
4.6.2	IMF Level.....	77
4.6.3	Channel Pair Type	80
CHAPTER 5	DISCUSSION	82
CHAPTER 6	CONCLUSIONS.....	90
APPENDIX A	Interictal Training Descriptive Statistics Figures	92
APPENDIX B	IMF-Coh Statistical Threshold Testing Connectivity Plots.....	105

APPENDIX C IMF-Coh _{max} Statistical Threshold Testing Connectivity Plots.....	109
APPENDIX D IMF-CCoef Statistical Threshold Testing Connectivity Plots.....	113
APPENDIX E IMF-SPLV Statistical Threshold Testing Connectivity Plots.....	117
APPENDIX F IMF-XCor Statistical Threshold Testing Connectivity Plots.....	121
APPENDIX G IMF-XCor _{max} Statistical Threshold Testing Connectivity Plots.....	125
APPENDIX H MATLAB Code.....	129
H.1 coh_ch_viz.m.....	130
H.2 eemd.m.....	137
H.3 feat_caselist2.m.....	139
H.4 freiburg.m.....	141
H.5 freiburg_dataprep.m	154
H.6 full_emd_coh_func.m	157
H.7 mcoh.m	161
H.8 patSelectinfo.m.....	163
REFERENCES.....	169
VITA.....	180

LIST OF TABLES

Table 3.1:	University Hospital of Freiburg Epilepsy Center Patient Database. Abbreviations used in the table are as follows: SP = simple partial, CP = complex partial, GTC = generalized clonic-tonic, NC = neocortex, H = hippocampus, d = depth, g = grid, s = strip.....	28
Table 3.2:	Associated channel pairings with channel pair ID number. Channel pairings with channel pair ID number indicate the 15 channel pairings of the 6 electrodes from the Freiburg Epilepsy Center Database (f = focal electrode, e = extrafocal electrode).	41
Table 3.3:	Naming convention for smoothed 20-point moving average data based on each synchronization measure.	46

LIST OF FIGURES

<p>Figure 1.1: The nomenclature of a seizure event. In an electroencephalographic recording, the seizure episode itself (shaded red) is known as the ictal period. A postictal period occurs directly after the seizure, and a preictal period (shaded yellow) occurs before the ictal event. The preictal period is difficult to determine and may extend from seconds to hours before a seizure. The combination of the preictal, ictal, and postictal periods can be collectively referred to as the periictal period. For epilepsy patients, the time periods between periictal periods are known as interictal. The preictal period is of key interest for researchers attempting to anticipate or predict upcoming seizures.</p>	6
<p>Figure 1.2: The timeline of seizure identification. Difficulty in identification of seizure activity depends on the timing at which the identification is made. In this chart, difficulty increases as researchers move to the right. For the current research presented, seizure anticipation is emphasized.</p>	8
<p>Figure 1.3: Seizure prediction parameters. A graphic indicating the method by which seizure prediction parameters are considered. According to Winterhalder <i>et al.</i>, an alarm must be initiated early enough (the seizure prediction horizon, or SPH) for the action of an intervention to drive the system away from a seizure state which would normally occur during a given time (the seizure occurrence period, or SOP). In their case, they evaluated an assumed fast-acting intervention such that the SPH was 5 seconds and maintained a SOP of 30 minutes (Note: This image is not shown at scale for their assertion). Image adapted from [28].</p>	9
<p>Figure 3.1: A schematic representation of intracranial electroencephalogram electrode types (Patient 4). Intracranial depth (<i>a</i>), subdural strip (<i>b</i>) and subdural grid (<i>c</i>) electrodes were used to collect brain activity recordings from epilepsy patients undergoing monitoring at the Epilepsy Center of the University Hospital of Freiburg. Note: IEEG electrode types and placement locations varied from patient to patient based on the monitoring needs of the clinicians.</p>	31

- Figure 3.2: Data preprocessing and decomposition block diagram. This block diagram shows the steps taken for initial IEEG electrode recording data preprocessing and data decomposition. The first three blocks in the upper left relate to information in Section 3.3. Ensemble Empirical Mode Decomposition is an extension of the EMD method and is performed by the repetitive (P trials) addition of white noise to the preprocessed data prior to EMD sifting. A set of n IMF levels is determined for each trial ($n = 12$ levels of separated IMFs for the IEEG data analyzed herein). (Notice that the first IMF level, IMF1, contains the highest frequency information, with the time scale of the signal increasing as the IMF level increases.) A more true, underlying representation of the IEEG signal is identified by taking the ensemble means of each IMF level across the P trials. For the analysis in this research work, the superimposed white noise was set to a variance of 0.1 and the number of trials P was 50..... 39
- Figure 3.3: Time-windowed representation of mean IMF coherence data. (a) A single IMF level for four consecutive time windows is shown for a pair of electrode recording channels. Vertical dashed lines indicate the start/end of each 16-second time window. (b) Concurrent IMF time windows are used to determine a channel pairs mean coherence, each producing a single, time-windowed representation of mean IMF coherence information. 43
- Figure 3.4: Moving average smoothing of mean IMF coherence data. This plot is an illustrative example of the mean IMF coherence data (blue thin line) smoothing using a 5 minute 20 second window to produce the IMF-Coh data (red thick line). The IMF-Coh data are used in the thresholding analyses detailed in Section 3.7. Note that the first 19 samples of the IMF-Coh data are zero and subsequently disregarded in the analyses. (One hour of preictal data is shown from patient 001, seizure 1, CH1-CH3 pair, IMF3.) 47
- Figure 3.5: Statistical threshold training and testing. IMF-Coh data for a single channel pair is shown for a subset of interictal validation data (a) and for one set of periictal test data containing a single seizure event (b). The threshold (dot-dash lines) in the validation and test data subplots illustrates zero false positives and seizure anticipation nearly an hour before onset, respectively. 50

- Figure 4.1: Frequency spectra of IMF levels. An example frequency analysis of the information contained at IMF levels 1 to 6 following EEMD of interictal data is shown. As IMF level increases, corresponding frequencies associated with the IMF level decrease. IMF 6 is the largest IMF level used in subsequent analyses. Example plots are generated from channel pair/16-second epoch for Patient 21 interictal data. 53
- Figure 4.2: Average mean coherence and standard deviation of average mean coherence of interictal training data. Statistical information for interictal training data for one measure (mean coherence) of the six synchronization measures is evaluated. (a) The image map shows each patient's average (across the 15 channel combinations) of the mean coherence at each IMF level. Note the increased coherence measure near the higher IMF levels. Higher IMF levels represent very low frequency ($< \sim 1$ Hz) and are subsequently disregarded in the analytical approach. (b) The image map shows the standard deviation of each patient's average (across the 15 channel combinations) of the mean coherence at each IMF level. 55
- Figure 4.3: Determination of statistical thresholds using the zero-FP approach on the validation set. Shaded boxes indicate that the threshold at the given multiple of σ of the channel-pair/IMF-level combination was exceeded. A statistical threshold is determined for each channel-pair/IMF-level combination. The minimum thresholds for seizure testing in the case above are subsequently determined to be 3.0σ and 3.5σ for (a) and (b), respectively. For visualization purposes, the data shown has been preferentially selected to illustrate the method and has been truncated to 30 minutes of the 3 total hours of validation data for the patient. The figures are representative of typical IMF- x interictal data used for developing the validation thresholds. (Data are shown for IMF-Coh for patient 015, (a) CH1-CH5 pair for IMF4 and (b) CH2-CH3 pair for IMF1.) 57
- Figure 4.4: Connectivity maps for IMF-Coh measure, Patients 1 to 6. Sample connectivity maps for IMF-Coh thresholded data are shown for Patients 1 to 6 across the first six IMF levels. Focal electrodes (red) and extra-focal electrodes (blue) show channel pair success rate in seizure anticipation. The TP ratio for each patient is represented by the weight of the line connecting channel pairs. Information regarding anticipation time is not included in the plots. (A complete set of connectivity maps can be found in Appendices B through G). 59

- Figure 4.5: Connectivity maps for IMF- x measures (Patient 5). Connectivity maps for IMF- x thresholded data are shown for Patient 5 across the first six IMF levels. Focal electrodes (red) and extrafocal electrodes (blue) show channel pair success rate in seizure anticipation. TP ratio for each patient is represented by the weight of the line connecting channel pairs. Information regarding anticipation time is not included in the plots. 61
- Figure 4.6: True positive ratio (channel pair mean). The true positive ratio for each patient and IMF level representing the mean TP ratio for all 15 channel pairs. 63
- Figure 4.7: Ratio of IMF- x data above threshold (channel pair mean). Ratio of IMF- x data above threshold (raT) are shown for all patients at each IMF level. The raT mean for all channel pairs is shown..... 64
- Figure 4.8: Ratio of IMF- x data above threshold (Patient 5). Ratio of IMF- x data above threshold (raT) are shown for Patient 5 at each channel-pair/IMF-level combination. 65
- Figure 4.9: Ratio of IMF- x data above threshold (Patient 10). Ratio of IMF- x data above threshold (raT) are shown for Patient 10 at each channel-pair/IMF-level combination. 66
- Figure 4.10: Anticipation optimality index (channel pair mean). The mean anticipation optimality (aO) indices for all channel pairs are shown at each IMF level for each patient's IMF- x measure. 68
- Figure 4.11: Anticipation optimality index (Patient 5). Anticipation optimality (aO) indices for Patient 5 are shown for each channel-pair/IMF-level combination in their respective IMF- x measure. 69
- Figure 4.12: Anticipation optimality index (Patient 10). Anticipation optimality (aO) indices for Patient 10 are shown for each channel-pair/IMF-level combination in their respective IMF- x measure. 71

- Figure 4.13: True positive ratio and anticipation optimality index versus seizure origin type. Kruskal-Wallis categorical test was used to generate notched box and whisker plots of the TP ratio (*a*) and the *aO* index (*b*) versus the seizure origin. The hippocampal (H) category was determined to be statistically different ($p < 0.01$) by the K-W test and showed significantly higher mean rank than the other two categories in both performance assessments (*a*) and (*b*). Implications of this statistical difference encourage the use of the proposed seizure anticipation algorithm in selective epilepsies. (NC = Neocortical, H = Hippocampal, H/NC = Hippocampal/Neocortical)..... 73
- Figure 4.14: True positive ratio and anticipation optimality index versus IMF-*x* measures (Patient 5). Kruskal-Wallis categorical test was used to generate notched box and whisker plots of the TP ratio (*a*) and the *aO* index (*b*) against the IMF-*x* measures evaluated in this study for Patient 5. No category of the six measures evaluated induces a statistically different mean rank in either case ((*a*) or (*b*)) for this patient (p -value can be referenced in Figure 4.15)..... 75
- Figure 4.15: Kruskal-Wallis categorical test for IMF-*x* measures. Kruskal-Wallis test was used to compare the TP ratio and the *aO* index against the IMF-*x* measures evaluated in this study. The p -values for each patient's pair of K-W tests is shown. The red (dotted) line indicates a statistical level of 0.01, while the blue (dash-dot) line indicates the statistical level of 0.05. Plotted p -values greater than a given statistical level indicate a lack of statistical difference in the mean ranks of all IMF-*x* measures tested..... 76
- Figure 4.16: Kruskal-Wallis categorical test for IMF levels. Kruskal-Wallis test was used to compare the TP ratio and (*aO*) index against the first six IMF levels. The p -values for each patient's pair of K-W tests is shown. The red (dotted) line indicates a statistical level of 0.01, while the blue (dash-dot) line indicates the statistical level of 0.05. Plotted p -values smaller than a given statistical level indicate a statistical difference in the mean ranks of at least one of the six IMF level's performance data. Each patient, except for Patient 9 where no TP was identified, showed at least one statistical difference when comparing the six IMF levels..... 78
- Figure 4.17: Anticipation optimality index versus IMF level (Patients 5 and 10). Kruskal-Wallis categorical test was used to generate notched box and whisker plots of the *aO* index against IMF levels 1 to 6 for Patients 5 (*a*) and 10 (*b*). Results of the K-W test indicate at least one statistically different IMF level ($p < 0.01$) for both patients..... 79

- Figure 4.18: Kruskal-Wallis categorical test for channel pair type. Kruskal-Wallis test was used to compare the TP ratio and (aO) index against the electrode pairing type: focal-focal, focal-extrafocal, and extrafocal-extrafocal. The p -values for each patient's pair of K-W tests is shown. The red (dotted) line indicates a statistical level of 0.01, while the blue (dash-dot) line indicates the statistical level of 0.05. In over half of the patients, performance data was statistically different for at least one channel pair type. 81
- Figure A.1: Average mean coherence indicating statistical information for mean coherence measure of interictal training data. The image map shows each patient's average (across the 15 channel pairs) of mean coherence at each IMF level. Note the increasing coherence measure at the higher IMF levels. Higher IMF levels represent very low frequency ($< \sim 1$ Hz) and are subsequently disregarded. 93
- Figure A.2: Standard deviation of average mean coherence indicating statistical information for mean coherence measure of interictal training data. The image map shows each patient's standard deviation of the average (across the 15 channel pairs) of the mean coherence at each IMF level. 94
- Figure A.3: Average maximum coherence indicating statistical information for maximum coherence measure of interictal training data. The image map shows each patient's average (across the 15 channel pairs) of maximum coherence at each IMF level. 95
- Figure A.4: Standard deviation of average maximum coherence indicating statistical information for the maximum coherence measure of interictal training data. The image map shows each patient's standard deviation of the average (across the 15 channel pairs) of the maximum coherence at each IMF level. 96
- Figure A.5: Average mean cross-correlation indicating statistical information for mean cross-correlation measure of interictal training data. The image map shows each patient's average (across the 15 channel pairs) of mean cross-correlation at each IMF level. 97
- Figure A.6: Standard deviation of average mean cross-correlation indicating statistical information for the mean cross-correlation measure of interictal training data. The image map shows each patient's standard deviation of the average (across the 15 channel pairs) of the mean cross-correlation at each IMF level. 98

- Figure A.7: Average maximum cross-correlation indicating statistical information for maximum cross-correlation measure of interictal training data. The image map shows each patient's average (across the 15 channel pairs) of maximum cross-correlation at each IMF level. 99
- Figure A.8: Standard deviation of average maximum cross-correlation indicating statistical information for maximum cross-correlation measure of interictal training data. The image map shows each patient's average (across the 15 channel pairs) of maximum cross-correlation at each IMF level.100
- Figure A.9: Average correlation coefficient indicating statistical information for correlation coefficient measure of interictal training data. The image map shows each patient's average (across the 15 channel pairs) of correlation coefficient at each IMF level. 101
- Figure A.10: Standard deviation of average correlation coefficient indicating statistical information for correlation coefficient measure of interictal training data. The image map shows each patient's average (across the 15 channel pairs) of correlation coefficient at each IMF level. 102
- Figure A.11: Average synchronized phase locking value indicating statistical information for synchronized phase locking value measure of interictal training data. The image map shows each patient's average (across the 15 channel pairs) of synchronized phase locking value at each IMF level. 103
- Figure A.12: Standard deviation of average synchronized phase locking value indicating statistical information for synchronized phase locking value measure of interictal training data. The image map shows each patient's average (across the 15 channel pairs) of synchronized phase locking value at each IMF level. 104
- Figure B.1: IMF-Coh connectivity plots for statistical threshold testing (Patients 1 to 6). IMF-Coh connectivity plots of channel pairs for Patients 1 through 6 show correct detection of periictal dynamics for statistical threshold testing. Channels 1-3 (red nodes) are identified as focal electrodes, while channels 4-6 (blue nodes) are extrafocal electrodes. The line width is proportional to the true positive (TP) rate. Information regarding anticipation time is not included in the plots. 106

- Figure B.2: IMF-Coh connectivity plots for statistical threshold testing (Patients 7 to 13). IMF-Coh connectivity plots of channel pairs for Patients 7 through 13 show correct detection of periictal dynamics for statistical threshold testing. Channels 1-3 (red nodes) are identified as focal electrodes, while channels 4-6 (blue nodes) are extrafocal electrodes. The line width is proportional to the true positive (TP) rate. Information regarding anticipation time is not included in the plots.107
- Figure B.3: IMF-Coh connectivity plots for statistical threshold testing (Patients 14 to 19). IMF-Coh connectivity plots of channel pairs for Patients 14 through 19 show correct detection of periictal dynamics for statistical threshold testing. Channels 1-3 (red nodes) are identified as focal electrodes, while channels 4-6 (blue nodes) are extrafocal electrodes. The line width is proportional to the true positive (TP) rate. Information regarding anticipation time is not included in the plots.108
- Figure B.4: IMF-Coh connectivity plots for statistical threshold testing (Patients 20 to 21). IMF-Coh connectivity plots of channel pairs for Patients 20 through 21 show correct detection of periictal dynamics for statistical threshold testing. Channels 1-3 (red nodes) are identified as focal electrodes, while channels 4-6 (blue nodes) are extrafocal electrodes. The line width is proportional to the true positive (TP) rate. Information regarding anticipation time is not included in the plots.108
- Figure C.1: IMF-Coh_{max} connectivity plots for statistical threshold testing (Patients 1 to 6). IMF-Coh_{max} connectivity plots of channel pairs for Patients 1 through 6 show correct detection of periictal dynamics for statistical threshold testing. Channels 1-3 (red nodes) are identified as focal electrodes, while channels 4-6 (blue nodes) are extrafocal electrodes. The line width is proportional to the true positive (TP) rate. Information regarding anticipation time is not included in the plots.110
- Figure C.2: IMF-Coh_{max} connectivity plots for statistical threshold testing (Patients 7 to 13). IMF-Coh_{max} connectivity plots of channel pairs for Patients 7 through 13 show correct detection of periictal dynamics for statistical threshold testing. Channels 1-3 (red nodes) are identified as focal electrodes, while channels 4-6 (blue nodes) are extrafocal electrodes. The line width is proportional to the true positive (TP) rate. Information regarding anticipation time is not included in the plots.111

- Figure C.3: IMF-Coh_{max} connectivity plots for statistical threshold testing (Patients 14 to 19). IMF-Coh_{max} connectivity plots of channel pairs for Patients 14 through 19 show correct detection of periictal dynamics for statistical threshold testing. Channels 1-3 (red nodes) are identified as focal electrodes, while channels 4-6 (blue nodes) are extrafocal electrodes. The line width is proportional to the true positive (TP) rate. Information regarding anticipation time is not included in the plots. 112
- Figure C.4: IMF-Coh_{max} connectivity plots for statistical threshold testing (Patients 20 to 21). IMF-Coh_{max} connectivity plots of channel pairs for Patients 20 through 21 show correct detection of periictal dynamics for statistical threshold testing. Channels 1-3 (red nodes) are identified as focal electrodes, while channels 4-6 (blue nodes) are extrafocal electrodes. The line width is proportional to the true positive (TP) rate. Information regarding anticipation time is not included in the plots. 112
- Figure D.1: IMF-CCoef connectivity plots for statistical threshold testing (Patients 1 to 6). IMF-CCoef connectivity plots of channel pairs for Patients 1 through 6 show correct detection of periictal dynamics for statistical threshold testing. Channels 1-3 (red nodes) are identified as focal electrodes, while channels 4-6 (blue nodes) are extrafocal electrodes. The line width is proportional to the true positive (TP) rate. Information regarding anticipation time is not included in the plots. 114
- Figure D.2: IMF-CCoef connectivity plots for statistical threshold testing (Patients 7 to 13). IMF-CCoef connectivity plots of channel pairs for Patients 7 through 13 show correct detection of periictal dynamics for statistical threshold testing. Channels 1-3 (red nodes) are identified as focal electrodes, while channels 4-6 (blue nodes) are extrafocal electrodes. The line width is proportional to the true positive (TP) rate. Information regarding anticipation time is not included in the plots. 115
- Figure D.3: IMF-CCoef connectivity plots for statistical threshold testing (Patients 14 to 19). IMF-CCoef connectivity plots of channel pairs for Patients 14 through 19 show correct detection of periictal dynamics for statistical threshold testing. Channels 1-3 (red nodes) are identified as focal electrodes, while channels 4-6 (blue nodes) are extrafocal electrodes. The line width is proportional to the true positive (TP) rate. Information regarding anticipation time is not included in the plots. 116

- Figure D.4: IMF-CCoef connectivity plots for statistical threshold testing (Patients 20 to 21). IMF-CCoef connectivity plots of channel pairs for Patients 20 through 21 show correct detection of periictal dynamics for statistical threshold testing. Channels 1-3 (red nodes) are identified as focal electrodes, while channels 4-6 (blue nodes) are extrafocal electrodes. The line width is proportional to the true positive (TP) rate. Information regarding anticipation time is not included in the plots.116
- Figure E.1: IMF-SPLV connectivity plots for statistical threshold testing (Patients 1 to 6). IMF-SPLV connectivity plots of channel pairs for Patients 1 through 6 show correct detection of periictal dynamics for statistical threshold testing. Channels 1-3 (red nodes) are identified as focal electrodes, while channels 4-6 (blue nodes) are extrafocal electrodes. The line width is proportional to the true positive (TP) rate. Information regarding anticipation time is not included in the plots.118
- Figure E.2: IMF-SPLV connectivity plots for statistical threshold testing (Patients 7 to 13). IMF-SPLV connectivity plots of channel pairs for Patients 7 through 13 show correct detection of periictal dynamics for statistical threshold testing. Channels 1-3 (red nodes) are identified as focal electrodes, while channels 4-6 (blue nodes) are extrafocal electrodes. The line width is proportional to the true positive (TP) rate. Information regarding anticipation time is not included in the plots.119
- Figure E.3: IMF-SPLV connectivity plots for statistical threshold testing (Patients 14 to 19). IMF-SPLV connectivity plots of channel pairs for Patients 14 through 19 show correct detection of periictal dynamics for statistical threshold testing. Channels 1-3 (red nodes) are identified as focal electrodes, while channels 4-6 (blue nodes) are extrafocal electrodes. The line width is proportional to the true positive (TP) rate. Information regarding anticipation time is not included in the plots.120
- Figure E.4: IMF-SPLV connectivity plots for statistical threshold testing (Patients 20 to 21). IMF-SPLV connectivity plots of channel pairs for Patients 20 through 21 show correct detection of periictal dynamics for statistical threshold testing. Channels 1-3 (red nodes) are identified as focal electrodes, while channels 4-6 (blue nodes) are extrafocal electrodes. The line width is proportional to the true positive (TP) rate. Information regarding anticipation time is not included in the plots.120

- Figure F.1: IMF-XCor connectivity plots for statistical threshold testing (Patients 1 to 6). IMF-XCor connectivity plots of channel pairs for Patients 1 through 6 show correct detection of periictal dynamics for statistical threshold testing. Channels 1-3 (red nodes) are identified as focal electrodes, while channels 4-6 (blue nodes) are extrafocal electrodes. The line width is proportional to the true positive (TP) rate. Information regarding anticipation time is not included in the plots. 122
- Figure F.2: IMF-XCor connectivity plots for statistical threshold testing (Patients 7 to 13). IMF-XCor connectivity plots of channel pairs for Patients 7 through 13 show correct detection of periictal dynamics for statistical threshold testing. Channels 1-3 (red nodes) are identified as focal electrodes, while channels 4-6 (blue nodes) are extrafocal electrodes. The line width is proportional to the true positive (TP) rate. Information regarding anticipation time is not included in the plots. 123
- Figure F.3: IMF-XCor connectivity plots for statistical threshold testing (Patients 14 to 19). IMF-XCor connectivity plots of channel pairs for Patients 14 through 19 show correct detection of periictal dynamics for statistical threshold testing. Channels 1-3 (red nodes) are identified as focal electrodes, while channels 4-6 (blue nodes) are extrafocal electrodes. The line width is proportional to the true positive (TP) rate. Information regarding anticipation time is not included in the plots. 124
- Figure F.4: IMF-XCor connectivity plots for statistical threshold testing (Patients 20 to 21). IMF-XCor connectivity plots of channel pairs for Patients 20 through 21 show correct detection of periictal dynamics for statistical threshold testing. Channels 1-3 (red nodes) are identified as focal electrodes, while channels 4-6 (blue nodes) are extrafocal electrodes. The line width is proportional to the true positive (TP) rate. Information regarding anticipation time is not included in the plots. 124
- Figure G.1: IMF-XCor_{max} connectivity plots for statistical threshold testing (Patients 1 to 6). IMF-XCor_{max} connectivity plots of channel pairs for Patients 1 through 6 show correct detection of periictal dynamics for statistical threshold testing. Channels 1-3 (red nodes) are identified as focal electrodes, while channels 4-6 (blue nodes) are extrafocal electrodes. The line width is proportional to the true positive (TP) rate. Information regarding anticipation time is not included in the plots. 126

- Figure G.2: IMF-XCor_{max} connectivity plots for statistical threshold testing (Patients 7 to 13). IMF-XCor_{max} connectivity plots of channel pairs for Patients 7 through 13 show correct detection of periictal dynamics for statistical threshold testing. Channels 1-3 (red nodes) are identified as focal electrodes, while channels 4-6 (blue nodes) are extrafocal electrodes. The line width is proportional to the true positive (TP) rate. Information regarding anticipation time is not included in the plots.127
- Figure G.3: IMF-XCor_{max} connectivity plots for statistical threshold testing (Patients 14 to 19). IMF-XCor_{max} connectivity plots of channel pairs for Patients 14 through 19 show correct detection of periictal dynamics for statistical threshold testing. Channels 1-3 (red nodes) are identified as focal electrodes, while channels 4-6 (blue nodes) are extrafocal electrodes. The line width is proportional to the true positive (TP) rate. Information regarding anticipation time is not included in the plots.128
- Figure G.4: IMF-XCor_{max} connectivity plots for statistical threshold testing (Patients 20 to 21). IMF-XCor_{max} connectivity plots of channel pairs for Patients 20 through 21 show correct detection of periictal dynamics for statistical threshold testing. Channels 1-3 (red nodes) are identified as focal electrodes, while channels 4-6 (blue nodes) are extrafocal electrodes. The line width is proportional to the true positive (TP) rate. Information regarding anticipation time is not included in the plots.128

ACKNOWLEDGMENTS

A multitude of people have shared with me their expertise, advice, friendship, and support during my graduate studies. Their contributions have propelled me toward a better place in my career and life.

I would like to sincerely thank my research advisor, mentor and friend, Dr. Alan W.L. Chiu for his continued support and guidance. He is a truly enlightened individual, and with his sharp intellect, he roots out the underlying fundamentals of any problem I bring to him. I hold him in the highest regard and am truly fortunate to have been the beneficiary of his wisdom.

I am deeply grateful to Dr. David Mills for providing me with an opportunity to be involved in the teaching and research cohort of GK-12, which gave me the tools and experience to pursue my passion for teaching. Additionally, the open and frank discussions he shared with me regarding life and work have been invaluable.

I cannot begin to express my sincere gratitude to the *Living with the Lab* faculty (Dr. David Hall, Dr. Kelly Crittenden, Dr. Michael Swanbom, Dr. Stan Cronk, Dr. Davis Harbour, Dr. John Easley, Dr. Katie Evans, Dr. Hisham Hegab, and Dr. Jim Nelson) for their clear perspectives and advice on educating burgeoning engineers. As part of the *Living with the Lab* faculty, I am very appreciative of their unreserved willingness to allow me to stand on their shoulders. A truly dynamic team, the *Living*

with the Lab faculty are the most dedicated and purely capable assembly of people of which I could ever hope to be a part.

I appreciate Dr. Mark DeCoster's shared expertise in neuroscience. Further, I cannot thank him enough for loaning me the computer platform upon which I have completed all of my analyses. Without this computer, I could not have accomplished the level of computation needed for this research work.

I am thankful to Dr. Steven Jones, whose clarity in prose is among the most advanced I have seen.

I wish to thank my research lab colleagues and close friends throughout my graduate experience. I have greatly enjoyed our time together and philosophical discussions. I truly appreciate Dr. Melanie Watson's efforts in sharing with me opportunities that have enabled me to both feed my family and pursue my career interests. In particular, I wish to thank Dr. Jude Savarraj for giving me some perspective at a crucial point in my research process.

I wish to thank Dr. Jim Spaulding for his extraordinary patience and lively conversation.

I greatly appreciate the efforts and practical guidance from Mrs. Arlene Hill, Mrs. Charlotte Wilkerson, Mrs. Joyce Bryan, Ms. Jane Petrus, Mrs. Gloria Skains, Mrs. Anita Hill, and Mrs. Marilyn Robinson.

I would like to thank Dr. Ramu Ramachandran for his support and opportunities provided to me.

I am very appreciative of the joint efforts by Dr. Bernd Schröder and Dr. Lisa Kuhn for development of the L^AT_EX dissertation template. I am particularly thankful for Dr. Schröder's emergency tech support.

I would like to acknowledge my graduate school financial support from the Louisiana Board of Regents, the National Science Foundation GK-12 Teaching Fellow Program, the *Living with the Lab* program, and the Louisiana Engineering Foundation.

PREFACE

The inability to forecast or recognize an upcoming seizure is one of the most debilitating aspects of epilepsy. The work of this study explores the potential for early anticipation of seizure events using signal processing, machine learning, and statistical techniques. The intermediate goal of this work is to develop a warning system for upcoming seizures. The ultimate goal of this work is to extend this warning system to one that can provide effective interventional therapy, such that the brain dynamics of an upcoming seizure can be redirected to a normal state.

CHAPTER 1

INTRODUCTION

Since the advent of the electroencephalogram (EEG), clinicians and researchers have sought the electrophysiological markers throughout seizure events. Identification of impending seizures has been an area of interest for the past several decades. With the advent and ubiquity of computing resources, researchers have investigated biopotential recordings leading to seizure activity in a highly quantitative way using signal processing, statistical, machine-learning and modeling techniques. The current knowledge of precursorial and generative biopotential activities that lead to seizures, however, still remains limited.

1.1 Epilepsy

Ranked as the third most common neurological disorder worldwide, epilepsy affects between 0.6% and 0.8% of the world's population [1]. Of this approximate 50 million people with epilepsy, about 3 million cases are found in the United States alone [2]. Additionally, the discovery rate of new epilepsy cases is increasing as low-income countries are gaining access to better medical diagnostic resources [2].

Seizures occur as a result of various acute or chronic problems, including infection, stroke, metabolic disorder, traumatic brain injury, dementia, Alzheimer's, illicit drug use, or other idiopathic or unknown causes. However, generally speaking,

epilepsy is a neurological disorder whose hallmark symptom is the recurrence of seizure episodes. Seizures manifest in a myriad of ways, ranging from subtle, short-lived absence seizures to the more overt, convulsive tonic-clonic seizures. Likewise, seizures may originate from an epileptogenic focus, a particular neuron or localized group of neurons that promote seizure activity, or from a less-defined cause or dispersed anatomical region. [3]

One of the most debilitating aspects of epilepsy is the suddenness by which a seizure can occur. While some epileptics (more prevalently for those with mesial temporal lobe epilepsy) experience a premonition, or aura, prior to a seizure event, many epileptics are unaware of an upcoming seizure [4–7]. The ramifications of this unpredictability can be severe for the patient’s overall quality of life and psychological well-being. This disorder can vastly limit the epileptic’s ability to perform typically routine activities found in both daily and work life, including examples such as driving and childcare. Further, it can lead to depression, confidence and other self-image issues, and even increased risk of injury or untimely death. [8–12]

1.2 Interventional Therapies and Their Side Effects

Currently, a number of interventional therapies may functionally limit or suppress seizure events. The primary clinical intervention by which epilepsy is most often managed is through the use of pharmacology. Antiepileptic drugs (AEDs), or antiseizure medication, have been shown to reduce or completely suppress seizure episodes for up to 65% of new-onset epileptic sufferers [3]. In some cases, ideal medication and dosage may not be adequately determined, leading to intractability

[13]. In other cases, the use of an AED may initially reduce seizures, but eventually lose its effectiveness due to increased patient tolerance [3]. Further, since the AEDs must be consistently present in the bloodstream in order to suppress seizures, their chronic use is subject to patient-compliance issues, particularly if the patient continues to have seizure episodes even if at a much reduced rate [14]. While AEDs are the most prevalent clinical therapy, researchers have shown several mild to even severe side effects associated with their chronic use. These side effects may manifest in a very broad array of general and idiosyncratic effects for each AED. Often seen side effects for many AEDs include dizziness, fatigue, insomnia, depression, reduced cognition speed, lowered IQ, limited memory, aggressiveness, and neuronal apoptosis [15–21].

In pharmacologically-intractable cases, surgical resection of focal regions is often a viable alternative. Seizures that consistently originate from a similar brain region (or epileptogenic focus) can be abolished by removing the seizure-generating tissue. While this intervention is only possible for well-defined foci found away from critical cognitive and speech brain regions, the potential risk involved in the highly invasive nature of these types of procedures is often regarded as a higher-tier measure. Surgical resection of epileptic foci can successfully eliminate seizures up to 60-70% of the time (with or without supplemental AED administration) [3]. Despite the relative success of surgical intervention, patients with concerns of surgical complications may be hesitant to pursue such therapy [22].

Yet another alternative for seizure suppression includes electrical stimulation therapies such as vagal nerve stimulation (VNS), deep-brain stimulation (DBS), electroconvulsive therapy (ECT), and subdural cortical stimulation. Although VNS and

DBS can reduce seizure frequency ranging from 50% to complete control in approximately half of the patients, these approaches have an open-loop, chronic stimulation frequency [22–24]. This blind stimulation is not designed to be responsive to real-time brain activities, and thus is poorly targeted toward addressing seizure-generative brain dynamics. Additionally, these treatment paradigms are often coupled with continued AED administration, so relief from chronic side effects of antiseizure medications is limited. Further, in some cases, the mere implantation of electrodes can have placebo effects on reduced seizure frequency, calling into question the efficacy of these open-loop electrical stimulation treatments [22]. The use of electroconvulsive therapy (ECT), previously known as electroshock therapy, has also been attempted as an additional method for simultaneously suppressing seizures and combating depression [25, 26]. Although effective in some cases, ECT itself imposes a type of seizure upon the patient and, thus, may simply be a measure for replacing a natural seizure event with an artificial one. Further, many people consider this treatment to be barbaric. These open-loop systems are inherently limited, by simply periodically stimulating brain tissue at a defined rate. Although in some systems the stimulations can be added by an external control device by the patient, responsive stimulation based on seizure-generative brain dynamics is not employed. However, recently, an advanced acute electrical stimulation system that actuates an adaptive response neurostimulation has been developed. The system from NeuroPace, Inc. (Mountain View, CA), is currently in clinical trials. While the system has shown some promise, it relies on the early detection of a seizure event, rather than employing a preemptive stimulation *prior to* a seizure episode. Nonetheless, the system from NeuroPace, Inc.,

is currently the state of the art in acute electrical stimulation for the treatment of epilepsy.

1.3 General Nomenclature in Epileptic Seizures

Traditionally, people suffering from epileptic seizures have undergone clinical diagnosis from medical doctors and epileptologists by EEG analysis. The diagnoses of seizure onset, duration, and end by these medical professionals are considered by researchers as the “gold standard.” The accepted nomenclature describing the brain activity of an electroencephalographic recording during a seizure episode is known as ictal activity. The brain dynamics during the time just prior to the seizure onset, or ictal event, is referred to as the preictal (sometimes written as pre-ictal) time period. The time period just following a seizure, or ictal event, is considered postictal, or post-ictal. For the purposes of this paper, we use the term periictal to indicate the combination of preictal and ictal time periods, and, in some cases, the addition of the postictal time period, though the postictal period holds less importance in the work shown here. In epilepsy, brain activity shown in electroencephalographic recordings during the time between seizures that does not include the preictal, ictal, and postical periods can be described as interictal (Figure 1.1).

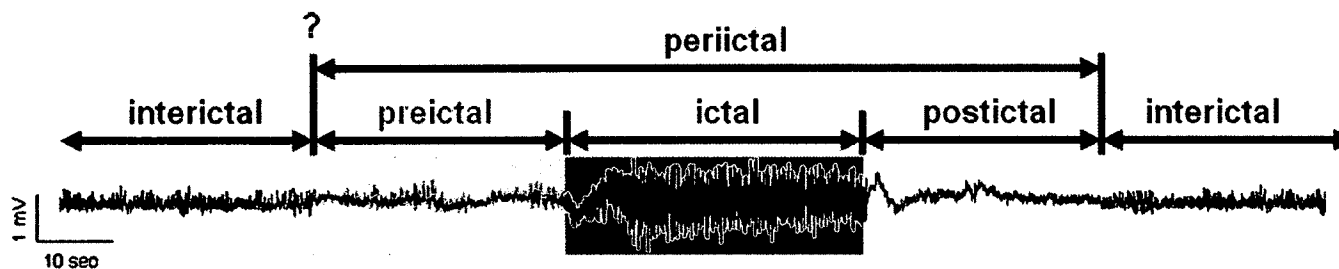


Figure 1.1: The nomenclature of a seizure event. In an electroencephalographic recording, the seizure episode itself (shaded red) is known as the ictal period. A postictal period occurs directly after the seizure, and a preictal period (shaded yellow) occurs before the ictal event. The preictal period is difficult to determine and may extend from seconds to hours before a seizure. The combination of the preictal, ictal, and postictal periods can be collectively referred to as the periictal period. For epilepsy patients, the time periods between periictal periods are known as interictal. The preictal period is of key interest for researchers attempting to anticipate or predict upcoming seizures.

While the ictal event is relatively well-defined time-wise by the assessment of the clinician, the preictal and postictal lengths are less certain and may vary from patient to patient as well as seizure to seizure. In particular, a great deal of research has been undertaken by others in an attempt to identify the existence and extent of the preictal brain state, but with only limited success and highly-varied estimates, ranging from seconds to hours. Additionally, characteristic brain activity that may indicate a preictal progression toward a seizure state may be intermittent or short-lived, further complicating the delineation between the interictal and preictal periods. Some researchers have suggested that in some seizure episodes no preictal period exists, and the seizure spontaneously initiates. Therefore, discernment of EEG brain activity that leads to a seizure episode is inherently challenging. [27]

1.4 Timing of Seizure Identification

Seizure identification can be accomplished through a number of scenarios, effectively related to the timing of the identification (Figure 1.2). In both post-seizure analysis and detection of a seizure episode, the electroencephalographic recordings at many electrode locations show a distinct, large amplitude, rhythmic activity. In these cases, the identification of an ictal event is relatively straightforward. Unfortunately, identification of a seizure after its end or during the event itself does not provide sufficient warning for any action to be made prior to the seizure onset, though there may be benefits for early detection that could lead to an intervention that shortens the duration of an active seizure.

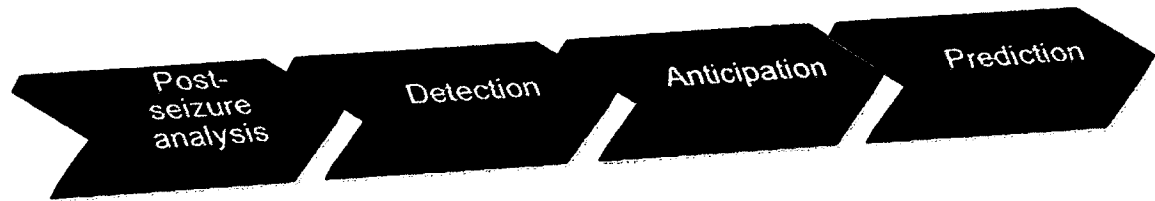


Figure 1.2: The timeline of seizure identification. The difficulty in identification of seizure activity depends on the timing at which the identification is made. In this chart, difficulty increases as researchers move to the right. For the current research presented, seizure anticipation is emphasized.

The main interest in the current research, however, is to identify an upcoming seizure before its onset, with the ultimate future goal to not simply shorten a seizure, but to eradicate it completely. To do so, knowledge of an upcoming seizure is necessary prior to the seizure onset, thus the anticipation or the prediction of a seizure is required. Although the idea of anticipation and prediction are relatively similar with regard to the timing at which a seizure is identified (i.e., before the seizure onset), the difference between the two terms is based on the estimation of *knowing when the actual seizure would occur* based on the anticipated or predicted identification. Perfect seizure prediction will identify the seizure onset time exactly, but in practice an acceptable seizure prediction produces an estimate that a seizure event will fall within a so-called seizure occurrence period (SOP) as described by Winterhalder *et al.* [28] (Figure 1.3). With the overarching intent of pre-seizure knowledge to be useful as a warning system or initiation of an interventional therapy, a seizure prediction horizon (SPH) has also been incorporated in Winterhalder *et al.*'s approach [28]. Seizure anticipation, however, holds less-stringent, more general forecasting that a seizure will occur in the “near future,” but implies more uncertainty of the actual time of the seizure activity onset and less concern for the SPH. The research proposed herein can

more accurately be described as seizure anticipation, rather than seizure prediction, by emphasizing the identification of an upcoming seizure within a relatively longer time frame (up to one hour before a seizure) without attempting to estimate a narrow seizure occurrence period. While the two can be considered to be relatively similar given the arbitrary lengths of SOPs, we feel that the phrase “seizure anticipation” is more appropriate in the context of this research.

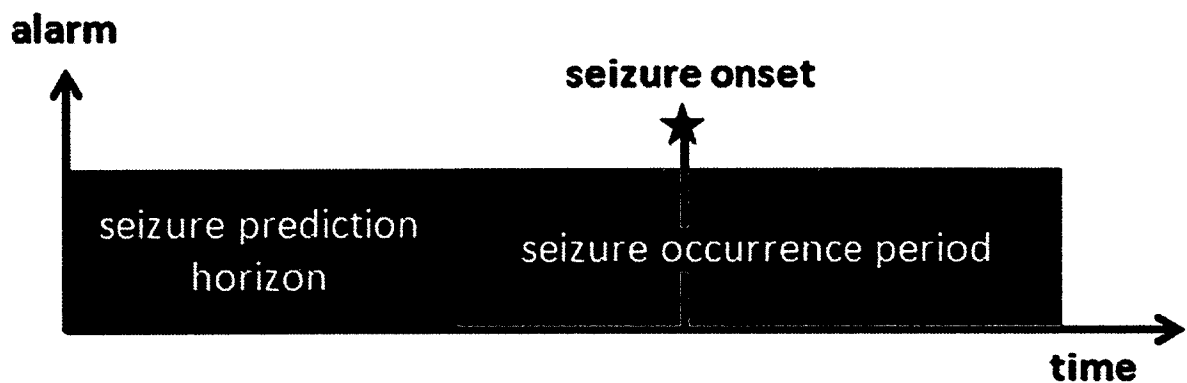


Figure 1.3: Seizure prediction parameters. A graphic indicating the method by which seizure prediction parameters are considered. According to Winterhalder *et al.*, an alarm must be initiated early enough (the seizure prediction horizon, or SPH) for the action of an intervention to drive the system away from a seizure state which would normally occur during a given time (the seizure occurrence period, or SOP). In their case, they evaluated an assumed fast-acting intervention such that the SPH was 5 seconds and maintained a SOP of 30 minutes (Note: This image is not shown at scale for their assertion). Image adapted from [28].

1.5 Purpose of Early Seizure Identification

Unfortunately, no interventional therapy at present has been found to be effective for all epileptic sufferers, and up to 25% eventually have medically intractable epilepsy, meaning that the patient’s disorder is not responsive to treatment [3]. Such individuals have little recourse in the management of seizures. As previously discussed, the ability to infer forecasted knowledge of an impending seizure from preictal EEG

activity could greatly enhance the quality of life for many epilepsy patients. In the simplest scenario, it could empower the individual by reducing the surprise of a sudden seizure episode, which could dramatically enhance the epileptic's sense of self within a social context. Not only would preconceived knowledge of an upcoming seizure aid in the reduction of the negative psychological effects of this disease, it could also enable the epilepsy patient to take precautions prior to a seizure, by moving to a safer environment or stopping activities that could be dangerous during a seizure occurrence. In such cases, a simple warning system could make a significant difference in the daily lives of epileptics.

For patients who respond well to treatments, a seizure warning system could also be employed in conjunction with acute interventional therapy in order to minimize the side effects of long-term, chronic use. This could circumvent problems associated with increased tolerance of medications, limitations on cognitive abilities and open-loop overstimulation. Depending on the lead time between alarm and seizure, administration of an AED, actuation of electrical stimulation, and/or use of other interventions are feasible as real-time treatments given an early enough anticipation.

1.6 Similarity and Synchronization as a Preictal Measure

A typical epileptic seizure results from an atypical, rhythmic hypersynchronization of regional or global neuronal masses. Since brain regions are entrained during a seizure, it may be possible to exploit an enhanced network connectivity in the time leading up to a seizure event for use in seizure anticipation. Similarity

and synchronization between different regions of the brain during the preictal period is a direct way of evaluating abnormal neuronal connectivity. Given that there are numerous signal pathways throughout the brain, dynamic activities can propagate to other regions as if through a black box with nonlinear filtering influences. We evaluate measures of similarity and synchronization as an early indicator of neuronal entrainment. Although similarity and synchronization are not the same, they can be considered analogous. Therefore, we will loosely refer to all of the measures investigated in this work as synchronization measures. In this work, we evaluate bivariate measures of coherence, cross-correlation, correlation coefficient and phase-locking synchrony.

1.7 Scope of the Research

The research work presented here provides a comparison between the preictal and interictal bivariate measures of synchronization for pairs of intracranial electroencephalogram recordings from epilepsy patients using an online seizure database. Extracted by the Ensemble Empirical Mode Decomposition algorithm, intrinsic mode functions of each electrode recording are evaluated in pairs for synchronization differences during “normal,” non-seizure brain activity and one hour of pre-seizure brain activity leading to a seizure event. Identification of appropriate parameters indicating increased preictal synchronization, without false positive identifications during interictal activity, is considered to be beneficial for use in seizure anticipation approaches.

1.7.1 Hypothesis

The signature of a seizure event is an abnormal hypersynchronization of regional or global neuronal tissue. We postulate that initial pre-seizure synchronization(s) occurs prior to the event itself. In order to identify the existence of this preictal synchronization, we evaluate spatial-temporal-frequency features of bivariate measures that relate the similarity and synchronization of electrode recordings. Our main hypothesis is:

- a seizure event is preceded by a notable increase (greater than two standard deviations) in preictal synchronization measures between spatial regions as compared to synchronization measures during interictal periods.

Our assumptions for this work are listed below.

- In the context of seizure progression, preictal dynamics are not required to constantly maintain a higher than normal level of synchronization, but may instead show intermittent increases. Therefore, the preictal period may contain a combination of both preictal and interictal dynamics.
- Increased abnormal synchronization between a particular pair of electrodes during the preictal period is useful as a measure for seizure anticipation given a relatively long time window so as not to be associated with cognitive task-related synchronizations.
- Increased synchronization can occur in clusters across electrode pairs (i.e., across spatial regions) individually, or simultaneously, as a pre-seizure state may propagate to numerous or different brain regions as time progresses.

- The use of Ensemble Empirical Mode Decomposition results in intrinsic mode functions that are more representative of the true underlying regional intracranial electroencephalogram (IEEG) signals in comparison to the original IEEG signals recorded at the electrode sites.

1.8 Organization of Work Presented

This research work is directed toward the ability to anticipate an upcoming seizure event from preictal electroencephalographic recordings. The primary goal of this work is to identify changes in synchronization between pairs of electrodes during the pre-seizure period, which could intimate an increased likelihood of an upcoming seizure event. A literature review is presented in Chapter 2 describing others' work that has been accomplished in the area of preictal brain dynamics synchronization. Chapter 3 illustrates the methods used in this study, along with the motivation for choosing the Ensemble Empirical Mode Decomposition algorithm. Chapter 4 shows the results of the computational analyses of the synchronization measures of interest. Chapter 5 discusses results, along with any limitations in the process. Chapter 6 offers insight gained from this research and areas of potential future work. Appendices are provided to provide a more thorough presentation of intermediate results as well as a portion of the MATLAB code developed and used for this project.

CHAPTER 2

BACKGROUND

The ability to forecast upcoming seizures has long been an area of active research in neuroscience. Coincident with the advancing state of mathematical techniques and robust computational platforms, numerous researchers and clinicians have actively investigated the preictal period for indications of changes in brain dynamics resulting in a seizure-progressive state. To this point, however, the mechanisms and markers associated with seizure-progenerative dynamics remain unclear.

2.1 Existence of a Preictal State

Epileptic seizures can occur in a wide variety of ways, and may manifest differently from patient to patient as well as seizure to seizure, owing to the multitude of epilepsy pathologies that can contribute to the vast differences in ictogenesis [3]. Based on efforts to identify preictal changes by a significant number of researchers over the past several decades, Lopes da Silva *et al.* [29] have theorized scenarios within which epileptic seizures may occur that include both spontaneous seizure generation and progressive changes in brain dynamics that lead to seizures. In the first case, they hypothesize that the seizure onset is identified as a sudden transition, such that the ability to predict a seizure is considered to be a fruitless effort. These types of abrupt, spontaneous dynamical changes have been theorized to be more likely

associated with absence-type or primary generalized (non-focal) seizures. However, for the latter case, they believe that progressive changes in brain dynamics leading up to a seizure could be detectable in the time before a seizure event. These slower changes in the brain state are more often considered to be associated with focal epilepsy, as the focal region would gradually entrain neighboring areas or produce clusters resulting in a seizure state [27, 30]. While often considered to be relegated to focus-originating seizures, preictal changes may not be limited to these cases only, as shown in recent studies [31, 32]. Further, some researchers hypothesize that the seizure itself is merely the culmination of events in preictal synchronization in an effort to “reset” the normal system dynamics [33–35]. Other studies [36, 37] using a measurement of neuronal excitability have indicated that the seizure onset itself may be unpredictable, though there may be an observable increased probability of ictogenesis. An increased excitability may, in effect, bridge the gap between the theories described above.

Currently, the existence of a preictal state is generally well-accepted for most seizure types [38–43], though the ability to precisely identify the preictal state is still limited. A portion of this shortcoming can be associated with the individuality of the pathology for the epileptic patient and the variation in seizure presentation. Herein lies a major challenge for researchers in the field of seizure prediction: the variability of seizure genesis. Although the idea of the existence of the preictal state hinges on some level of constancy across patients, it is not contradictory to consider that the preictal state may be represented in various ways across patients. As such, researchers have moved toward patient-specific analyses for seizure-predictive

approaches. There is an inherent limitation of determining global measures that adequately anticipate upcoming seizure events for all seizures across a multipatient data set [27, 38]. Rather, selective, patient-specific measures may produce higher prediction performance results. However, researchers have shown seizure-to-seizure correlations and lack thereof [44], so the challenges also extend to the inpatient scenario.

Supporting evidence from clinical studies of pre-seizure physiological changes in heart rate, cerebral blood flow, and oxygen levels also suggest a broader, more global impact of the preictal period on the individual [45–49]. These physiological changes indicate the likelihood of detectable signs of a seizure-progenerative, or, at a minimum, a seizure-premonitory, preictal state. Further, some epileptic patients with temporal lobe epilepsy (a focal epilepsy) experience a pre-seizure “aura” [50]. Beyond patients experiencing auras, it has been shown that some epileptics in cases of focal or generalized seizures also may anticipate upcoming seizures [6, 7]. Thus, there is additional compelling evidence toward the potential of distinguishing preictal dynamics from interictal activities that falls outside of the context of quantitative EEG analysis.

It should be noted that the epileptic brain may inherently hold some subtle differences in dynamics in comparison to the normal brain. Some foundational studies using synchronization measures have been performed to localize the seizure focal region during interictal time periods. Bialonski and Lehnertz [30] used a multivariate approach for analysis of synchronization clusters. While their objective was seizure focus localization rather than seizure prediction, their clustering method elucidated an

increased synchronization in interictal dynamics precisely where the focal region was determined to be by independent presurgical analysis. Additionally, Osterhage *et al.* [51] were able to correctly lateralize the focal region for all of the synchronization measures they tested during the interictal period. Others have observed similar enhanced interictal synchronization [52, 53]. It is uncertain whether or not these studies simply denoted a pervasive difference in the interictal dynamics of epilepsy patients or, perhaps, “happened upon” long-duration preictal dynamical changes that were assigned to be interictal in nature. While these discoveries do not disprove the idea of a preictal period and subsequently indicate a basic differentiation between epileptic and normal brains, further evaluation of the preictal period’s existence is needed.

2.1.1 Testing Null Hypotheses

While knowledge of a distinct preictal state would be beneficial, many researchers have approached this uncertainty in a different way. In one such effort to explore a method to discount the possibility of a pre seizure state, Andrzejak *et al.* [54] tested the null hypothesis of the absence of the preictal state. They were unable to reject the null hypothesis, but their work was only exploratory, using a single-patient analysis with only one measure (degree of nonlinear determinism). In many cases, the practical, straightforward approach for determining a clinically-viable method of seizure prediction is simply based on the sensitivity of the measure coupled with an “acceptable” false positive rate [28, 55]. While, generally speaking, a false positive rate (FPR) of 0.15 false positives per hour is a commonly accepted number based

on the maximum average seizure frequency [56], these rates may become inflated or deflated based on the individual's seizure frequency and effectiveness of the seizure-control therapy [57]. Winterhalder *et al.* [28, 58] used a method of comparison of measures with a random predictor based on a nominal false positive rate. They showed that certain measures and electrode combinations were capable of successfully performing better than chance. Others [38, 43, 59–65] have also made comparisons of their seizure prediction methods to random predictors with similar success and expectation of preictal changes. Andrzejak *et al.* [66], however, suggests that while these studies may be promising for the end goal of detecting preictal changes, the ability to truly reject the null hypothesis is questionable since distinct null hypotheses in these studies may not be appropriately devised. In the end, the true test of seizure prediction schemes must fall to relevance in the clinical setting and acceptance by the patient population [67].

2.1.2 Duration of the Presumed Preictal Period

While generally-accepted, but not explicitly proven, the preictal state is conjectured to occur somewhere within a broad range of durations (from seconds to hours), based on researchers' results from seizure predictive measures. As early as the 1980's, Rogowski *et al.* [68] used an autoregressive analysis and found changes seconds before the seizure onset. Others [69] have also observed preictal differences seconds before seizure onset. An inherent problem with pre-seizure anticipation, however, is the time frame of potential interventions. While knowledge of a seizure only seconds before onset could be useful for certain therapies (e.g., electrical stimulation such as

employed by the NeuroPace system), other intervention types are not feasible. In fact, electrographical changes that are identifiable a few seconds before clinical signs of a seizure are exhibited may simply indicate that these short-term changes are a subclinical start of the seizure episode and can be considered to be seizure detection, rather than seizure anticipation.

Longer-term preictal analysis has thus been evaluated to enable a broader range of feasible interventional therapies as well as eliminate questions regarding seizure prediction versus seizure detection. Litt *et al.* [70] found indicators of seizure behavior as much as seven hours prior to seizure and observed accumulated energy measure differences nearly one hour before ictal onset. Iaşemidis *et al.* [71] observed preictal changes of their T -index from the maximum short term Lyapunov exponent as far as three hours in advance of seizure events. Through their work, Morman *et al.* [38] analyzed data from four time durations of preictal data, derived from the original studies of many of the measures they reevaluated. They found that several measures showed more distinct separation between interictal and preictal phenomena for longer preictal time frames, often observing the best performance for a 240-minute preictal period of bivariate analysis, while well-performing univariate measures typically ranged from 5-30 minutes.

2.1.3 Long-Duration Preictal Periods

One might conclude that the changes of measures during a long preictal duration is linked to an increased propensity for a seizure event over the course of larger time scales. In some ways, this can be considered to be more akin to

seizure anticipation, rather than seizure prediction. To be sure, however, the effects of antiepileptic drug concentration tapering, the state of vigilance, or the influence of circadian rhythms may have some influence in this observation of long-term nonstationarity and the preictal state, as suggested by many researchers [38, 61, 72–74]. As a result, researchers can adopt an adaptive baseline (threshold) approach or maintain a constant baseline when identifying differences between interictal and preictal measures. In their comparison study, Mormann *et al.* [38] investigated both scenarios and observed a notably better performance when the baseline was maintained as a constant as compared to an adaptive one. While the parameters governing the “adaptability” of the measure can hold significant influence on the outcome, it is possible that the changing baseline itself may carry important information regarding a change in the probability of ictogenesis.

2.2 Role of Hypersynchrony in Seizure Anticipation

In the 1950’s, Penfield and Jasper promoted the idea that seizures are manifested as abnormal hypersynchronous activities of brain tissue [75]. Although some recent studies have shown seizures themselves hold more complex changes in synchronization than previously thought [76–82], Penfield and Jasper’s classical theory holds insight into the nature of seizure events. By extension, many researchers have sought to identify the elusive features indicative of a preictal state by using measures of synchronization and interdependency across brain regions in the time leading up to a seizure. Given that the seizure state involves enhanced synchrony, an effort to determine precursorial, subclinical synchrony holds promise in better

understanding the mechanism of seizure progression and in the ability to employ warning or interventional therapy systems.

2.3 Bivariate Measures of Synchronization

While the use of univariate measures of EEG patterns prior to seizure has been studied extensively, in more recent years, interest has been directed toward bivariate preictal data analysis. Early work by Mormann *et al.* [83] promoted the potential benefits of bivariate analyses. They evaluated mean phase coherence as a measure of phase synchronization. They observed synchronization changes minutes to hours before the seizure event. Later work by the same group [60, 84] showed similar results between mean phase coherence and two other adaptations of phase synchronization: a Shannon entropy-based index and a conditional probability-based index stemming from work by Tass *et al.* [85]. Finally, Mormann *et al.* [38] used over 30 univariate and bivariate measures to compare interictal and preictal EEG signals. Their findings suggest an advantage of bivariate measures over univariate measures. They observed better performance for bivariate analyses when a patient-individualized, channel-specific scheme was used. Their results imply that certain channel combinations may indicate synchronization changes across brain regions, while others may not indicate similar changes. In other words, a global (patient-generic) analysis scheme may have less relevance when detecting preictal changes. Mormann *et al.*'s work has provided a springboard for researchers' expansion into the use of bivariate measures.

Winterhalder *et al.* [58] have also shown benefits of bivariate measures with their analyses of phase synchronization and lag synchronization. Through their work,

they analyzed various durations for the seizure prediction horizon (SPH) and seizure occurrence period (SOP) (refer to Figure 1.3). Evaluating preictal differences for both decrease and increase in these measures in comparison to a random prediction scheme, they observed a highly patient-dependent capability of one or both of these measures to exceed critical sensitivity values based on a nominal false prediction rate. Their approach showed success for approximately half of the patients tested. They found that the lag synchronization measure was most sensitive when used with a focal-extrafocal paired combination of electrodes. They conjecture that the synchronization delay across these regions pertains to the increasing global synchronization during the preictal period.

In their study to determine ictal and interictal differences of phase synchronization, Gupta *et al.* [34] observed potential indicators of phase synchronization value changes during the preictal period. Although their dataset was limited, they saw a typically seizure-coincident cyclical pattern in a relative feature composed of two frequency bands' phase synchronization measures. They conjecture that these cyclical changes relate to a set-reset type of mechanism of synchrony for pre-seizure and seizure dynamics, respectively. Additionally, they observe that the measure's interictal trend is "pulled away" from normal at times leading up to a seizure event.

Mirowski *et al.* [86, 87] used a pattern recognition method with six bivariate measures (and three classification schemes) over multiple time frames. They found that frequency-based bivariate features, such as wavelet coherence and synchronized phase locking value, performed better on average. They also showed success with a nonlinear interdependence measure. The success for certain measures was observed

in the case of certain patients' data while other measures proved to be much more appropriate for other patients' data. This notable difference provides insight into the highly variable nature of seizure pathologies and correct identification of patient-specific measures.

In 2009, Myers and Kozma [88] investigated a synchronized phase-locking value (PLV or SPLV) for potential incorporation into a VNS implant control scheme. They found that the increased levels of synchronization (i.e., a high PLV) effectively identified seizure events. Additionally, they observed higher than normal synchronization values at times during the preictal period as well. A limitation of their study is their use of *a priori* knowledge, by developing a threshold value for each patient that satisfied both seizure predictive and identifying constraints retrospectively. They relied on the PLV measure to first identify the seizure, then slowly lowered their threshold to still include some predictive high-synchrony value, rather than basing their measure simply on using interictal synchrony values for the threshold value selection. Nevertheless, the use of a synchronized phase-locking value showed promise from their study.

Feldwisch-Dentrup *et al.*'s [89] work with combined univariate and bivariate measures indicates the potential benefit of multi-feature approaches. They investigated alarms for both mean phase coherence and dynamic similarity index in a Boolean "AND" operation within a limited time period. They found that the specificity and performance were better than a random prediction scheme upon application of this requirement. This multi-feature method may be the optimum pathway to provide a clinically-relevant tool for use of synchronization measures, particularly in

the context of limitations due to electrode placement, and is further supported by later work from the same group [90].

Recently, bivariate synchronization features have been derived from wavelet transform data from EEG signals as an additional means of extracting important and, perhaps, subtle information beneficial to the differentiation between preictal and ictal dynamics. Nesaei and Nesaei [91] applied a discrete wavelet transform and determined a measure of phase synchronization for three IEEG focal electrodes across different frequency bands below 32 Hertz. They predicted seizure events at times ranging from seconds to nearly an hour in advance of the onset, based on a drop below threshold for their synchronization measure. They reported two of the three combinations of focal electrodes that performed well, with relatively high sensitivities and specificities. They did not see a particular optimum in performance for any particular level of frequencies across the global dataset for either of the electrode combinations. Such an optimum might have been observed at the patient-specific level, however. In an animal study, Suarez *et al.* [92] performed cross-correlation analysis on wavelet coefficients of Pilocarpine-induced seizures with notably high sensitivity ($> 90\%$).

2.3.1 Contraindications for the Use of Bivariate Synchronization Measures

Not all bivariate measures of synchronization have produced desired results. Jouny *et al.*'s [93] use of a complexity measure (Gabor Atom Density) and a synchrony measure (known as measure S) failed to correctly detect preictal changes, though these measures were able to identify ictal and postictal dynamics. Jerger *et al.* [94] did not see good performance in their one-patient study using a linear

discriminator for cross-correlation and phase synchronization. However, they trained their discriminator on ictal and interictal data for testing of the preictal data. By doing so, they are essentially requiring that the measures during the preictal state resemble that of the ictal state, which likely understates the subtleties of pre-seizure dynamics. In their modeling study of coupled oscillators, O’Sullivan-Greene *et al.* [95, 96] question the observability of synchronization, however they acknowledge that local synchrony may provide enhanced capability. They have shown some potential of synchrony measures in the context of input stimulation response of their models.

2.3.2 Predisposition of Synchronization Measures

Morman *et al.* [38] suggest that there is no essential difference in presupposing directionality of synchronization (increasing or decreasing). Based on their results, they often observed increased synchronization in one region coupled with a corresponding decreased synchronization in an adjacent region. They hypothesize that a region of excitable brain tissue is entrained by an ever-growing cluster, while simultaneously separating its dynamics from a previous interaction with a different brain region from an opposing direction [83, 84]. Similar results of directionality were observed by Aarabi *et al.* [31] in their analysis of preictal dynamics for absence seizures. Winterhalder *et al.* [58] draw from their own work support for the arbitrary nature of increasing versus decreasing synchronization assigning relevance of the directionality as based on intracranial electrode placement to nearby anatomical structures. While knowledge of directionality in synchronization could enhance seizure anticipation

schemes, there is limited evidence to compel researchers to incorporate directionality in their approaches at this point.

2.4 Empirical Mode Decomposition in Seizure Anticipation

Neuroscientists have often separated EEG signals into frequency bands for subsequent analysis using techniques such as the fast Fourier transform and the wavelet transform. A relatively new approach, known as Empirical Mode Decomposition (EMD) [97], provides an analytical analogue to this often applied technique. Recently, a few researchers have explored the potential for this new decomposition method in quantitative EEG analysis. Tafreshi *et al.* [98] used the EMD technique to obtain intrinsic mode functions (IMFs) from which an autoregressive (AR) model could be used to extract features in a seizure prediction approach. The AR coefficients were submitted to a self-organizing map clustering approach for classification purposes. The authors determined that their classification was more accurate when the AR model was applied to the IMF components than it was when the AR model or IMF features were used individually. Tianqiao *et al.* [99] have also shown the potential benefit of EMD. They evaluated the preictal period using a univariate complexity measure derived from the IMFs along with an artificial neural network for classification. With this method, they obtained a reasonably high accuracy (75%), but it may not be suitable for the clinical scenario due to a relatively poor sensitivity (67%). Orosco *et al.* [100] and Oweis and Abdulhay [101] have also used EMD to investigate descriptive statistics at the IMF component-level with good success for seizure detection.

CHAPTER 3

METHODS

3.1 Computational Platform and Software

Data for this study were analyzed on 32-bit Microsoft Windows XP and Vista operating systems. MATLAB versions R2008a and R2009a (The MathWorks, Inc., Natick, Massachusetts) were used for computational analysis. Custom MATLAB codes were written by the author for this work. Additionally, some available toolboxes were used.

3.2 Intracranial Electroencephalogram Data Set

Intracranial electroencephalogram (IEEG) data from intracranial grid, strip and depth electrodes were obtained through a publicly-available database of invasive pre-surgical epilepsy monitoring at the Epilepsy Center of the University Hospital of Freiburg. Data from a total of twenty-one patients are available (Table 3.1). The database includes a minimum of twenty-four hours of interictal data for each patient, either from 24 hours of continuous recording (13 patients) or from a combination of non-continuous interictal recordings (8 patients). Between two and five seizure episodes for each patient are available. Patients included both female and male subjects, ranging in ages of 14 to 50 years old. Patients experienced simple partial

(SP), complex partial (CP), and/or generalized tonic-clonic (GTC) seizure types originating from either the hippocampus or neocortex.

Table 3.1: University Hospital of Freiburg Epilepsy Center Patient Database. Abbreviations used in the table are as follows: SP = simple partial, CP = complex partial, GTC = generalized clonic-tonic, NC = neocortex, H = hippocampus, d = depth, g = grid, s = strip.

Patient	Sex	Age	Seizure Type	H/NC	Origin	Electrodes	Seizures
001	f	15	SP,CP	NC	Frontal	g,s	4
002	m	38	SP,CP,GTC	H	Temporal	d	3
003	m	14	SP,CP	NC	Frontal	g,s	5
004	f	26	SP,CP,GTC	H	Temporal	d,g,s	5
005	f	16	SP,CP,GTC	NC	Frontal	g,s	5
006	f	31	CP,GTC	H	Temporal/Occipital	d,g,s	3
007	f	42	SP,CP,GTC	H	Temporal	d	3
008	f	32	SP,CP	NC	Frontal	g,s	2
009	m	44	CP,GTC	NC	Temporal/Occipital	g,s	5
010	m	47	SP,CP,GTC	H	Temporal	d	5
011	f	10	SP,CP,GTC	NC	Parietal	g,s	4
012	f	42	SP,CP,GTC	H	Temporal	d,g,s	4
013	f	22	SP,CP,GTC	H	Temporal/Occipital	d,s	2
014	f	41	CP,GTC	H,NC	Frontal/Temporal	d,s	4
015	m	31	SP,CP,GTC	H,NC	Temporal	d,s	4
016	f	50	SP,CP,GTC	H	Temporal	d,s	5
017	m	28	SP,CP,GTC	NC	Temporal	s	5
018	f	25	SP,CP	NC	Frontal	s	5
019	f	28	SP,CP,GTC	NC	Frontal	s	4
020	m	33	SP,CP,GTC	NC	Temporal/Parietal	d,g,s	5
021	m	13	SP,CP	NC	Temporal	g,s	5

Data were acquired at the Epilepsy Center of the University Hospital of Freiburg, Germany, with a 128-channel Neurofile NT digital video electroencephalograph (EEG) system. Data were digitized using a 16-bit analog-to-digital converter. Using

the video EEG system, a certified epileptologist has identified interictal and ictal activities. Database files are downloadable as either interictal or ictal sets of tarred and zipped compressed archive files for each patient. Once uncompressed, files are ASCII-type and include a single column of voltage recordings in the scale of millivolts. The files are presented typically as one-hour datablocks, except in specific cases where the data were lost due to data acquisition difficulties (e.g., electrode box disconnections and other technical difficulties). Throughout the dataset, a period of less than three seconds of data was omitted between these one-hour datablocks due to technical and computing resource reasons. Each filename is unique (e.g., 010403ba_0006_1.asc), including an identifier based on recording start date, patient initials, sequential datablock numbering, and channel number, respectively. No notch or bandpass filtering was performed by the Epilepsy Center on the IEEG data; thus, electrode disconnection and 50 Hertz (Hz) power line noise were present in the available database recordings. It should be noted that any movement artifacts are inherently limited due to the intracranial placement of electrodes. IEEG data were acquired at 256 Hz for all but one patient (512 Hz for patient 012, the data for which was omitted from this analysis). As of this writing, the data can be accessed following approval of the registered user from the website administrators of the Seizure Prediction Project Freiburg (<https://epilepsy.uni-freiburg.de/freiburg-seizure-prediction-project/eeg-database>).

For each patient, a schematic representation of the intracranial grid, strip, and depth electrode locations are provided (see example in Figure 3.1). Although multiple electrode sites were recorded, the epileptologist selected three recording sites (i.e.,

channels or electrodes) found to be involved in the early stages of the seizure activities observed. These channels (named CH1-CH3) were deemed as in-focus, or focal, electrodes. Similarly, the epileptologist selected another three channels considered to not be involved in the early onset of the patient's seizures. These channels (CH4-CH6) were identified as out-of-focus, or extrafocal, electrode sites. The available dataset for each patient, therefore, contains recordings for both interictal and ictal activities from the six concurrently recorded channels as identified above. Seizure event onsets and ends, as identified by certified epileptologist post-seizure analysis of the video EEG record, were determined at the University Hospital of Freiburg. For each patient's seizure events, data sample numbers indicating the onset and end within particular database files are supplied.

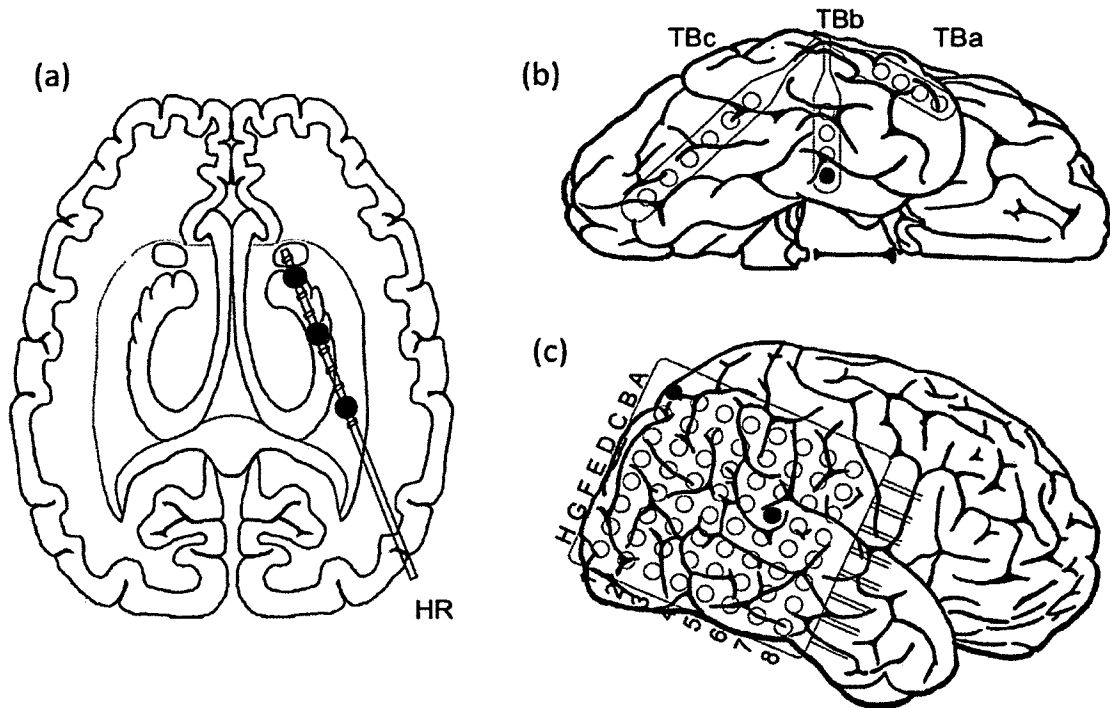


Figure 3.1: A schematic representation of intracranial electroencephalogram electrode types (Patient 4). Intracranial depth (a), subdural strip (b) and subdural grid (c) electrodes were used to collect brain activity recordings from epilepsy patients undergoing monitoring at the Epilepsy Center of the University Hospital of Freiburg. Note: IEEG electrode types and placement locations varied from patient to patient based on the monitoring needs of the clinicians.

3.3 Data Preparation, Partitioning, and Preprocessing

Custom code was used to read the ASCII data into the MATLAB environment, and the data structures composed of multiple matrices were saved in the native **.mat* format. For interictal data, a 60-minute block of data was saved, following the data organization structure of the Epilepsy Center Patient Database files. For periictal data, 60 minutes of preictal and 15 minutes of ictal/postictal data were combined to create a 75-minute datablock. In assembling the periictal datablock, the data acquisition gap of less than three seconds was ignored during concatenation of data from sequential files.

IEEG recordings for each of the six channels were partitioned into non-overlapping 16-second time windows. The 60-minute interictal datablock was, therefore, divided into 225 time windows, while the 75-minute periictal datablock has 281 time windows. Sampled at 256 Hz, each 16-second time window included N samples, such that $N = 4096$. The division points for these time windows were temporally-coincident across the six available channels (i.e., the relative start and end time of each partitioned window was maintained consistently across all concurrent channel recordings). Sample data for each time window were normalized to have a zero mean ($\mu = 0$) and unit standard deviation ($\sigma = 1$), for later introduction to the Ensemble Empirical Mode Decomposition (EEMD) algorithm.

To determine the zero-mean normalization of the sample time window m , the arithmetic mean μ (Equation 3.1) is removed from the original time series signal, $y_i^{k,m}$, where i is the index value of a set of N samples for m^{th} window of the k^{th} channel,

or electrode. The resulting zero-mean time series of the m^{th} time window can be denoted as $\hat{y}_i^{k,m}$ (Equation 3.2).

$$\mu^{k,m} = \frac{1}{N} \sum_{i=1}^N y_i^{k,m} \quad (3.1)$$

$$\hat{y}_i^{k,m} = y_i - \mu \quad (3.2)$$

The standard deviation σ of the zero-mean time series for time window m and channel k is determined by the square root of the mean squared error (Equation 3.3). The subsequent normalization of the data to unit standard deviation (also referred to as the z -score) is accomplished by dividing the zero-mean samples of a given time window by the standard deviation (Equation 3.4).

$$\sigma^{k,m} = \sqrt{\frac{1}{N} \sum_{i=1}^N (\hat{y}_i^{k,m} - \mu^{k,m})^2} \quad (3.3)$$

$$z_i^{k,m} = \frac{\hat{y}_i^{k,m}}{\sigma^{k,m}} \quad (3.4)$$

3.4 Data Decomposition

3.4.1 Empirical Mode Decomposition

Empirical Mode Decomposition (EMD), first introduced by Huang *et al.* in 1998, is a useful technique for decomposing non-stationary and non-linear time series data [97]. The analyzed data are decomposed into a relatively small number of intrinsic mode functions (IMFs) using a sifting process with stopping criteria. The EMD method itself is an adaptive, data driven approach which decomposes a signal $x(t)$

into IMF components c_j and a residual r_n following n extracted IMFs (Equation 3.5).

$$x(t) = \sum_{j=1}^n c_j + r_n \quad (3.5)$$

Huang *et al.* have adopted the name intrinsic mode function “because it represents the oscillation mode imbedded in the data” and have provided a strong argument for its use in their original paper [97]. An IMF captures the physically meaningful, local instantaneous frequency, unlike the more general and global Hilbert transform, thereby enabling application to non-stationary data (i.e., data with more than one oscillatory mode). Each intrinsic mode function has two conditions that must be met. The first condition requires that the number of local extrema and the number of zero crossings in IMF time-frequency space cannot be different by more than one. This condition provides for an analogous representation of narrow bandwidth requirements typically used with stationary data. The second condition requires that the mean value of the envelope of the local maxima and envelope of the local minima is zero. Each upper or lower envelope is defined by a cubic spline of the respective extrema (along the local maxima or along the local minima), rather than using a local instantaneous mean. Forcing the envelope mean, rather than the local mean, of the data to be zero circumvents difficulties with determining the local averaging time scale, particularly with non-stationary data.

3.4.2 The EMD Sifting Process

In order to decompose complicated data into its IMFs and residual, a sifting process is employed. The upper and lower envelopes’ mean m_1 is determined and

removed from the original data $x(t)$ (Equation 3.6).

$$x(t) - m_1 = h_1 \quad (3.6)$$

In an ideal case, h_1 would be the first IMF, however, in more complicated data with wide bandwidth, subsequent sifting processes are typically necessary. A second sifting process would then be accomplished (Equation 3.7), where h_1 would be treated as the data, m_{11} would be the mean of the upper and lower envelopes from the extrema of h_1 , and h_{11} would be the evaluated to determine if it is in fact an IMF.

$$h_1 - m_{11} = h_{11} \quad (3.7)$$

The process is repeated k times following

$$h_{1(k-1)} - m_{1k} = h_{1k}, \quad (3.8)$$

until h_{1k} is a true IMF and can be designated as the first IMF component c_1 of the data, such that

$$c_1 = h_{1k}, \quad (3.9)$$

once the riding waves have been eliminated and uneven amplitudes smoothed. In order for these stopping criteria to be assessed for the sifting process, the size of the standard deviation σ_h can be set to be between 0.2 and 0.3 for consecutive sifting results k and $(k - 1)$ following

$$\sigma_h = \sum_{t=0}^T \left[\frac{|(h_{1(k-1)}(t) - h_{1k}(t))|^2}{h_{1(k-1)}^2(t)} \right]. \quad (3.10)$$

The first IMF c_1 (also referred to as IMF1 in the following text) contains the smallest scale (highest frequency) information of the signal. IMF1 can be removed

from the original data by

$$x(t) - c_1 = r_1, \quad (3.11)$$

producing a residue r_1 . This residue which may contain lower frequency components is further decomposed using the sifting process described above to obtain subsequent n IMF components and a residue r_n by

$$r_1 - c_2 = r_2, \dots, r_{n-1} - c_n = r_n. \quad (3.12)$$

The final stopping criteria of the analytical decomposition is when the final IMF component c_n or the residue r_n is appropriately small enough to have inconsequential effect on the data (selected in the decomposition parameters) or when the residue r_n is a monotonic function (i.e., trend data without local extrema).

Recall Equation 3.5, indicating that the simple linear superposition of the n IMFs and the residue provide the original data sequence:

$$x(t) = \sum_{j=1}^n c_j + r_n. \quad (3.5)$$

The EMD method separates scales of the original data during the sifting process and results in a relatively small number of intrinsic mode functions representative of the signal itself. However, there are limitations to the EMD algorithm for complex natural systems, including EEG brain dynamics. The most notable drawback of the EMD algorithm is its tendency toward mode mixing, particularly for signals with poor scale separability such as EEG recordings. Mode mixing occurs as a result of signal intermittency and can manifest in two distinct ways. In the first case, a single IMF may include signal information that is more appropriately partitioned into several

IMFs due to a wide variation in the time-frequency representation, or scale. In the other case, a portion of the signal having a similar scale, which presumably would be represented in a single IMF, may be spread across a number of IMFs. Another limitation of the EMD algorithm relates more to the signal itself and how the algorithm decomposes the data. In a natural system like the human brain, the EEG recording may not accurately represent the actual underlying signal. Inherently, EEG and IEEG recordings are influenced by the local and regional effects of the surrounding neuronal tissue, resulting in a weighted summation of biopotential activities of nearby neuronal masses. Thus, the electrode recording represents multiple action potentials and ion movements from numerous cells, with the end result as a measure of local field potential. This local field potential is heavily influenced by the timing of neighboring neuronal activities, and is, therefore, laden with broadband noise. The resulting IMFs from the EMD algorithm may erroneously represent the true nature of the system dynamics in the presence of this broadband noise.

3.4.3 Ensemble Empirical Mode Decomposition

In order to more appropriately represent the true, or natural, underlying signal of the electrode region, it is beneficial to employ a noise-assisted data analysis (NADA) approach. The data analysis accomplished in this study uses this noise-assisted extension of the EMD computational technique by determining the ensemble means of the identified intrinsic mode functions of noise-added input signals. This method is known as Ensemble Empirical Mode Decomposition (EEMD) and was developed by Wu and Huang [102]. By superimposing finite white noise onto a signal prior to

submission to the decomposition algorithm, variants of each IMF are obtained. If this process is repeated with different white noise sequences over an adequate number of trials, the noisy background from neighboring regional activity influencing the local field potential can, in effect, be canceled out by obtaining the ensemble mean of these IMF variants. This follows the statistical definition of error across multiple trials of added white noise shown by

$$\varepsilon_p = \frac{\varepsilon}{\sqrt{P}}, \quad (3.13)$$

where ε is the amplitude of the white noise, P is the number of trials and ε_p is the standard deviation of error between the signal and IMF. The NADA EEMD algorithm essentially behaves as a dyadic filter bank [103]. In doing so, mode mixing is effectively eliminated. Therefore, the EEMD method offers the advantage of a more robust and true representation of the actual underlying signal based on the ensemble mean.

Figure 3.2 illustrates the methodology for data preparation and decomposition using the EEMD approach, a straightforward NADA extension of the original EMD method. Following the data preparation in Section 3.3, a white noise sequence $w(t)$ with a small variance ($\sigma^2 = 0.1$) is introduced to the preprocessed time window data sequence $z_p^{k,m}(t)$ and is determined using

$$\hat{z}_p^{k,m}(t) = z_p^{k,m}(t) + w_p(t) \quad (3.14)$$

for the p^{th} trial of the k^{th} channel and m^{th} time window. The data $\hat{z}_p^{k,m}(t)$ are decomposed with the EMD sifting process until each IMF is extracted. Twelve levels of IMFs were obtained from the decomposition of the data. An ensemble mean at each IMF level was calculated from the P trials' results. These IMF ensemble means

were considered the fundamental oscillating modes of the data and were used in the subsequent analysis of the synchronization measures of interest.

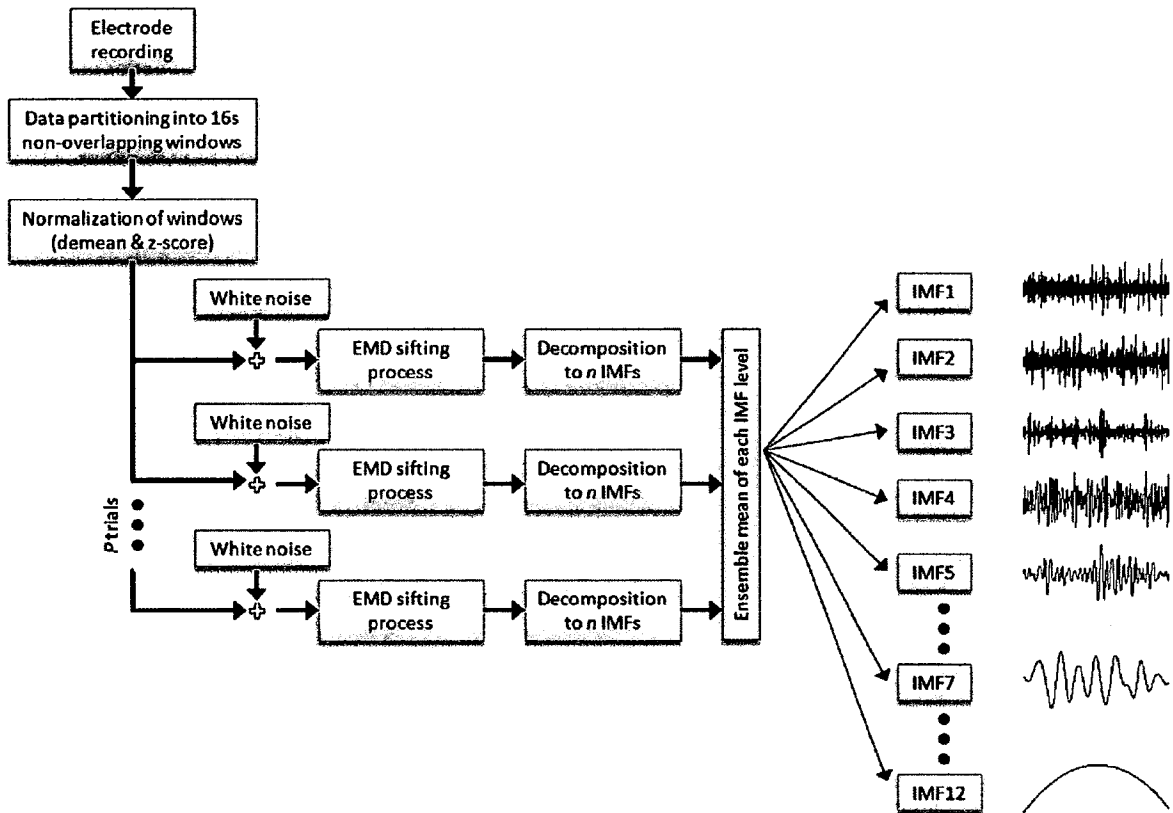


Figure 3.2: Data preprocessing and decomposition block diagram. This block diagram shows the steps taken for initial IEEG electrode recording data preprocessing and data decomposition. The first three blocks in the upper left relate to information in Section 3.3. Ensemble Empirical Mode Decomposition is an extension of the EMD method and is performed by the repetitive (P trials) addition of white noise to the preprocessed data prior to EMD sifting. A set of n IMF levels is determined for each trial ($n = 12$ levels of separated IMFs for the IEEG data analyzed herein). (Notice that the first IMF level, IMF1, contains the highest frequency information, with the time scale of the signal increasing as the IMF level increases.) A more true, underlying representation of the IEEG signal is identified by taking the ensemble means of each IMF level across the P trials. For the analysis in this research work, the superimposed white noise was set to a variance of 0.1 and the number of trials P was 50.

3.4.4 EEMD Computation Time Limitations

The EEMD algorithm requires multiple trials of decomposition to obtain the ensemble means. The computational resources (described above in Section 3.1) provide very modest capability for the combination of the algorithm and large size of the IEEG data files. Completion of EEMD on a single hour of IEEG data routinely required in excess of ~ 10 hours. Due to the relatively large number of patients to be analyzed (20 patients, recall that patient 012 was omitted from analysis), only the first six hours of interictal data was submitted to the EEMD algorithm. Additionally, each patient's periictal dataset contains a 75-minute block of information, thus increasing the computation time in those cases. The computation time alone for the EEMD algorithm of this limited data set is roughly three months.

3.5 Measures of Synchronization

The signature of a seizure event is an abnormal hypersynchronization of regional or global neuronal tissue. We postulate that initial pre-seizure synchronization(s) occurs prior to the event itself. In order to identify the existence of this preictal synchronization, we evaluate spatial-temporal-frequency components between the decomposed data of electrode recording pairs at similar IMF levels. The research presented here investigates bivariate measures that relate the similarity and synchronization of signals, such as coherence, cross-correlation, correlation coefficient, and phase-locking synchrony.

The preprocessed and decomposed data time windows of the six electrode (channel) recordings were used to calculate each synchronization measure. Channel pairings were developed from the six available electrodes, providing fifteen (15) channel pair combinations (Table 3.2). For each channel pair, IMFs at the same level were used to compute each measure. Only concurrent time windows were evaluated in the bivariate computation.

Table 3.2: Associated channel pairings with channel pair ID number. Channel pairings with channel pair ID number indicate the 15 channel pairings of the 6 electrodes from the Freiburg Epilepsy Center Database (f = focal electrode, e = extrafocal electrode).

Channel Pair ID	Channel A	Channel B	Pair Type
1	1	2	f-f
2	1	3	f-f
3	1	4	f-e
4	1	5	f-e
5	1	6	f-e
6	2	3	f-f
7	2	4	f-e
8	2	5	f-e
9	2	6	f-e
10	3	4	f-e
11	3	5	f-e
12	3	6	f-e
13	4	5	e-e
14	4	6	e-e
15	5	6	e-e

3.5.1 Coherence

Coherence is a measure of similarity between two signals. Coherence has a bounded value of $[0, 1]$, where a perfect correlation of the two signals at all frequencies holds a value of 1. This work uses magnitude-squared coherence and can be described by

$$C_{xy}(f) = \frac{|P_{xy}(f)|^2}{P_{xx}(f)P_{yy}(f)}, \quad (3.15)$$

where P_{xx} and P_{yy} are the autospectral density functions for x and y , respectively, and P_{xy} is the cross-spectral density function. As functions of frequency (f), the magnitude squared coherence (C_{xy}), i.e. the real portion of the coherence, provides what can be considered to be a frequency-varying cross-correlation measure representing the linear relationship of the two signals. The MATLAB command `mscohere` was used for determining the magnitude-squared coherence.

The coherence was analyzed to determine the coherence of concurrent time windows for each channel pair at each IMF level (Figure 3.3). An overall, mean coherence ($C_{\mu}^{q,m,j}$), and a maximum coherence ($C_{max}^{q,m,j}$), was determined across all frequencies and recorded as the mean (maximum) coherence value for a particular time window m , IMF level j , and channel pair q . This coherence value is therefore representative of the coherence between a particular channel pair at a specific IMF level for one 16-second time window.

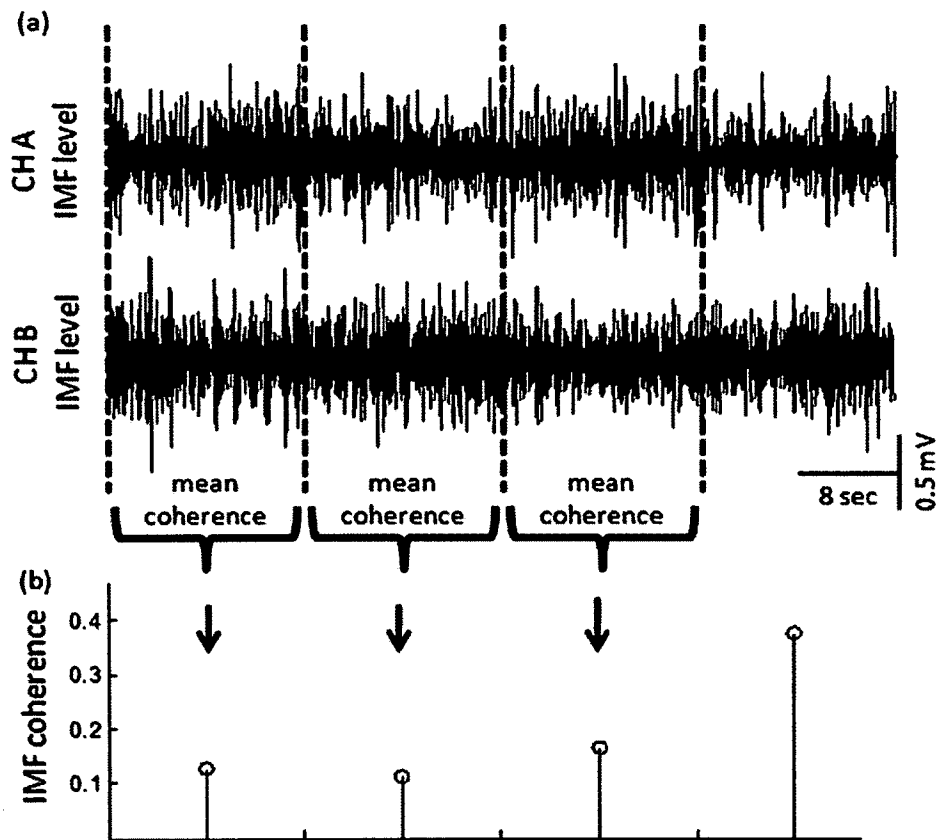


Figure 3.3: Time-windowed representation of mean IMF coherence data. (a) A single IMF level for four consecutive time windows is shown for a pair of electrode recording channels. Vertical dashed lines indicate the start/end of each 16-second time window. (b) Concurrent IMF time windows are used to determine a channel pairs mean coherence, each producing a single, time-windowed representation of mean IMF coherence information.

3.5.2 Cross-Correlation

The cross-correlation can appropriately provide an indication of time-shifted features of similarity between two signals. The normalized cross-correlation ($\rho_{xy}(\tau)$) is bounded as $[-1, 1]$ and is shown by

$$\rho_{xy}(\tau) = \frac{\gamma_{xy}(\tau)}{\sigma_x \sigma_y}, \quad (3.16)$$

where γ_{xy} is the cross-covariance of $x(t)$ and $y(t)$ such that

$$\gamma_{xy} = E[(x_t - \mu_x) E(y_t - \mu_y)], \quad (3.17)$$

and σ represents the standard deviation and τ represents the time-lag. For the purposes of this study and to limit the influence of significant time delay which may cause inappropriate associations of neuronal activity between spatial regions, the maximum lag evaluated for the signals was five. Since the cross-correlation can fall within $[-1, 1]$ and the directionality of the signals is not of interest, $|\rho_{xy}|$ was used to determine the mean and maximum cross-correlation data for each 16-second time window. The MATLAB command used to determine the normalized cross-correlation was `xcorr` with the 'coeff' option enabled.

3.5.3 Correlation Coefficient

The correlation coefficient (r_{xy}) is a summarizing value of linear dependence between x and y based on the zeroth lag cross-correlation, and is similar to Equation 3.16 as shown by

$$r_{xy} = \frac{\gamma_{xy}}{\sqrt{\gamma_{xx} \gamma_{yy}}}. \quad (3.18)$$

Like the cross-correlation, the correlation coefficient is a bounded value within $[-1, 1]$. The output from the MATLAB command `corrcoef` is a symmetric 2×2 matrix (including the autocorrelation coefficients of x and y on the diagonal) providing the correlation coefficient of x and y in the off-diagonal.

3.5.4 Synchronized Phase-Locking Value

Phase-locking synchrony, or synchronized phase-locking value (SPLV), uses the Hilbert transform to determine the instantaneous phase of the signal contained in the 16-second time window at a particular IMF level. Following the scale separation by the EEMD algorithm, the Hilbert transform of the decomposed data for each intrinsic mode function is much better behaved. The synchronized phase-locking value is determined by

$$SPLV = \left\| \frac{1}{N} \sum_{n=1}^N e^{i[\phi_1(t) - \phi_2(t)]} \right\|, \quad (3.19)$$

where N is the number of data points and ϕ_1 and ϕ_2 are the instantaneous phases for each signal as determined from the Hilbert transform result. The SPLV value range is $[0, 1]$, where a value of 0 indicates signals with completely independent phases and a value of 1 indicates signals with a constant phase-lag.

3.6 Measure Data Smoothing

Following the computations for the measures as described above, a 20-point running average was used to produce a smoothed data window of 5 minutes 20 seconds (i.e., 20 data points times the 16-second length of each time window). A 5-minute time window is consistent with the extensive review of numerous measures by Mormann

et al. [38] as well as the enhanced feature separation between preictal and interictal dynamics as discussed by Mirowski *et al.* [87] and Netoff *et al.* [104]. This rectangular smoothing window provides a robust approach for minimizing transient influences of local oscillations and for representing more noteworthy general, though still short-term, effects or trends. While a rectangular smoothing window may introduce ripples, these ripples should not affect subsequent analyses. The smoothed data for each of the measures is hereafter referred to as indicated by Table 3.3, using a generic reference to any of the measures as IMF- x . A sample representation of the relation between IMF coherence data and IMF-Coh is shown (Figure 3.4).

Table 3.3: Naming convention for smoothed 20-point moving average data based on each synchronization measure.

Measure	Name of Smoothed Measure Data
Coherence	
mean	IMF-Coh
maximum	IMF-Coh _{max}
Cross-Correlation	
mean	IMF-XCor
maximum	IMF-XCor _{max}
Correlation Coefficient	IMF-CCoef
Synchronized Phase-Locking Value	IMF-SPLV

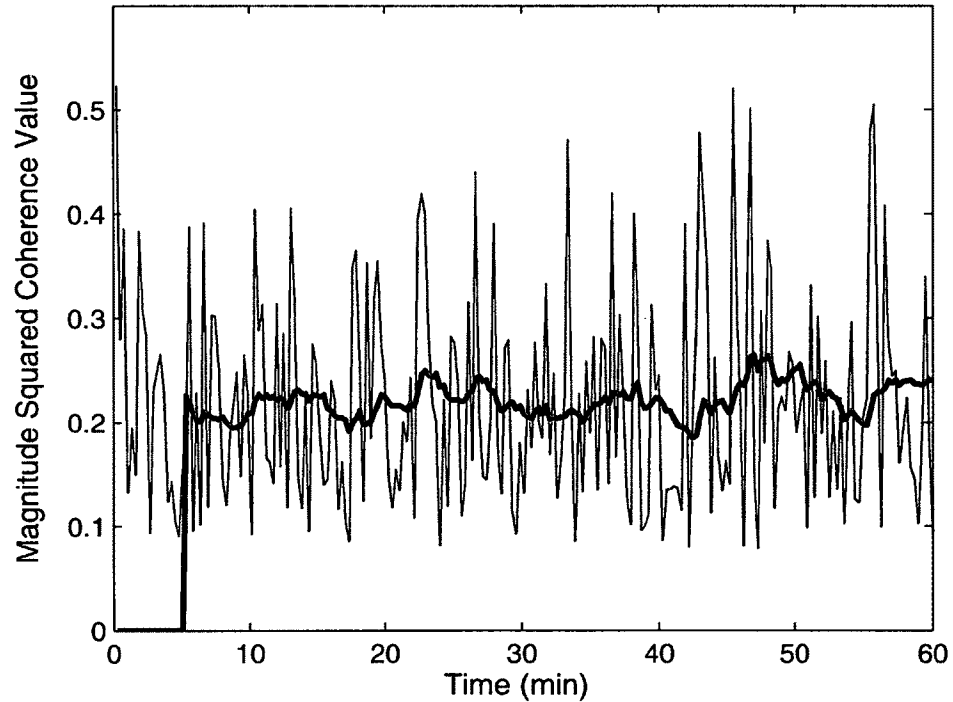


Figure 3.4: Moving average smoothing of mean IMF coherence data. This plot is an illustrative example of the mean IMF coherence data (blue thin line) smoothing using a 5 minute 20 second window to produce the IMF-Coh data (red thick line). The IMF-Coh data are used in the thresholding analyses detailed in Section 3.7. Note that the first 19 samples of the IMF-Coh data are zero and subsequently disregarded in the analyses. (One hour of preictal data is shown from patient 001, seizure 1, CH1-CH3 pair, IMF3.)

3.7 Threshold Analyses

Our hypothesis promotes that the spatial similarity, or synchronization, of brain dynamics increases during the time leading up to a seizure episode (i.e., during the preictal period). It is unclear if the state changes progressively toward seizure activity or, possibly, intermittently transitions between preictal and interictal dynamics prior to a seizure event. Using a straightforward threshold approach relaxes the requirements for identification of an upcoming seizure when applied to a more strict “progression” scenario and, thus, becomes inclusive of the “intermittent” case. With the relatively large smoothing window, a single preictal IMF- x value exceeding the threshold derived from interictal IMF- x data is considered here to be important within the context of seizure identifying dynamics. This less-constraining approach may prove to be a beneficial way of viewing and identifying seizure development, considering the number of epilepsy types and origins as well as broad variety in seizure manifestation of interpatient and inpatient episodes.

3.7.1 Statistical Training, Validation, and Testing

A statistical training, validation and testing method using threshold analysis was employed to identify differences in the IMF- x between interictal and periictal data. The first six (6) hours of interictal data for each patient were used for the statistical training and validation. The training data set consisted of alternating 30-minute blocks (three hours total) of the interictal IMF- x information from each patient. The standard deviation (σ) of the IMF- x training data at each IMF level was calculated and used as the basis for determining the IMF- x thresholds. The

appropriate IMF- x thresholds, which were allowed to range from 2 to 5 (in steps of 0.5) times σ , were identified using the validation set consisting of the remaining three hours of IMF- x data. The criterion to determine a minimum threshold is referred to as a zero-false-positive (zero-FP) threshold method, wherein the false positive rate of seizure detection in the validation set is forced to be zero (i.e., all of the IMF- x data in the validation set is below the threshold). Patient-specific IMF- x information containing 60-minute preictal and 15-minute ictal/postictal (i.e., periictal) data were used as the test set. Seizure events were considered to be correctly detected when its IMF- x value first exceeded the lowest validation threshold meeting the zero-FP criterion (Figure 3.5). The sensitivity, or true positive (TP) rate, for each patient's test set was calculated from the ratio of correctly identified seizures to total number of tested seizures. The seizure anticipation time (maximum of 54 minutes 40 seconds, due to the smoothing parameter) was noted for each detected seizure.

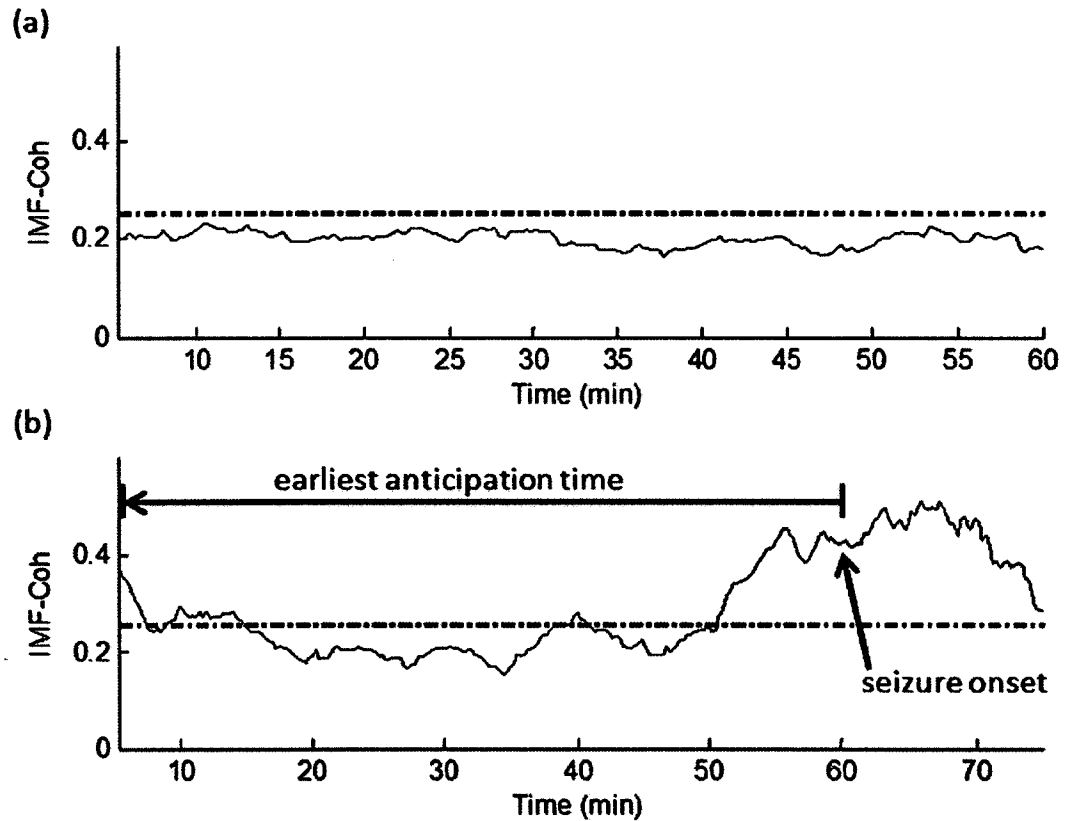


Figure 3.5: Statistical threshold training and testing. IMF-Coh data for a single channel pair is shown for a subset of interictal validation data (a) and for one set of periictal test data containing a single seizure event (b). The threshold (dot-dash lines) in the validation and test data subplots illustrates zero false positives and seizure anticipation nearly an hour before onset, respectively.

3.7.2 Performance Assessment

An optimality index [105] was modified to assess the performance of our anticipation algorithm for the IMF- x data for each channel pair. We define our anticipation optimality index (aO) as

$$aO = \frac{TP + (1 - FP)}{2} + \frac{T_a}{T_d}, \quad (3.20)$$

where FP is forced to be zero by the threshold selection method, T_d is the time of smoothed preictal data available (here, 54 minutes 40 seconds), and T_a is the average anticipation time of seizures that were identified (positive if prior to the seizure onset, negative if after). For IMF-level/channel-pair cases in which no seizure was detected, T_a was set to be zero. In this analysis, the possible range for the anticipation optimality measure is $0.23 \leq aO \leq 2$, where higher aO values indicate better sensitivity and earlier detection anticipation.

CHAPTER 4

RESULTS

4.1 Selection of Critical Intrinsic Mode Functions

The frequencies of interest in this study are considered to be greater than 1 Hz, as these contain the majority of the frequency information of the signal. Because we have used a z-score transformation on zero-meaned data, very low (offset) frequencies may not accurately represent the signal information, in any case. By selection of IMF levels 1 to 6, we can effectively eliminate very low frequencies as if by high pass filtering, but without the introduction of time delays to the data being investigated. Only a slight overlap of frequency content can be seen between pairs of IMF levels, indicating that a relatively well-attenuated amount of mode mixing is occurring (Figure 4.1).

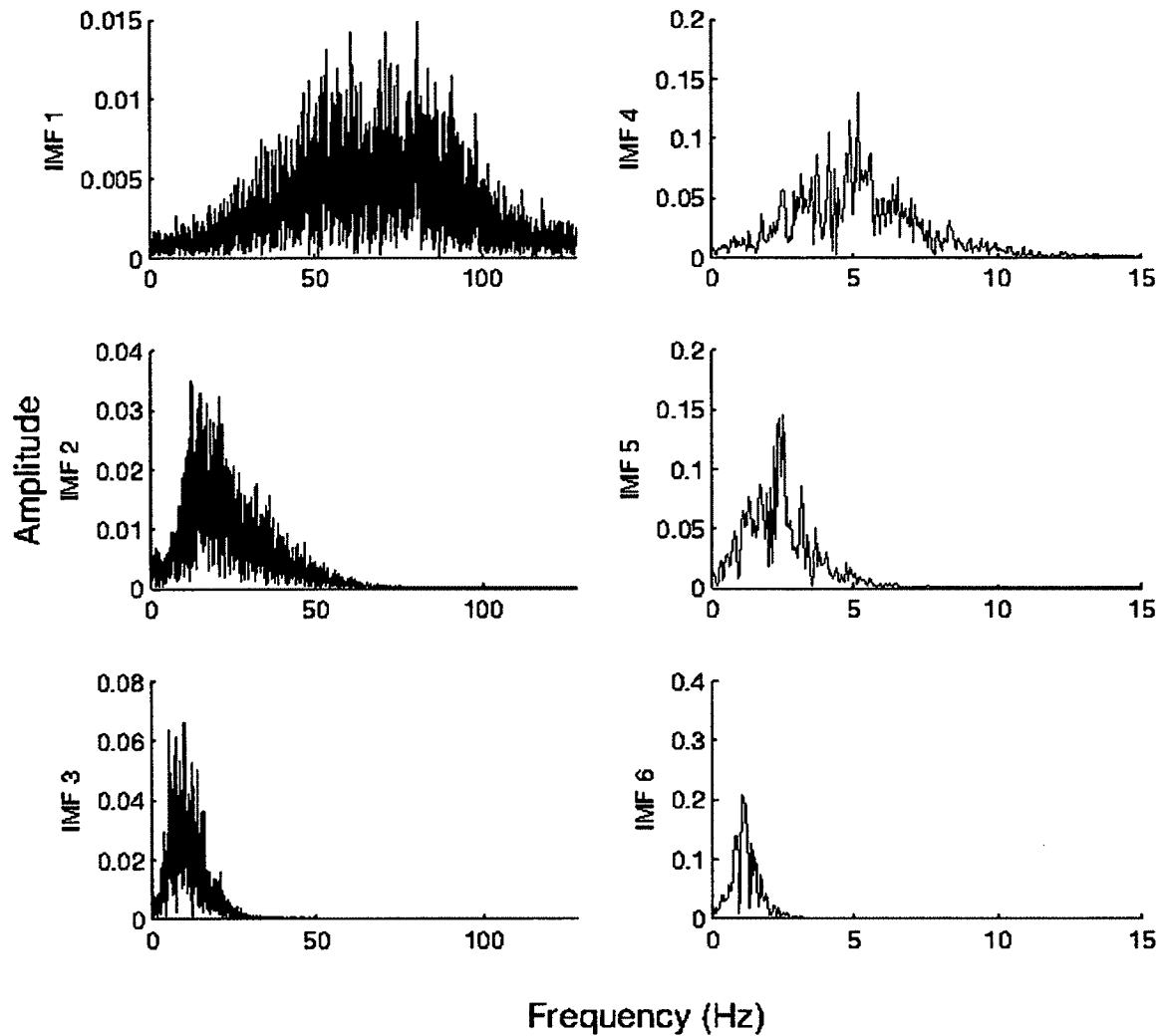


Figure 4.1: Frequency spectra of IMF levels. An example frequency analysis of the information contained at IMF levels 1 to 6 following EEMD of interictal data is shown. As IMF level increases, corresponding frequencies associated with the IMF level decrease. IMF 6 is the largest IMF level used in subsequent analyses. Example plots are generated from channel pair/16-second epoch for Patient 21 interictal data.

To gain a better understanding of the response of these synchronization measures for each patient across the IMF levels during normal interictal dynamics, the averages of the IMF measure data were calculated across all 15 channel pairs. A sample image map (Figure 4.2a) is shown for the average mean coherence interictal training information for all patients. Data for each of the patients (vertical axis) and each IMF level (horizontal axis) are shown. Blue regions represent low IMF- x values, and red regions represent high IMF- x values. The standard deviation of the average mean coherence measure is provided for additional information (Figure 4.2b). Similar images for the remaining measures can be found in Appendix A. Synchronization measures at the higher IMF levels (lower frequencies) appear to show relative consistency (i.e., limited variation) and, as expected, offer little to the analyses of this study. As such, we will not use these higher IMF levels in our subsequent analyses. We will restrict the analyses to IMF levels 1-6 which contain the frequency information of which we are most interested (i.e., $> \sim 1$ Hz),

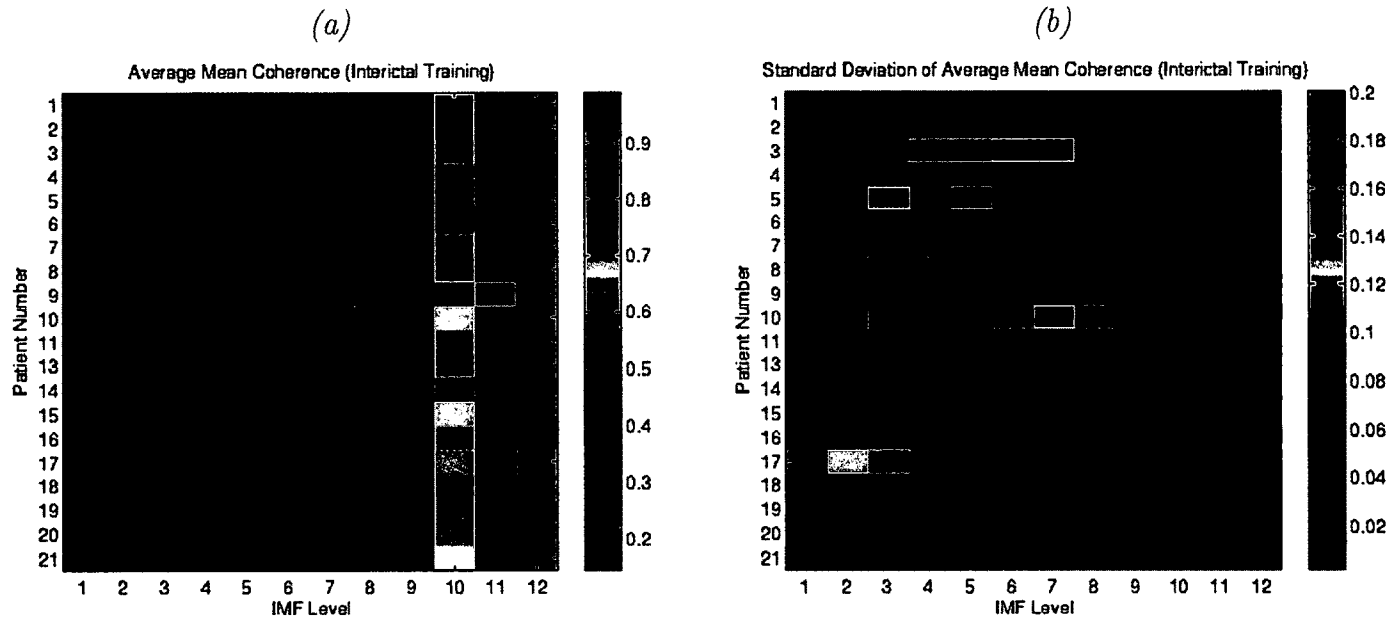


Figure 4.2: Average mean coherence and standard deviation of average mean coherence of interictal training data. Statistical information for interictal training data for one measure (mean coherence) of the six synchronization measures is evaluated. (a) The image map shows each patient's average (across the 15 channel combinations) of the mean coherence at each IMF level. Note the increased coherence measure near the higher IMF levels. Higher IMF levels represent very low frequency ($< \sim 1$ Hz) and are subsequently disregarded in the analytical approach. (b) The image map shows the standard deviation of each patient's average (across the 15 channel combinations) of the mean coherence at each IMF level.

4.2 Statistical Threshold of Synchronization Measures

The zero-FP validation approach (Section 3.7.1) was accomplished by automated selection of appropriate multiples of σ for each channel-pair/IMF-level combination in the patient's interictal validation set of IMF- x data (Figure 4.3). Shaded boxes in the figure indicate that the threshold at the given multiple of σ of the channel-pair/IMF-level combination was exceeded. A statistical threshold is determined for each channel-pair/IMF-level combination at the first multiple of σ without a false positive. Following these automated selections, the periictal IMF- x data were compared against the thresholds to determine successful identification (true positive, or TP) of a seizure event.

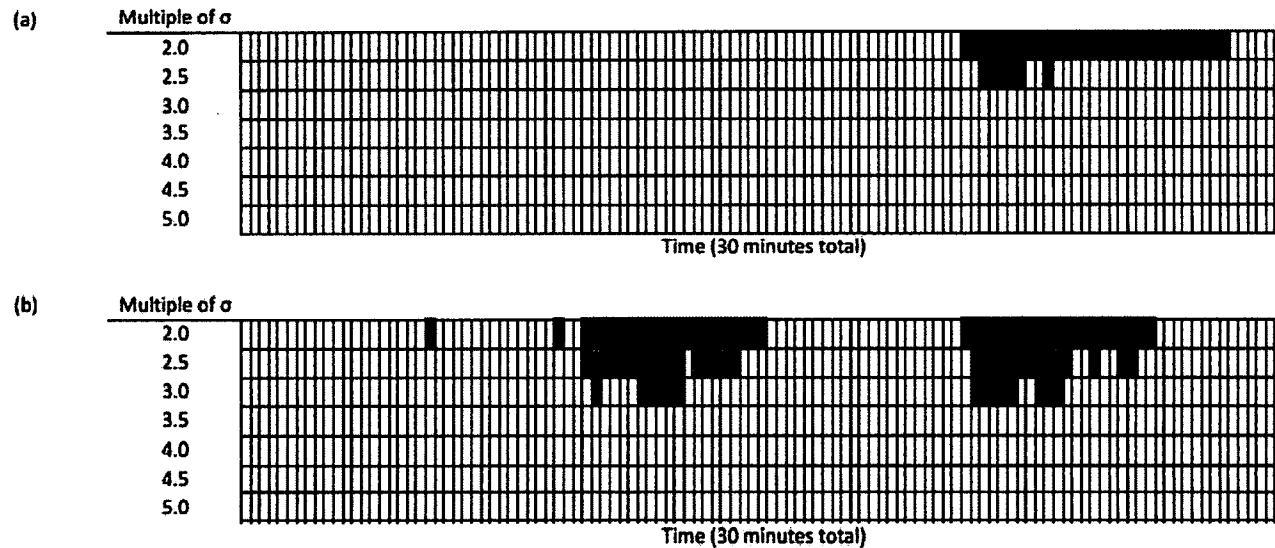


Figure 4.3: Determination of statistical thresholds using the zero-FP approach on the validation set. Shaded boxes indicate that the threshold at the given multiple of σ of the channel-pair/IMF-level combination was exceeded. A statistical threshold is determined for each channel-pair/IMF-level combination. The minimum thresholds for seizure testing in the case above are subsequently determined to be 3.0σ and 3.5σ for (a) and (b), respectively. For visualization purposes, the data shown has been preferentially selected to illustrate the method and has been truncated to 30 minutes of the 3 total hours of validation data for the patient. The figures are representative of typical IMF- x interictal data used for developing the validation thresholds. (Data are shown for IMF-Coh for patient 015, (a) CH1-CH5 pair for IMF4 and (b) CH2-CH3 pair for IMF1.)

4.3 Channel Pair Connectivity Maps

Connectivity maps were developed to indicate true positives of periictal seizure testing for channel pairings at each IMF level and for each measure (Figure 4.4 and Appendices B through G). Lines connecting representative electrodes (numbered dots, where electrodes 1, 2, and 3 in red are considered focal electrodes and electrodes 4, 5, and 6 in blue are considered extrafocal electrodes) indicate that the channel pair was successful in identifying a seizure event. Line weight indicates the TP ratio of the seizures tested (thicker lines for higher ratios). Channel pairs without connections did not identify a seizure event. The connectivity maps do not represent the time at which a tested seizure was identified as a TP, only whether or not the threshold value was exceeded.

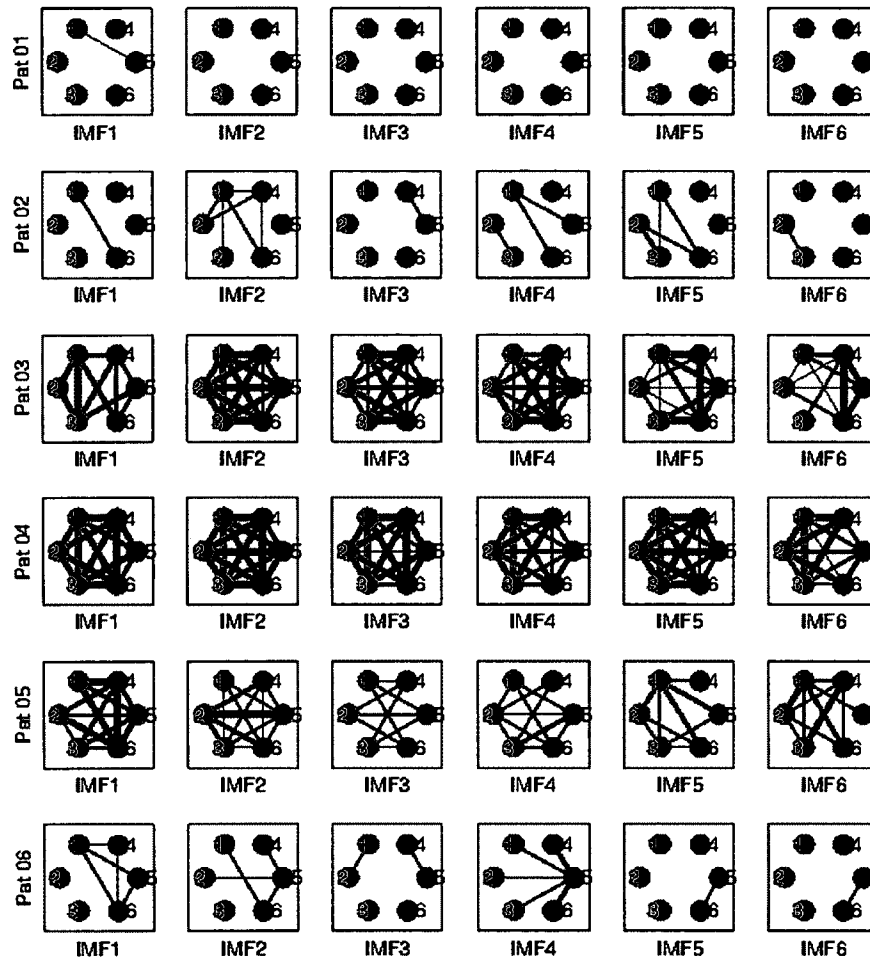


Figure 4.4: Connectivity maps for IMF-Coh measure, Patients 1 to 6. Sample connectivity maps for IMF-Coh thresholded data are shown for Patients 1 to 6 across the first six IMF levels. Focal electrodes (red) and extra-focal electrodes (blue) show channel pair success rate in seizure anticipation. The TP ratio for each patient is represented by the weight of the line connecting channel pairs. Information regarding anticipation time is not included in the plots. (A complete set of connectivity maps can be found in Appendices B through G).

Our results indicate that IMF- x data from some channel pairs distinguished between interictal and periictal dynamics. IMF- x analyses of some channel pairs anticipated none of the tested seizure events (no connectivity shown), while many others correctly identified some or all test cases. Channels and/or channel pairs associated with successful seizure anticipation at one particular IMF level did not always support presupposition of success at other IMF levels, evincing that increased levels in IMF- x measures between channels result from narrow-band preictal frequency information not present in the interictal validation data.

The connectivity maps do not show trends that can be generalized for all patients. For example, whereas IMF-1 was highly successful in Patient 4, it was generally unsuccessful in Patients 1 and 2. As such, comparison of TP ratios between measures in a patient-specific scenario may provide benefits to better understand the similarities and differences in use of these measures for individuals (Figure 4.5). Throughout the dataset, analysis for some patients (e.g., Figure 4.5) showed relatively high connectivity in all six IMF levels suggesting the potential presence of broadband information inherent to the patient-specific manifestations of the seizure events. These results indicate applicability of these IMF- x measures should be evaluated on a patient-specific basis, though specific channel pairs may be sufficient to provide good sensitivity. Similarly, consistencies amongst the IMF- x measures also imply a generalization in anticipation measures and further support the directive for patient-specific analysis.

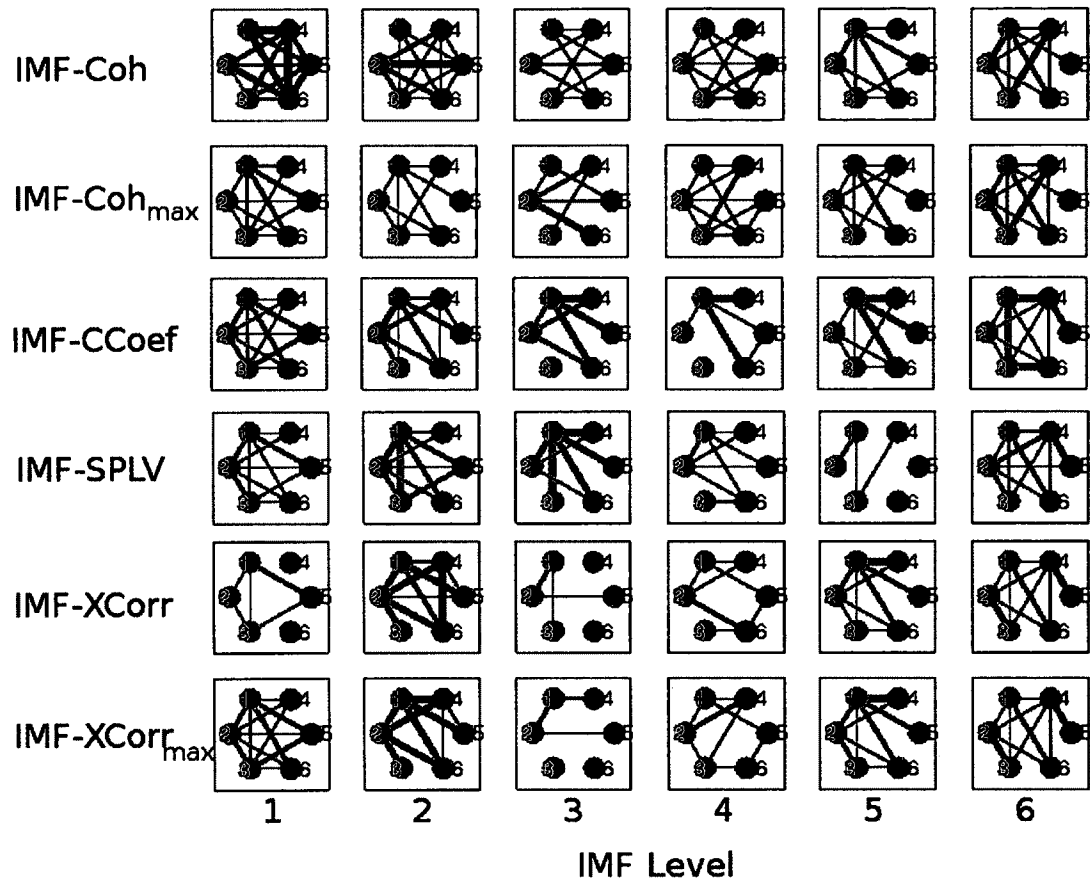


Figure 4.5: Connectivity maps for IMF- x measures (Patient 5). Connectivity maps for IMF- x thresholded data are shown for Patient 5 across the first six IMF levels. Focal electrodes (red) and extrafocal electrodes (blue) show channel pair success rate in seizure anticipation. TP ratio for each patient is represented by the weight of the line connecting channel pairs. Information regarding anticipation time is not included in the plots.

4.3.1 Ratio of IMF- x Data Above Threshold

The connectivity maps above (Section 4.3) require only a single, smoothed, IMF- x data point to exceed the threshold in order to be considered to be a TP. While the data preprocessing, smoothing, and coarse delineation of multiples of σ is intended to squelch transient signal and IMF- x measure noise, the connectivity maps may not adequately represent the efficacy of a single-point threshold method (Figure 4.6). To evaluate this limitation, a ratio of IMF- x data above threshold (raT) has been produced from the threshold testing algorithm (Figure 4.7). The highest mean raT are found within the highest frequency IMF levels (low IMF number). This observation indicates the potential benefit of IMF-level selection in the anticipation algorithm. However, relatively low channel pair mean raT values do not necessarily indicate poor performance if the benefits of more isolated high-impact channel pairs are considered. In some cases, a patient may have a limited number of high-impact channel-pair/IMF-level combinations (Figure 4.8), while another patient may have several (Figure 4.9). Furthermore, it has been shown to be difficult to ascertain whether preictal dynamics manifest themselves in a continued progression toward seizure state or by intermittent “forays” toward seizure dynamics (Section 2.1). Thus, the relative weight of the ratio above threshold (raT) values may hold limited value.

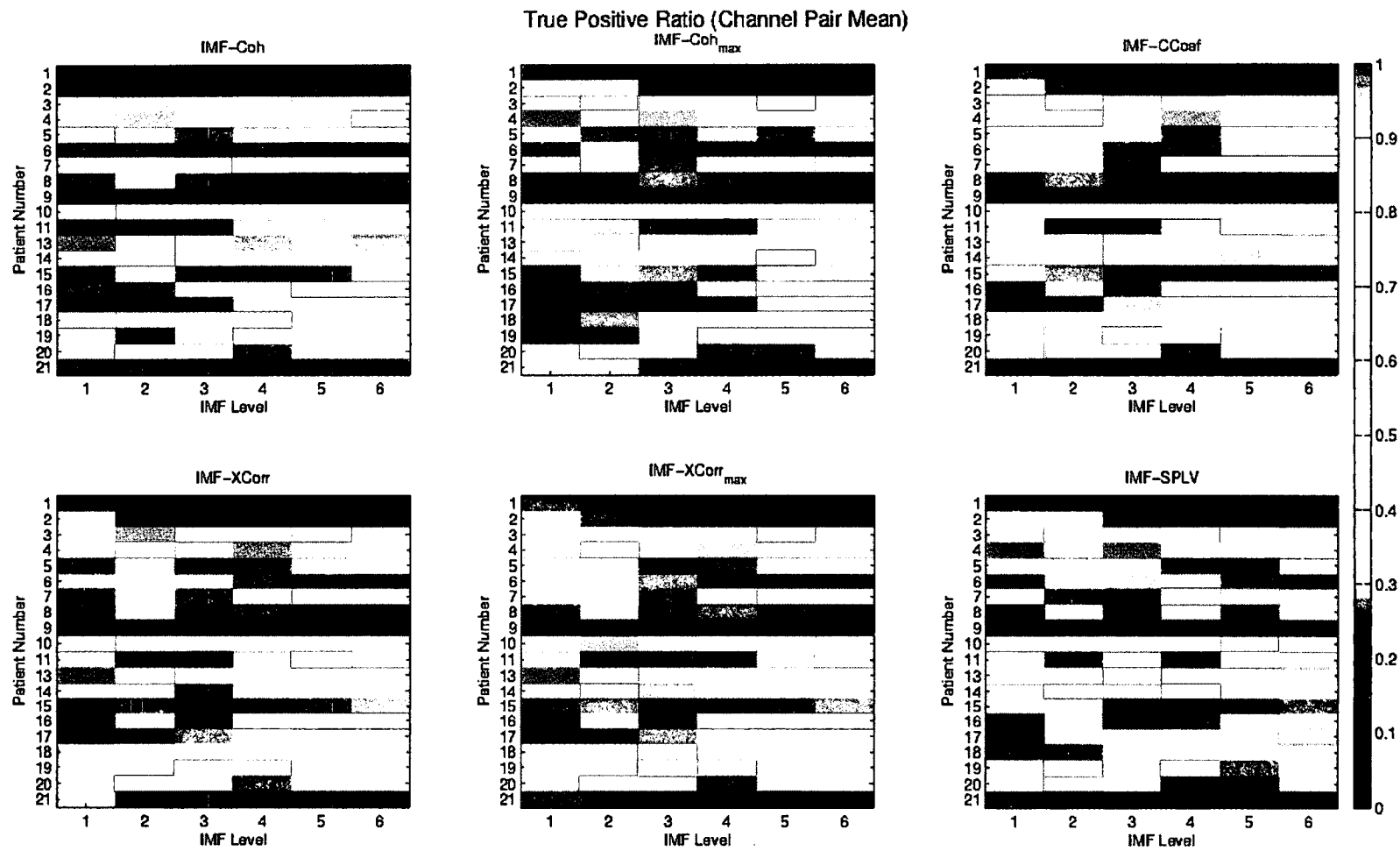


Figure 4.6: True positive ratio (channel pair mean). The true positive ratio for each patient and IMF level representing the mean TP ratio for all 15 channel pairs.

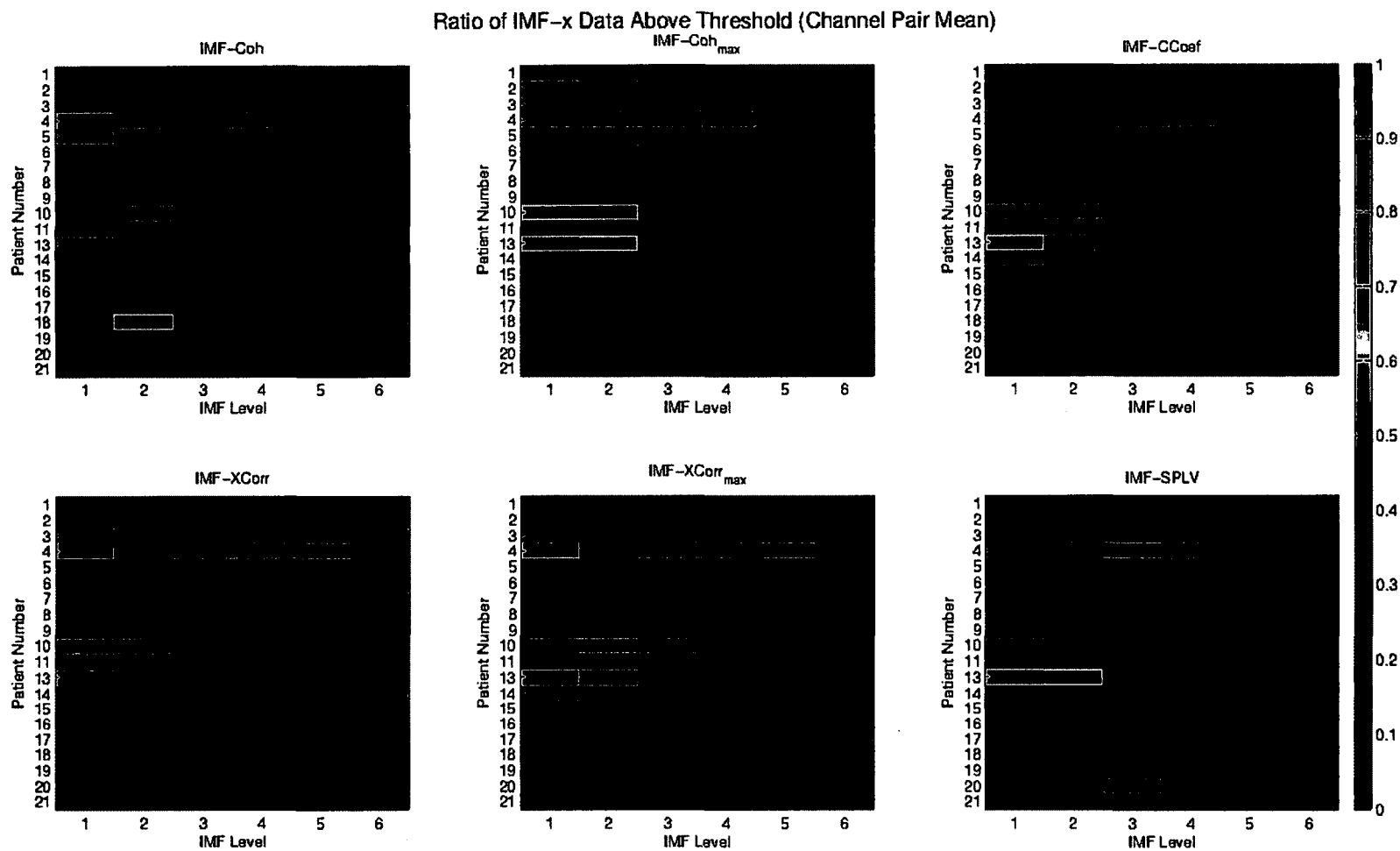


Figure 4.7: Ratio of IMF- x data above threshold (channel pair mean). Ratio of IMF- x data above threshold (raT) are shown for all patients at each IMF level. The raT mean for all channel pairs is shown.

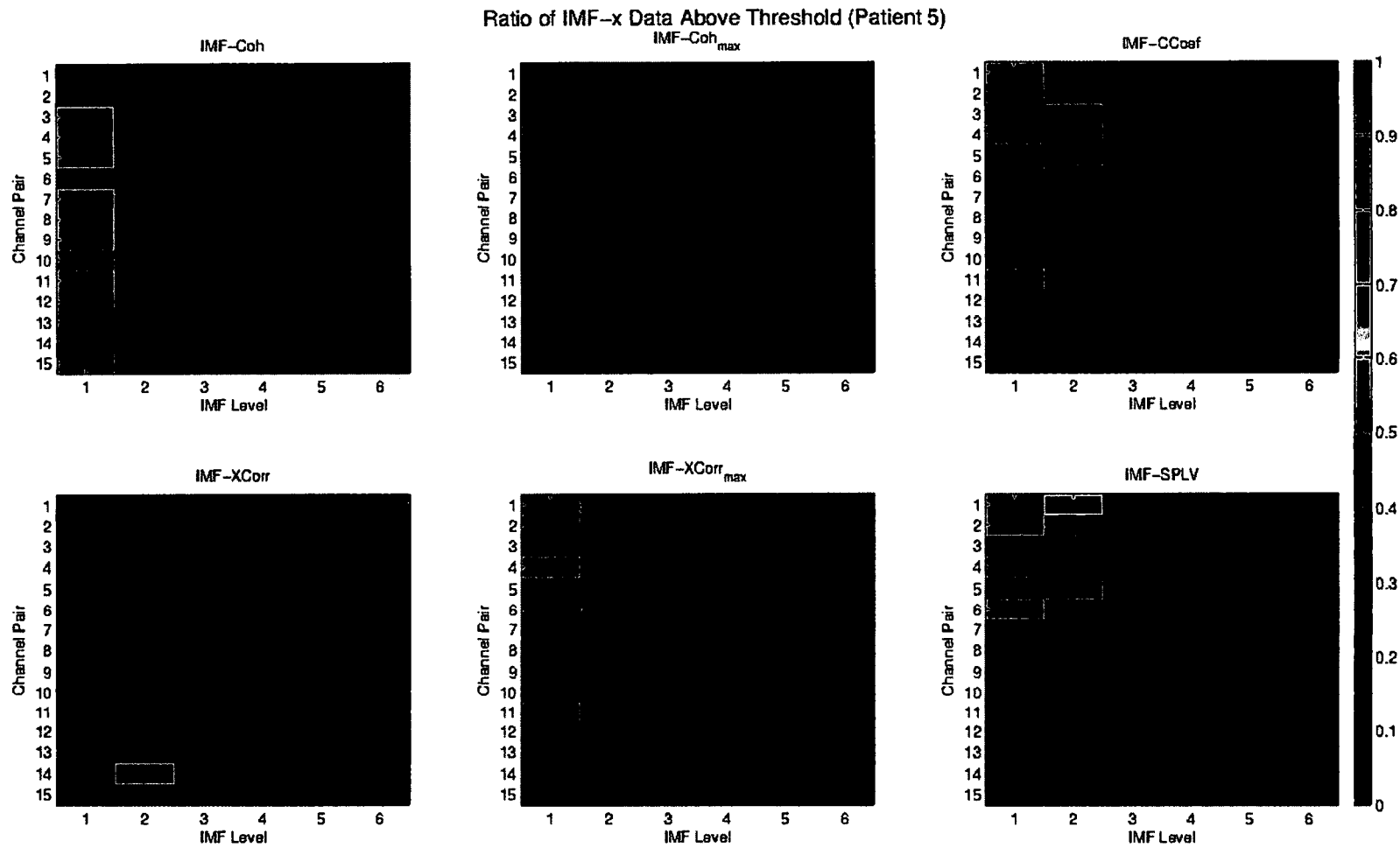


Figure 4.8: Ratio of IMF- x data above threshold (Patient 5). Ratio of IMF- x data above threshold (raT) are shown for Patient 5 at each channel-pair/IMF-level combination.

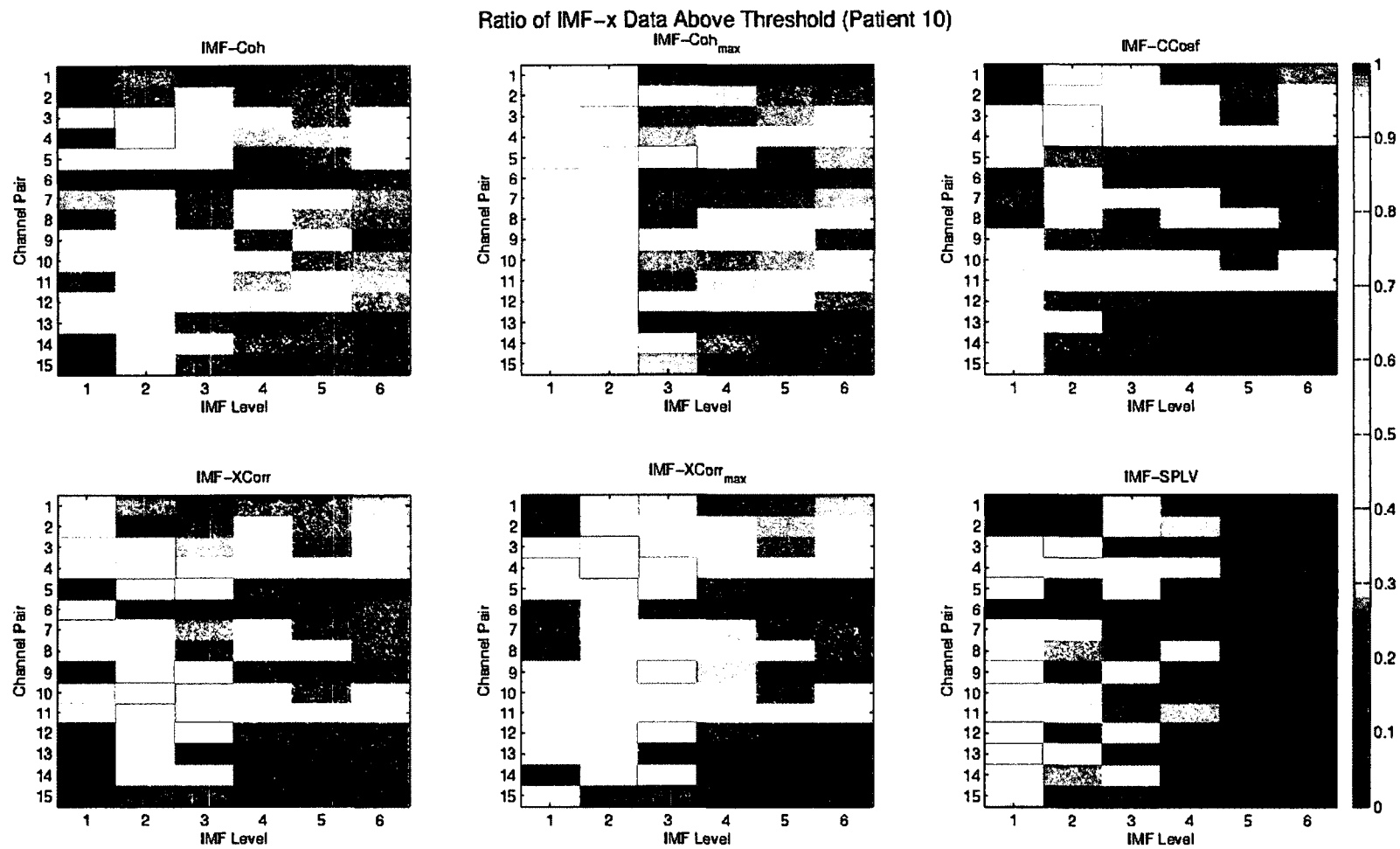


Figure 4.9: Ratio of IMF- x data above threshold (Patient 10). Ratio of IMF- x data above threshold (raT) are shown for Patient 10 at each channel-pair/IMF-level combination.

4.4 Anticipation Optimality Index

The TP ratio and raT data above do not incorporate the timing of the seizure identification in their representations. In order to better identify successful and early seizure anticipation, an anticipation optimality (aO) index is offered (Section 3.7.2). While the aO index shares a somewhat similar pattern to the TP ratio due to its reliance on the ratio in its calculation, the separating factor is the inclusion of the anticipation time. The aO index provides a unified indicator of the sensitivity and anticipation window available for IMF- x testing and was used to obtain a general estimation of performance (Figure 4.10), in addition to identifying high-impact pairings of channels (Figure 4.11).

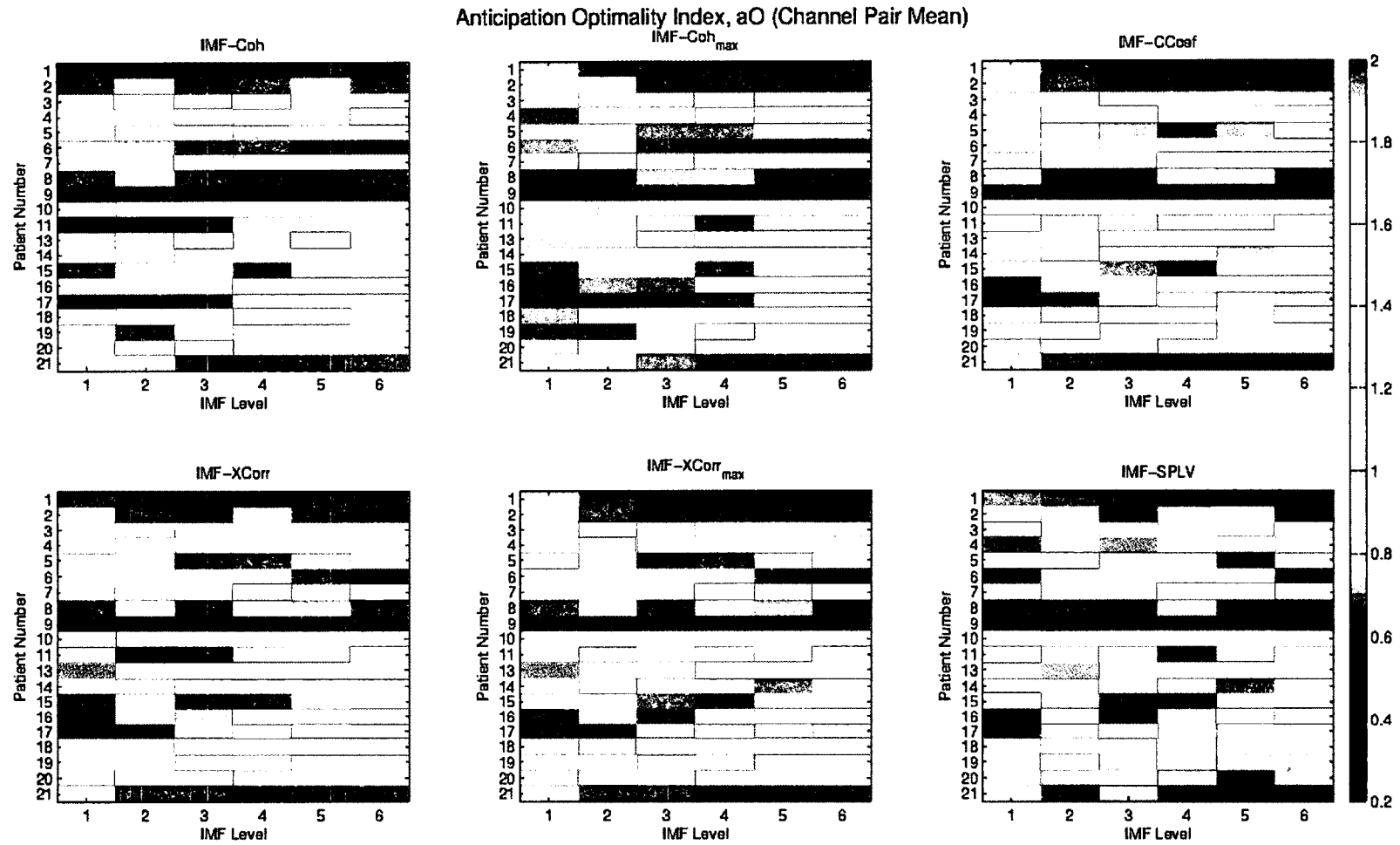


Figure 4.10: Anticipation optimality index (channel pair mean). The mean anticipation optimality (aO) indices for all channel pairs are shown at each IMF level for each patient's IMF- x measure.

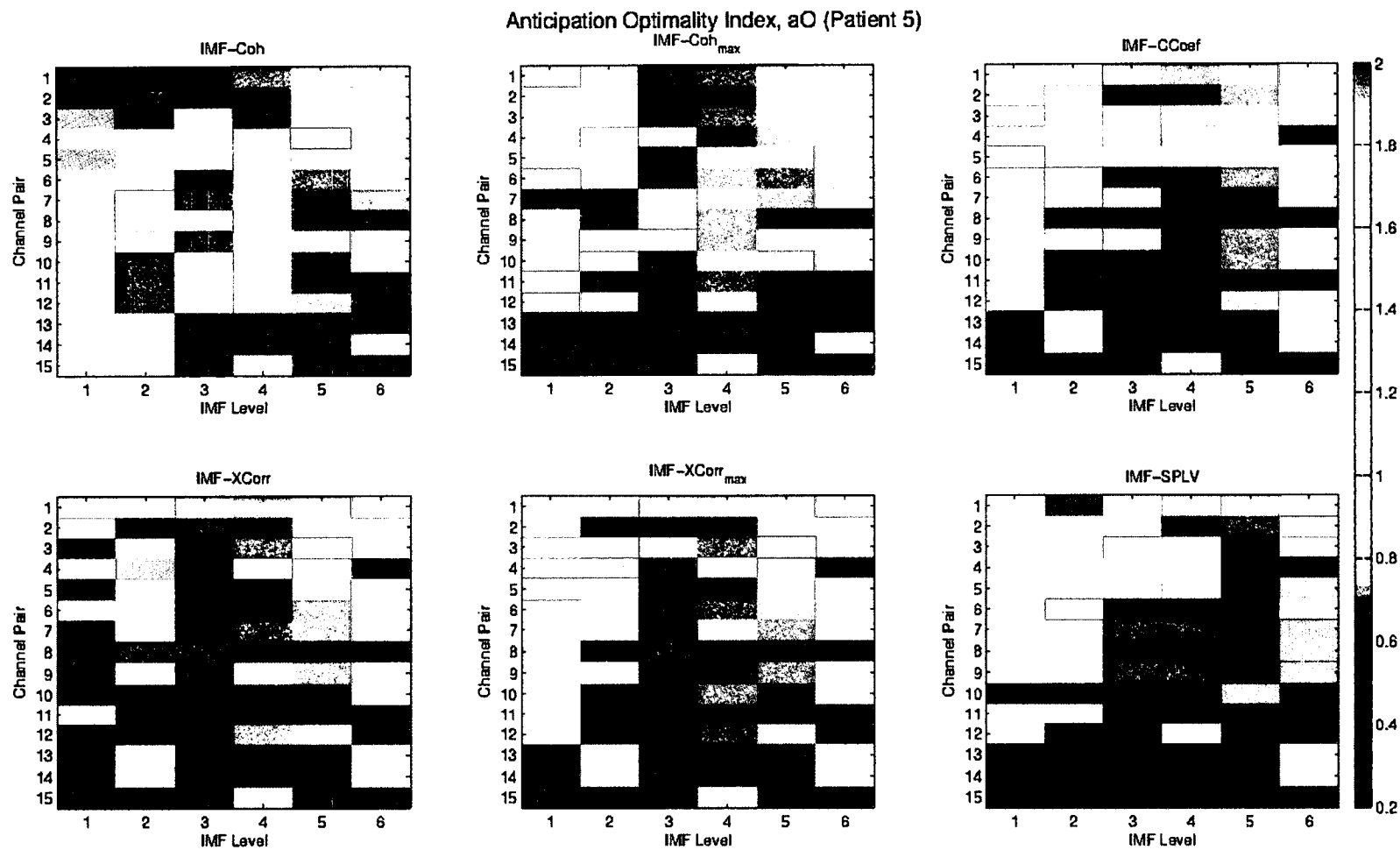


Figure 4.11: Anticipation optimality index (Patient 5). Anticipation optimality (aO) indices for Patient 5 are shown for each channel-pair/IMF-level combination in their respective IMF- x measure.

We found long anticipation times for the majority of the correctly detected seizure events. Channel pairs showing perfect TP rates had earliest anticipation times ranging within 30 to 53 minutes prior to seizure onset almost exclusively. While certain cases had shortened anticipation times, they often remained on the order of several minutes prior to the seizure onset. For the patient data providing higher anticipation performance, the aO index values are often considerably high for many channel-pair/IMF-level combinations (Figure 4.12). In several cases, the maximum aO index value was exhibited by multiple channel pairs at the same IMF level.

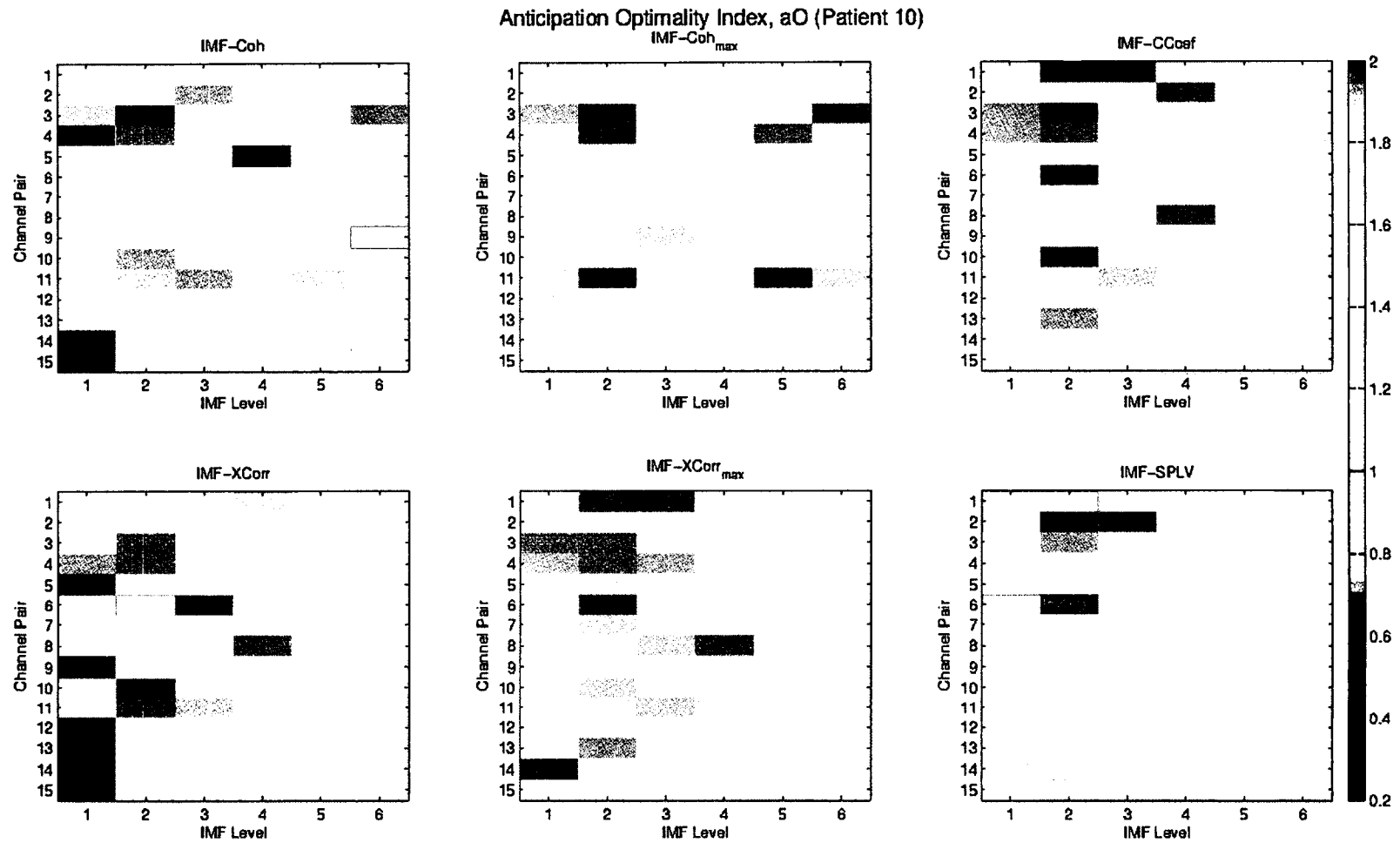


Figure 4.12: Anticipation optimality index (Patient 10). Anticipation optimality (aO) indices for Patient 10 are shown for each channel-pair/IMF-level combination in their respective IMF- x measure.

4.5 Generalization Based on Focal Origin

Seizure anticipation algorithms have typically been used in a patient-specific scenario. However, in certain scenarios, particular types of focal epilepsies lend toward potential generalizations of algorithms. The University Hospital of Freiburg Epilepsy Center Patient Database (Table 3.1) includes patients with focal epilepsies having hippocampal (H) origin, neocortical (NC) origin, or a combined (H/NC) origin. An analysis across the patient database was used to determine if the TP ratio and the aO indices show a statistical difference based on seizure origin. A Kruskal-Wallis (K-W) test (`kruskalwallis` in MATLAB) was used to produce notched box and whisker plots, as well as p values, for the different categories of seizure origin (Figure 4.13). The results of the K-W test indicate that, indeed, there is a statistical difference in the successful identification of seizure events by the algorithm when seizure origin is considered. The proposed algorithm and methodology shows the highest sensitivity for the anticipation of seizure events of hippocampal origin.

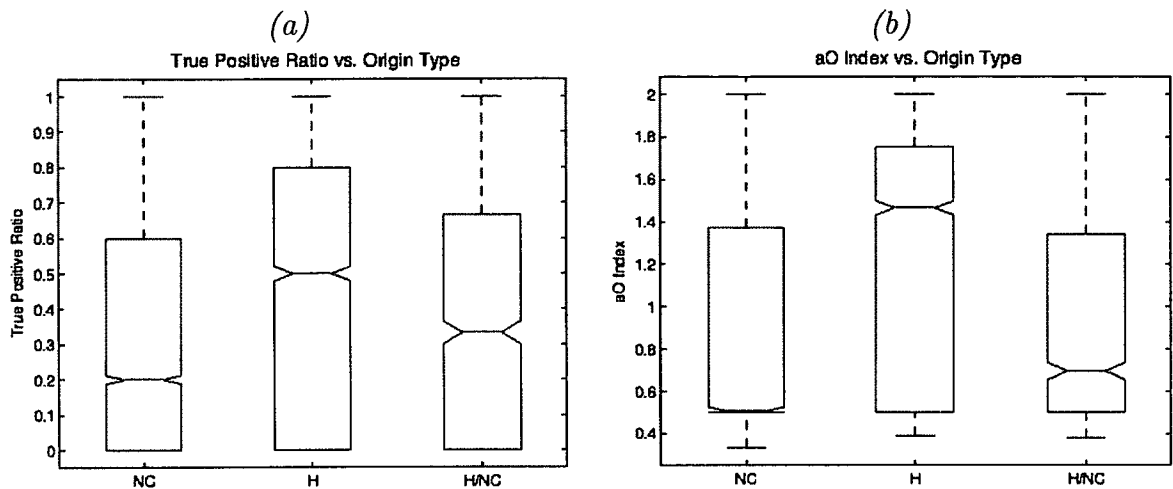


Figure 4.13: True positive ratio and anticipation optimality index versus seizure origin type. Kruskal-Wallis categorical test was used to generate notched box and whisker plots of the TP ratio (a) and the *aO* index (b) versus the seizure origin. The hippocampal (H) category was determined to be statistically different ($p < 0.01$) by the K-W test and showed significantly higher mean rank than the other two categories in both performance assessments (a) and (b). Implications of this statistical difference encourage the use of the proposed seizure anticipation algorithm in selective epilepsies. (NC = Neocortical, H = Hippocampal, H/NC = Hippocampal/Neocortical)

4.6 Patient-Specific Generalizations

Since seizures often manifest differently from patient to patient, a patient-specific approach is appropriate and more meaningful than broader generalizations across the patient database. As such, comparisons related to the IMF- x measure, channel pair type and IMF level are analyzed using the Kruskal-Wallis categorical test to determine the influence of these variables at the individual patient level. While it is not expected that all patients will exhibit similar statistical characteristics, potential trends may be elucidated.

4.6.1 IMF- x Measure

Statistical differences in the mean ranks of the TP Ratio and aO index for each IMF- x measure evaluated are examined. For some patients, no significant difference was found in the seizure anticipation capability of the six IMF- x measures (Figure 4.14), while for others, at least one measure's performance was statistically significant (Figure 4.15). Although large p -values indicate a lack of statistical difference, the overall generalization of whether or not particular IMF- x measures are most appropriately applied for a specific patient may be skewed by an overall poor anticipation performance. The K-W test only seeks one category with a significant difference as compared to the other categories, so even in the instance of small p -values, a majority of IMF- x measures may perform similarly. Given the trend across the patient performance results (Figure 4.15), a coarse assessment may be made that the choice of IMF- x measure holds less importance in the seizure anticipation algorithm.

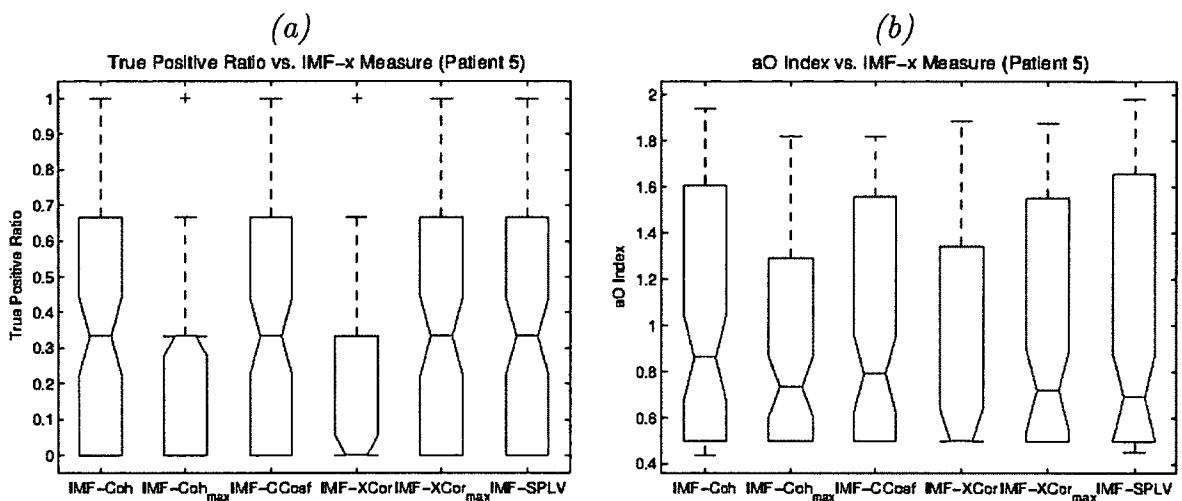


Figure 4.14: True positive ratio and anticipation optimality index versus IMF- x measures (Patient 5). Kruskal-Wallis categorical test was used to generate notched box and whisker plots of the TP ratio (a) and the aO index (b) against the IMF- x measures evaluated in this study for Patient 5. No category of the six measures evaluated induces a statistically different mean rank in either case ((a) or (b)) for this patient (p -value can be referenced in Figure 4.15).

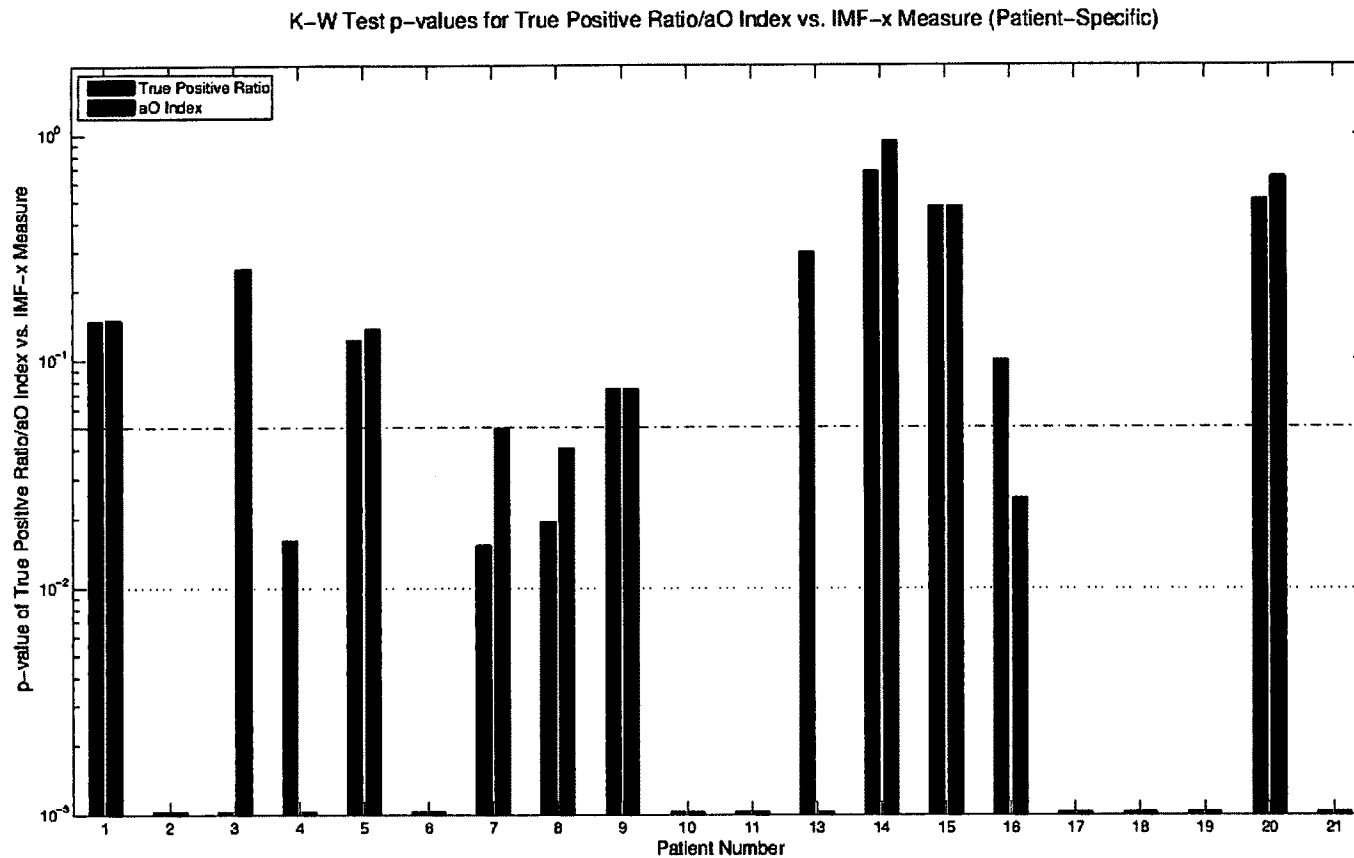


Figure 4.15: Kruskal-Wallis categorical test for IMF- x measures. Kruskal-Wallis test was used to compare the TP ratio and the aO index against the IMF- x measures evaluated in this study. The p -values for each patient's pair of K-W tests is shown. The red (dotted) line indicates a statistical level of 0.01, while the blue (dash-dot) line indicates the statistical level of 0.05. Plotted p -values greater than a given statistical level indicate a lack of statistical difference in the mean ranks of all IMF- x measures tested.

4.6.2 IMF Level

A comparison between the influence of IMF levels on the TP Ratio and aO index was made with the K-W test in the patient-specific case (Figure 4.16). Sample results from patients 5 and 10 are also shown (Figure 4.17) to illustrate the relatively large variations in the scope of the performance data while statistical difference is maintained for at least one IMF level. Despite the performance data variation amongst patients, the K-W test results indicate that the underlying signals represented by performance results within the context of each IMF level should be considered in a patient-specific manner. IMF levels may directly relate to patient-specific, limited-bandwidth, pre-seizure dynamics associated with particular manifestations of the seizure type and evolution.

K-W Test p -values for True Positive Ratio/ aO Index vs. IMF Level (Patient-Specific)

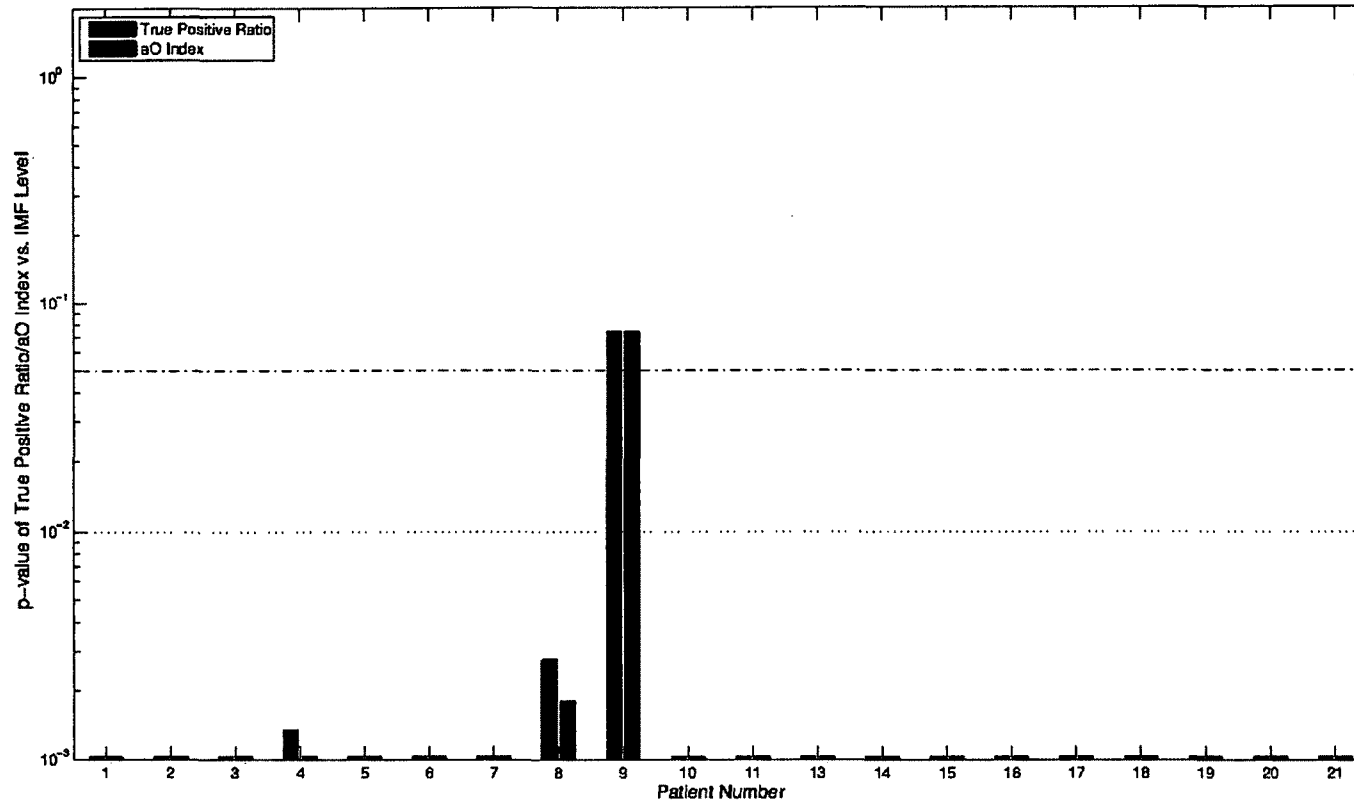


Figure 4.16: Kruskal-Wallis categorical test for IMF levels. Kruskal-Wallis test was used to compare the TP ratio and (aO) index against the first six IMF levels. The p -values for each patient's pair of K-W tests is shown. The red (dotted) line indicates a statistical level of 0.01, while the blue (dash-dot) line indicates the statistical level of 0.05. Plotted p -values smaller than a given statistical level indicate a statistical difference in the mean ranks of at least one of the six IMF level's performance data. Each patient, except for Patient 9 where no TP was identified, showed at least one statistical difference when comparing the six IMF levels.

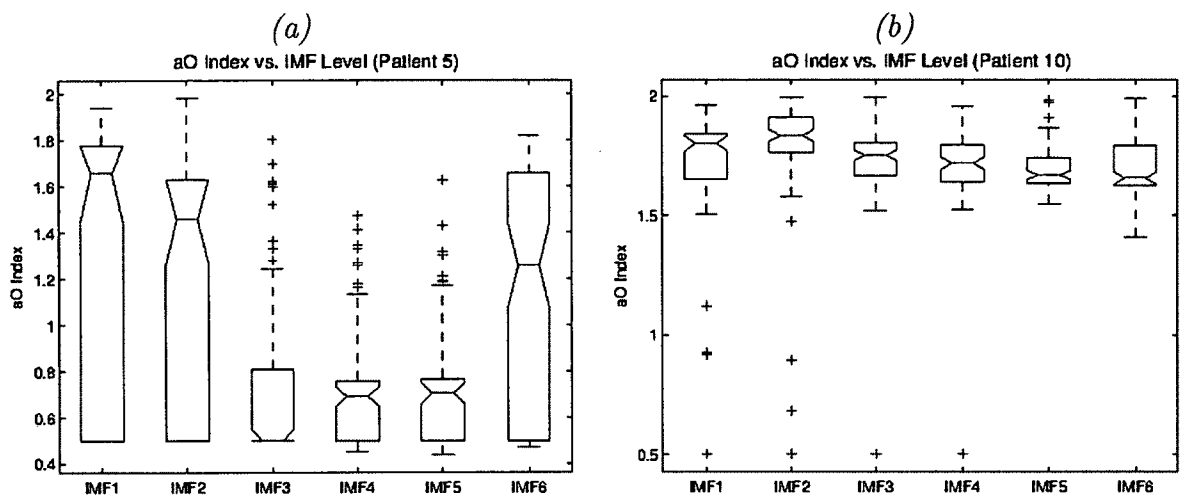


Figure 4.17: Anticipation optimality index versus IMF level (Patients 5 and 10). Kruskal-Wallis categorical test was used to generate notched box and whisker plots of the aO index against IMF levels 1 to 6 for Patients 5 (a) and 10 (b). Results of the K-W test indicate at least one statistically different IMF level ($p < 0.01$) for both patients.

4.6.3 Channel Pair Type

Connectivity maps suggest the presence of high-impact channel pairs for use in anticipation algorithms. However, generalization of channel pairings by grouping the electrode pairs into three types, focal-focal (f-f), focal-extrafocal (f-e), and extrafocal-extrafocal (e-e), could provide information for preferential selection and/or surgical placement of channel pairs. Using the Kruskal-Wallis test, the three channel pair types were analyzed against performance results (Figure 4.18). In over half of the patients, performance data were statistically different for at least one channel pair type. No noteworthy, identifying characteristics in the electrodes' form (grid, strip, or depth), placement, or spatial interrelation were found for the patients with statistically similar ($p > 0.01$) performance results.

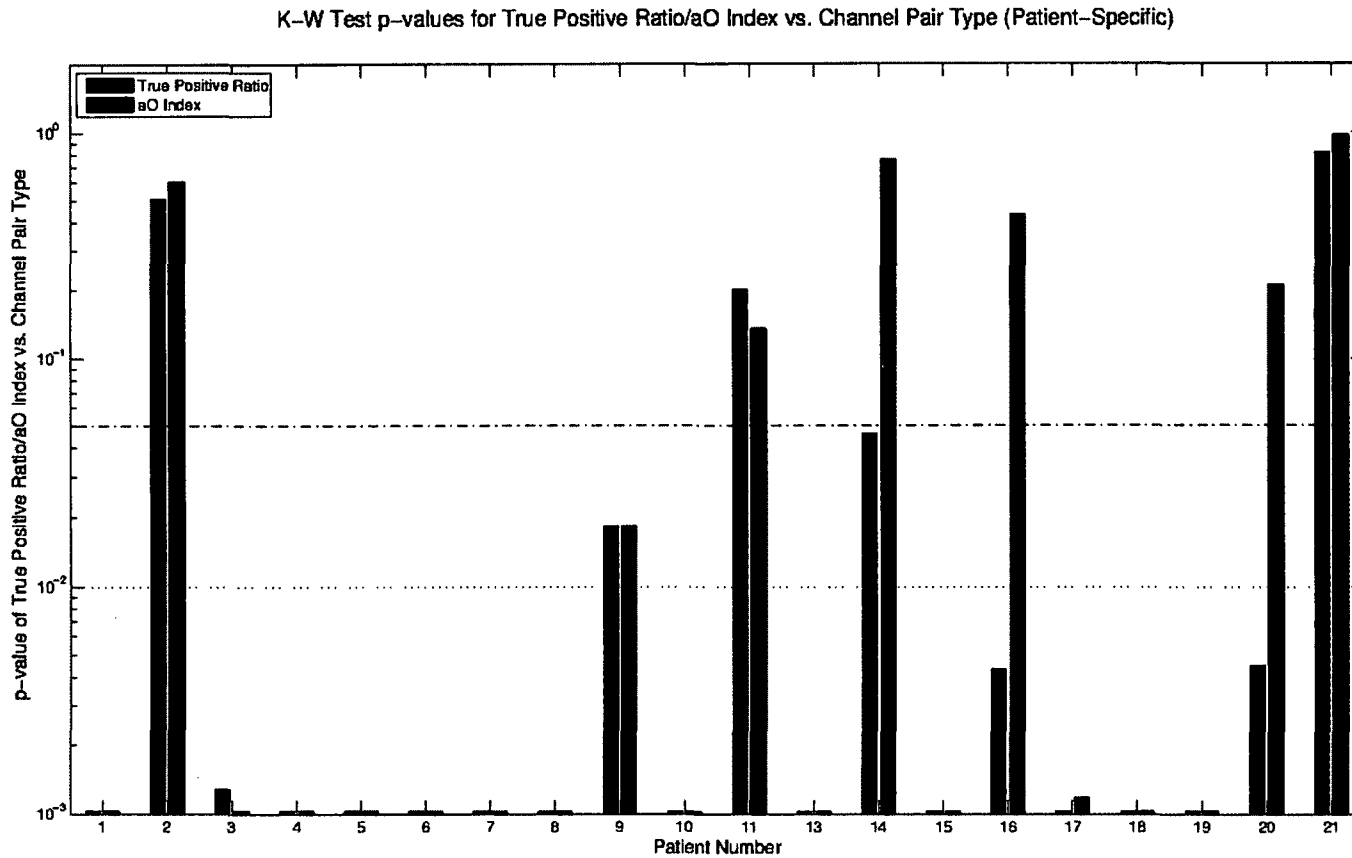


Figure 4.18: Kruskal-Wallis categorical test for channel pair type. Kruskal-Wallis test was used to compare the TP ratio and (aO) index against the electrode pairing type: focal-focal, focal-extrafocal, and extrafocal-extrafocal. The p -values for each patient's pair of K-W tests is shown. The red (dotted) line indicates a statistical level of 0.01, while the blue (dash-dot) line indicates the statistical level of 0.05. In over half of the patients, performance data was statistically different for at least one channel pair type.

CHAPTER 5

DISCUSSION

Our results suggest that intrinsic mode function synchronization measures (IMF- x measures) may provide a useful approach for patient-specific seizure anticipation. In many cases, periictal dynamics were successfully identified by one or more channel-pair/IMF-level combination(s) using the zero-FP threshold outlined earlier (Section 3.7.1). High-impact channel-pair/IMF-level combinations may provide benefit in patient-specific algorithms when preferentially selected. A modified anticipation optimality (aO) index is proposed as a relevant measure jointly representing sensitivity and anticipation information for comparisons in the performance of this algorithm. Statistical analyses for generalizations of anticipation performance were accomplished to identify relevant distinctions between seizure origin, IMF- x synchronization measures, IMF levels and focal/extrafocal electrode pairing type. Patients with a hippocampal seizure origin showed a higher success rate in early anticipation of seizure events in the context of our algorithm. In the patient-specific scenario, the IMF level appeared to hold the most significant categorical relation to our performance measure, indicating that the frequency bands of periictal dynamics holds highly relevant information. Similarly, the electrode pairing type showed distinctive differences in a majority of patients. We also found that for a slight majority

of patients, the synchronization measures used could be generalized such that the selection of a particular measure is not significantly important as a distinguishing factor for performance assessment.

Noise-assisted Ensemble Empirical Mode Decomposition (EEMD) was used in this exploratory analysis. This method was selected in order to better represent the true dynamics underlying the recorded intracranial electroencephalogram (IEEG) signals. Though twelve intrinsic mode function (IMF) levels were produced, we chose the first six IMFs for analysis since they contained the majority of the IEEG signal content (frequency information greater than ~ 1 Hz). Selection of these IMF levels is consistent with noted frequencies relevant to preictal dynamics as discussed in the literature [40, 101, 106, 107]. This frequency constraint does not preclude possible benefits in dynamical analysis of the very low frequency components associated with higher IMF levels. However, the potential of minor variations in the DC bias of electrode recordings could have severe effects on the resulting synchronization measures at higher IMFs. As illustrated in Figure 4.2, high IMF levels (at or above IMF8) generally have large synchronization measures and limited variation. To eliminate the potential concerns of using extreme values, we chose to disregard the upper half of the IMF levels. With a presumably more accurate representation of the true underlying signals through EEMD and retention of the majority of the information present in the signals, we believe that synchronization measures were appropriately applied.

Generalization of the IMF measure information by reduction to a single mean value for each time window, and subsequent smoothing across several time windows, allows for a meaningful comparison of trends between interictal and periictal activities.

The approximate 5-minute sliding average we have employed appears to adequately represent feature differences in IMF- x measures between normal and abnormal algorithm input data. While a wide array of lengths for moving averages have been implemented by researchers [38], our choice of an approximately 5-minute window was motivated by the enhanced feature separation observed by Mirowski *et al.* [87] and Netoff *et al.* [104]. The smoothing helps to squelch transient noise induced by cognitive tasks, but appears to retain adequate detail to identify major transitions in preictal dynamics.

We intentionally constrained the IMF- x thresholds to produce a zero FP rate. The reasons for this choice are twofold. Firstly, our preliminary analysis is limited to only about one quarter of the available interictal data for each patient. Requiring higher expectations for FP rate may offset variations in the resulting analysis of the remaining interictal data which may lead to higher FP rates in general. Future work should include training and validation of the statistical distributions for all available interictal data for each patient in order to evaluate this consideration. Secondly, use of a zero FP rate IMF- x threshold can help to circumvent potential negative effects in acute interventional therapy. By forcing a zero FP rate, the detection rates and anticipation times of ictal events may be reduced. We also utilized relatively coarse threshold steps in our analysis, which could result in underestimation of sensitivity. However, threshold tuning could be adapted to allow for higher sensitivity, though potentially at the expense of lower specificity. In a patient application, the thresholds could be easily adjusted to more accurately reflect the particular patient's seizure occurrence rate.

In recent years, some researchers have proposed the use of random predictor comparisons [27, 28, 58] to seizure prediction methods. A limitation of our zero-FP approach is in the inability to adequately compare our algorithm's results against a meaningful random predictor since we have required a false positive rate (FPR) of zero. A potential shortcoming in this exploratory study relates to the method of selection and amount of interictal (training and validation) data used. Our selection of the first six disconnection-free hours of interictal data may influence the overall FPR of the interictal validation data. The computationally expensive EEMD algorithm limited the data analyzed. This omission may result in the inclusion or exclusion of pharmacological, vigilance-state, and/or immune response influences when compared to the overall set of interictal data. These influences could skew the validation IMF- x threshold values we have determined and thus promote higher or lower sensitivity and specificity. Further validation and testing of interictal data would be appropriate and may help poise the method for a comparison with a random predictor, but is beyond the scope of this exploratory study. With regard to the computational expense of the EEMD algorithm in practical applications, we expect that a real-time application is possible through analysis of intermittent, short-time blocks (~ 5 minutes) of data.

Our results as shown by the connectivity maps (Figures 4.4 and 4.5 and Appendices B through G) are relatively consistent with the sensitivities determined by Winterhalder *et al.* [58] and Mirowski *et al.* [87]. In general, the level of interconnectivity for all IMF levels may provide a rough estimate of the applicability of intrinsic mode function synchronization measures for patient monitoring. However, even poorly interconnected plots could include high-sensitivity channel pairs which may

prove adequate in seizure anticipation analysis. Based on our statistical analysis of the relation of IMF levels to performance assessment, it may be more appropriate to view these high-impact channel pairs as coupled with particular IMF levels. If multiple, appropriately sensitive channel-pair/IMF-level combinations are present for the patient-specific level, the development of preferentially-designed anticipation algorithms is feasible. In such a scenario, an extrapolation of the patient-specific channel-pair/IMF-level high-impact combinations could employ algorithmic fine-tuning by requiring two or more true positives to be identified by these high-impact combinations. Further tuning is possible by use of weighted votes by the committee of channel-pair/IMF-level combinations. The possibilities of patient customization are far-reaching and could afford the clinician a wide variety of approaches for setting the balance of sensitivity and specificity. Certainly, the use of specified, high-impact channel-pair/IMF-level combinations would be highly individualized, and thus potentially difficult to manage, but given the current state of limited practical seizure predictive methods, it could prove beneficial to pursue.

Anticipation optimality aO indices appear useful and may aid in distinction of high-impact channel-pair/IMF-level combinations. During the trial stage of patient implementation, the aO could produce beneficial criteria from which interventional therapies or simple warning systems are selected. Further, if a particular channel-pair/IMF-level combination has data that has exceeded the threshold, matching the aO value with the alarm combination could inform the patient of a general seizure horizon, as well as a loose estimation of confidence in an impending seizure occurrence. Results from Schulze-Bonhage *et al.* [108] indicate overwhelmingly that patients

surveyed would prefer a seizure prediction device to indicate impending seizures only up to one hour prior to a seizure event. Empowering the patient with the aO measure related to the combination that has exceeded the threshold could perhaps make them more open to longer anticipation times than reported preferences from the survey. For instance, if a relatively high aO -valued channel-pair/IMF-level combination exceeds threshold, the patient may recognize and more willingly accept that a seizure is highly likely to occur sometime over a longer horizon. For a low-value aO index combination, the patient may regard an upcoming seizure to likely occur within a shorter time period, but may have less confidence in the likelihood of the seizure occurring at all. From the same study, the majority of patients are willing to forgo individualized seizure predictions and would be satisfied with an impending seizure probability type of feedback framework. Within the scope of these considerations, the aO index could be directly applicable as a long-running measure of seizure probability. Even a simple sum of the aO index values associated with multiple combinations above threshold at any given time could provide user feedback for an estimation of seizure probability. If this running sum of aO values was further compared with perhaps a minimum value, it could aid in limiting false positives (similar to the committee method above) as well as provide information of horizon time.

Patients with hippocampal seizure origins held a statistically significant ($p < 0.01$) higher aO index than patients with neocortical origins in our intrinsic mode function synchronization measure method. This higher predictability was also found by Winterhalder *et al.* [58] when they used other preprocessing and synchronization methods. While the group of individual patients selected for the dataset may be

the reason for this notable difference in performance between seizure origins, the focal origin may provide researchers with selection criteria for potential application of our seizure anticipation method. The population of the patient set undergoing the presurgical monitoring may experience exaggerated effects from seizure and pre-seizure activities as compared to other patients who have been able to control seizures with pharmacological or other interventions short of surgical resection. It is uncertain if the dataset analyzed can truly represent the “average” epilepsy sufferer. However, it is in these same non-surgically intractable patient cases that a warning system would likely be highly sought after.

At the patient-specific level, we observed that the IMF- x measures for a majority of patients did not vary in a statistically significant manner. For the patients with Kruskal-Wallis categorical test p -values less than 0.01, one or more of the six measures was statistically different from the others. It is possible that, in many of those cases, only one of the six measures was statistically different from the other five while still maintaining a very low p -value. Given that possibility and the limited number of patients with low p -values, it appears that, in general, IMF- x bivariate synchronization measures hold less importance in exhibiting distinctions in algorithm performance. This concept is fairly well-supported in the literature [27, 58].

Consideration of the channel pair types of focal-focal, focal-extrafocal, or extrafocal-extrafocal indicates that for over half of the patients there is a distinction between these pair groupings’ capability in seizure anticipation performance. Intuitively, focal-focal pairs may be expected to hold higher synchronization values than other pair types, but this is not always the case [58]. If one considers the seizure

progenerative dynamics to approximate seizure dynamics, one would expect higher synchronization between focal and extrafocal regions during the preictal state. It is still unclear what effect electrode pair type may have on seizure anticipation, but our results suggest that it may have at least some relevance in the patient-specific scenario.

The most significant difference in our categorical statistical tests appears to be the distinctions between IMF levels for seizure anticipation performance. These results are consistent with the general consensus of the importance of frequency bandwidth in the successful separation between interictal and preictal dynamics. Because of the highly individual nature of epilepsies and seizure manifestations, it is reasonable to expect that these seizure-pertinent frequency ranges may vary from patient to patient, and possibly seizure to seizure. When coupled with high-sensitivity channel pairs, this information may allow for a robust, yet selectively focused, patient-specific seizure anticipation algorithm.

CHAPTER 6

CONCLUSIONS

In this exploratory analysis, we used noise-assisted Ensemble Empirical Mode Decomposition (EEMD) of intracranial electroencephalogram data of twenty presurgical epilepsy patients as a preprocessing platform upon which to evaluate intrinsic mode function (IMF) bivariate measures for potential application in seizure anticipation. Synchronization measures of coherence, correlation coefficient, cross-correlation and synchronized phase-locking value were determined from decomposed patient data for each IMF level and electrode pair. Using training and validation interictal IMF- x data for the development of patient-specific, channel-pair/IMF-level combination thresholds, we compared periictal IMF- x data to the determined thresholds for identification of preictal and ictal dynamics. A true positive ratio of correctly identified periictal dynamics, along with a proposed anticipation optimality index incorporating both sensitivity and anticipation time, were evaluated. Statistical analyses were accomplished to identify generalizations relating the anticipation algorithm's successful performance with considerations of seizure origin, IMF- x measure, IMF level and channel pair type.

The approach outlined in this paper may be useful in the development of a seizure anticipation algorithm. It appears that certain high-impact channel-pair/IMF-level combinations can provide adequate seizure anticipation, but should be preferentially selected in a patient-specific manner. The proposed anticipation optimality index appears useful for determination of periictal-relevant intrinsic mode function levels and channel pairings, and may also provide selection criteria if evaluating patient candidacy for implementations of seizure anticipation techniques. Of the synchronization measures analyzed, it appears that generalization of these measures is appropriate for some patients, while others may require preferential selection. For the majority of patients, the electrode pairing type does hold some relevance to performance assessment values. A strong indication of IMF level dependence of anticipation performance data was shown, suggesting seizure dynamics manifest within certain frequency bandwidths. The patients with a hippocampal seizure origin show better sensitivity with our algorithm than patients with neocortical seizure origin.

APPENDIX A

**INTERICTAL TRAINING DESCRIPTIVE
STATISTICS FIGURES**

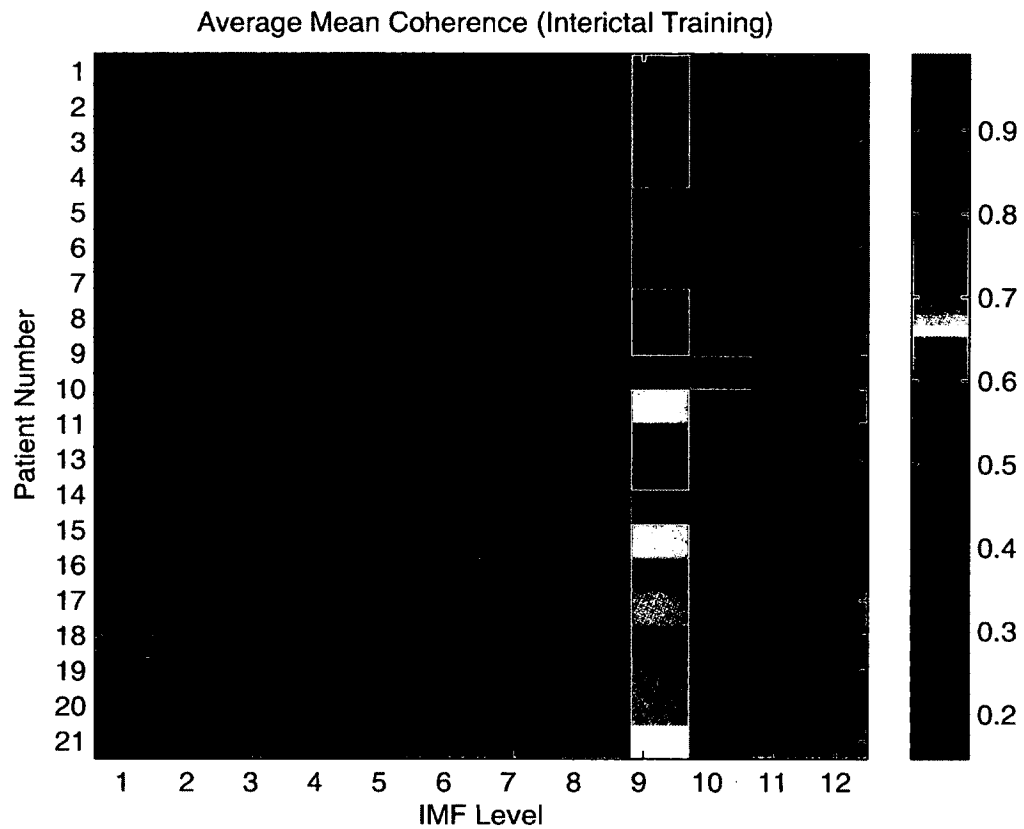


Figure A.1: Average mean coherence indicating statistical information for mean coherence measure of interictal training data. The image map shows each patient's average (across the 15 channel pairs) of mean coherence at each IMF level. Note the increasing coherence measure at the higher IMF levels. Higher IMF levels represent very low frequency ($< \sim 1$ Hz) and are subsequently disregarded.

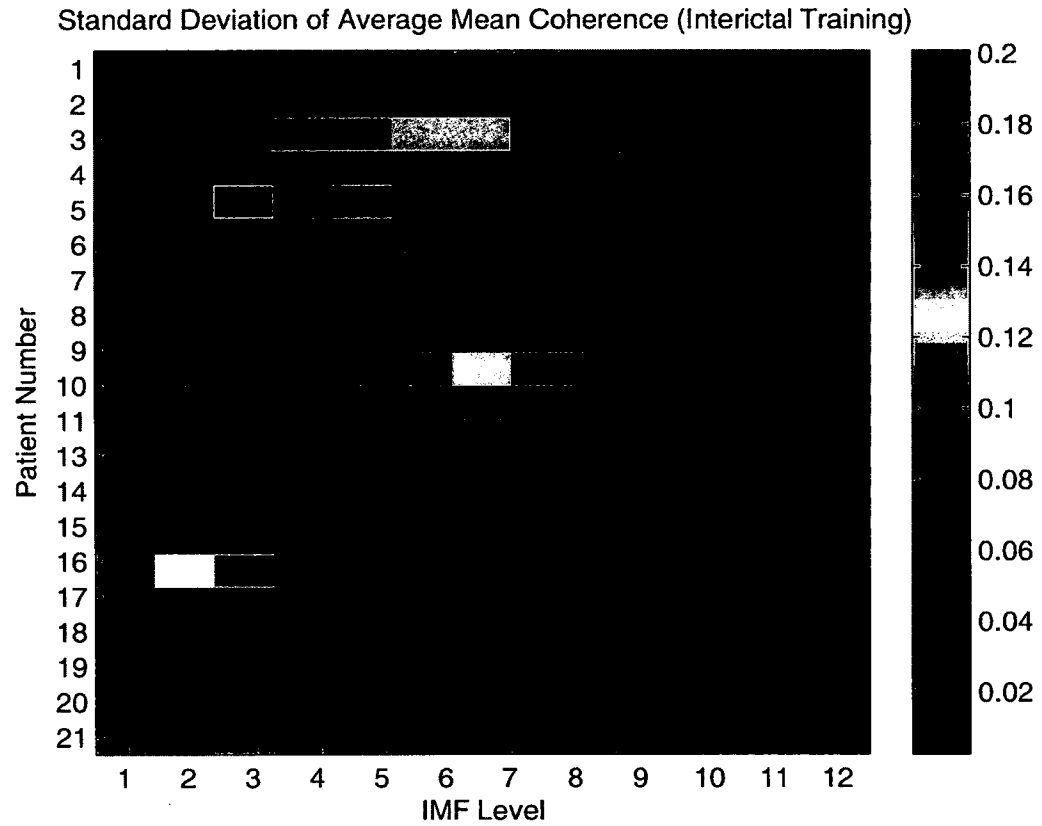


Figure A.2: Standard deviation of average mean coherence indicating statistical information for the mean coherence measure of interictal training data. The image map shows each patient's standard deviation of the average (across the 15 channel pairs) of the mean coherence at each IMF level.

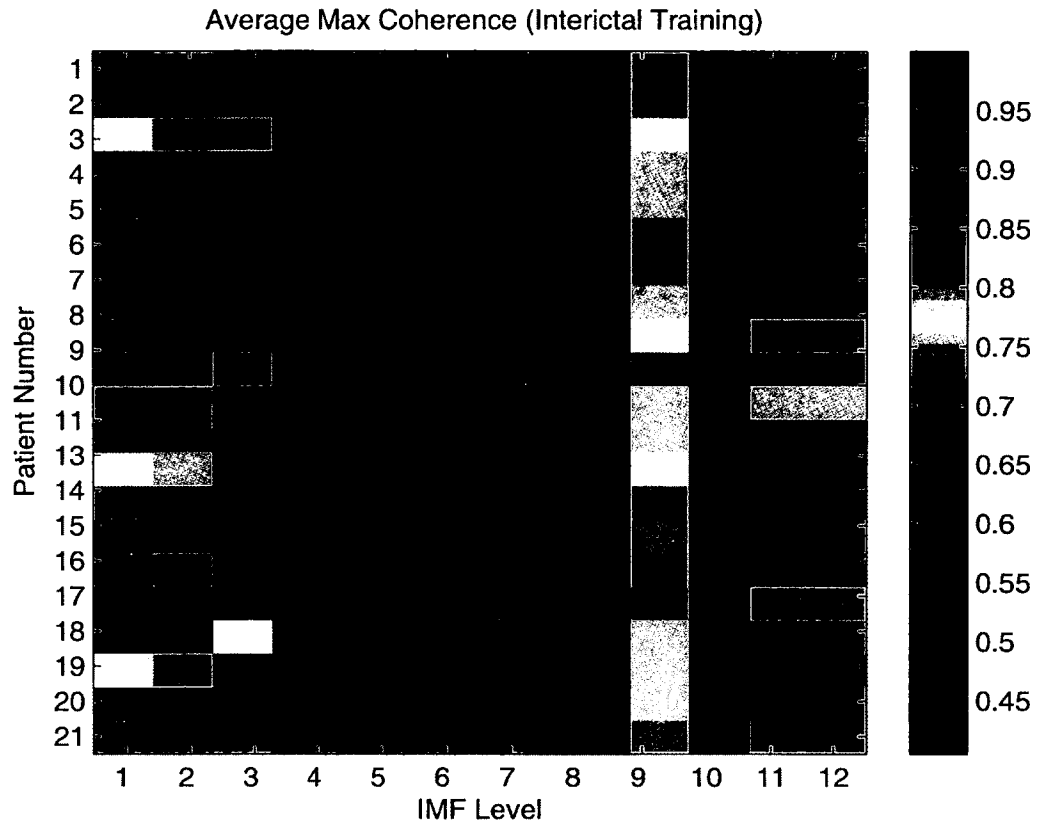


Figure A.3: Average maximum coherence indicating statistical information for maximum coherence measure of interictal training data. The image map shows each patient's average (across the 15 channel pairs) of maximum coherence at each IMF level.

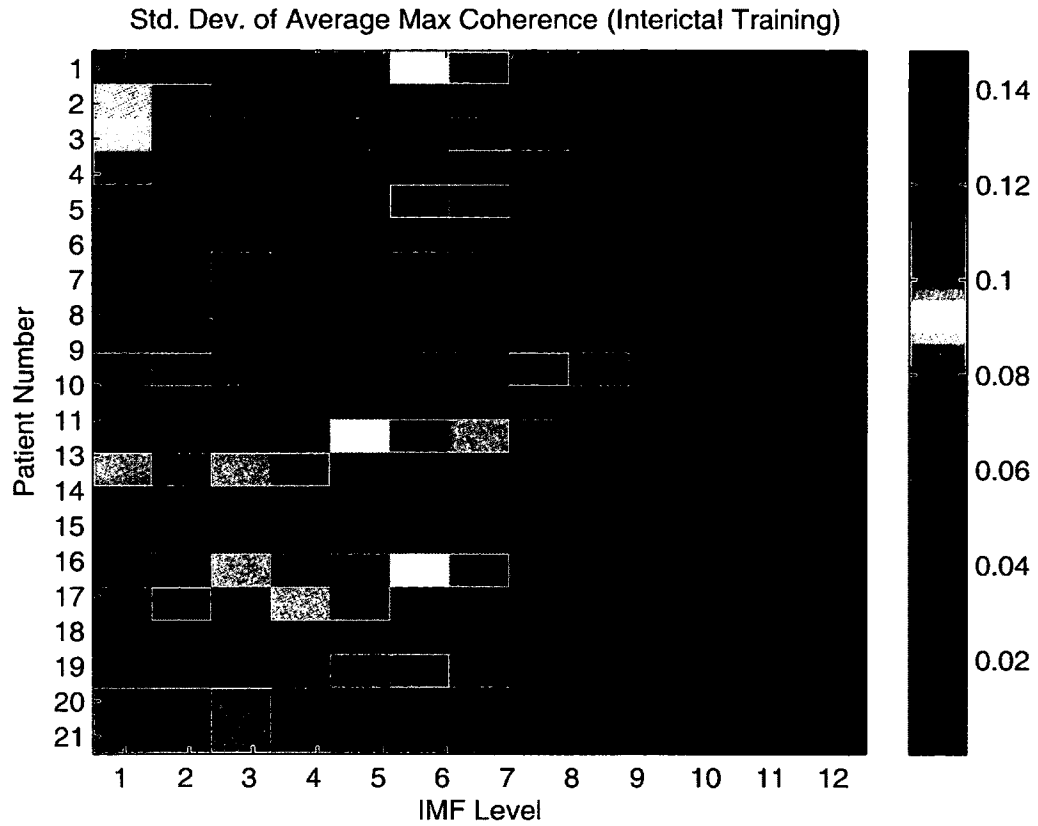


Figure A.4: Standard deviation of average maximum coherence indicating statistical information for the maximum coherence measure of interictal training data. The image map shows each patient's standard deviation of the average (across the 15 channel pairs) of the maximum coherence at each IMF level.

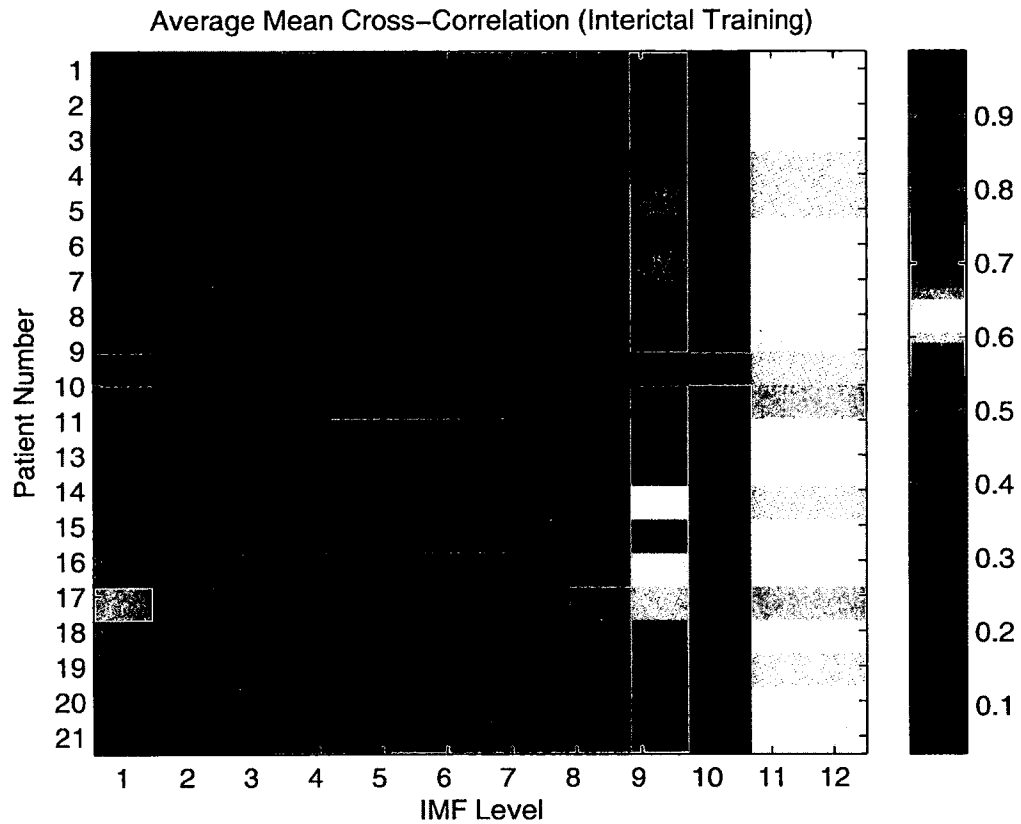


Figure A.5: Average mean cross-correlation indicating statistical information for mean cross-correlation measure of interictal training data. The image map shows each patient's average (across the 15 channel pairs) of mean cross-correlation at each IMF level.

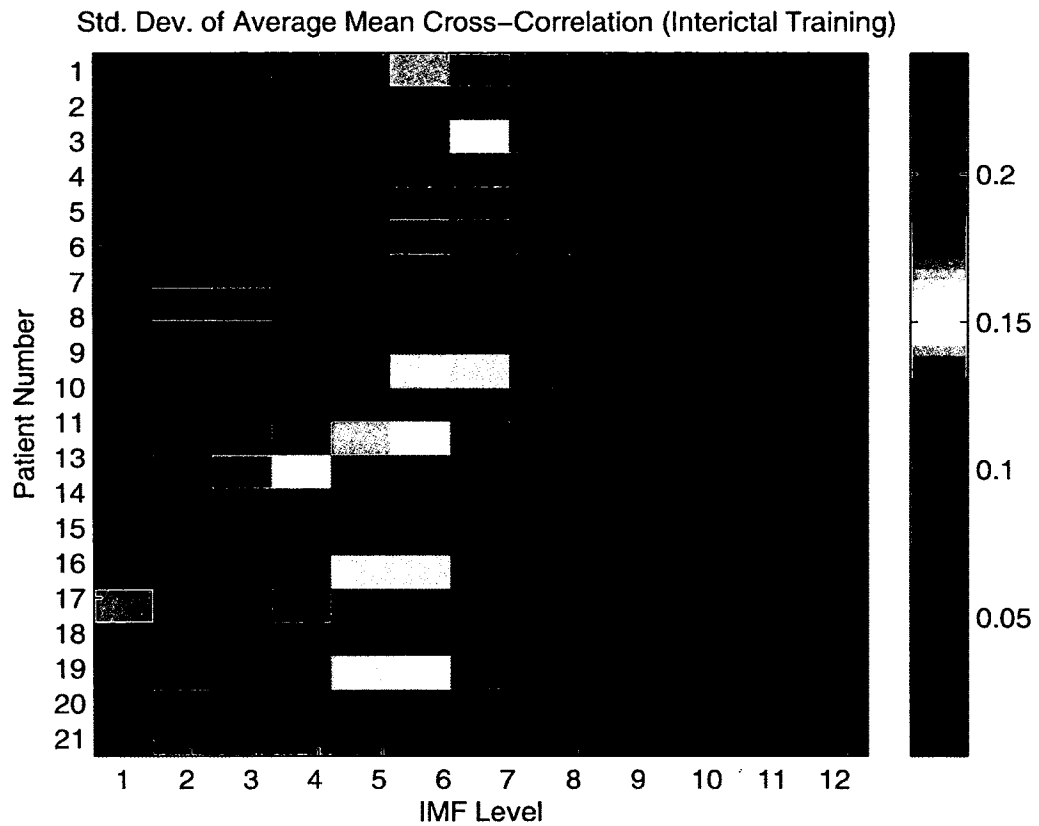


Figure A.6: Standard deviation of average mean cross-correlation indicating statistical information for the mean cross-correlation measure of interictal training data. The image map shows each patient's standard deviation of the average (across the 15 channel pairs) of the mean cross-correlation at each IMF level.

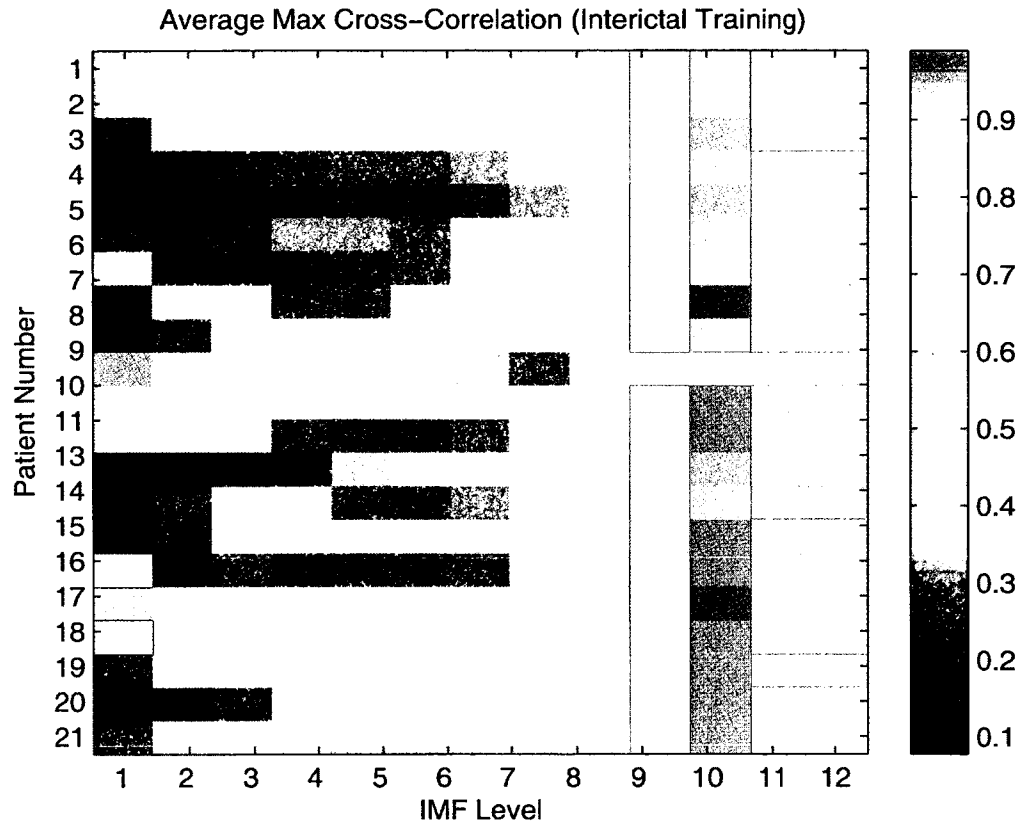


Figure A.7: Average maximum cross-correlation indicating statistical information for maximum cross-correlation measure of interictal training data. The image map shows each patient's average (across the 15 channel pairs) of maximum cross-correlation at each IMF level.

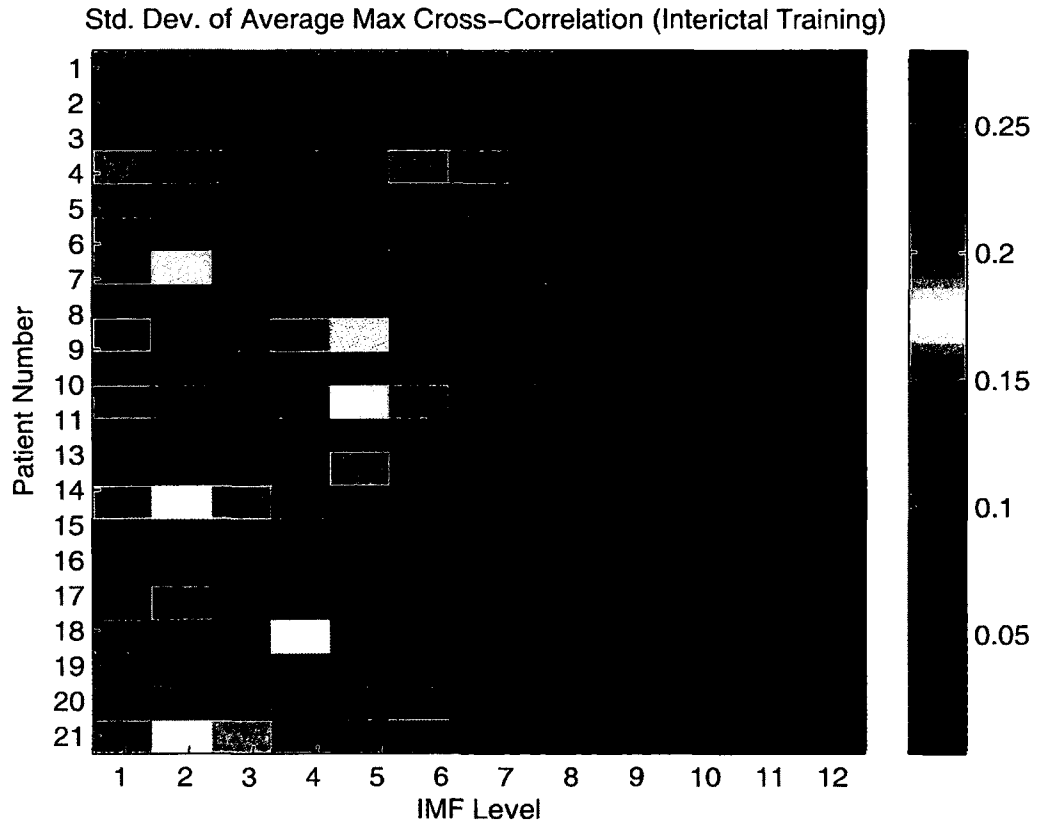


Figure A.8: Standard deviation of average maximum cross-correlation indicating statistical information for maximum cross-correlation measure of interictal training data. The image map shows each patient's average (across the 15 channel pairs) of maximum cross-correlation at each IMF level.

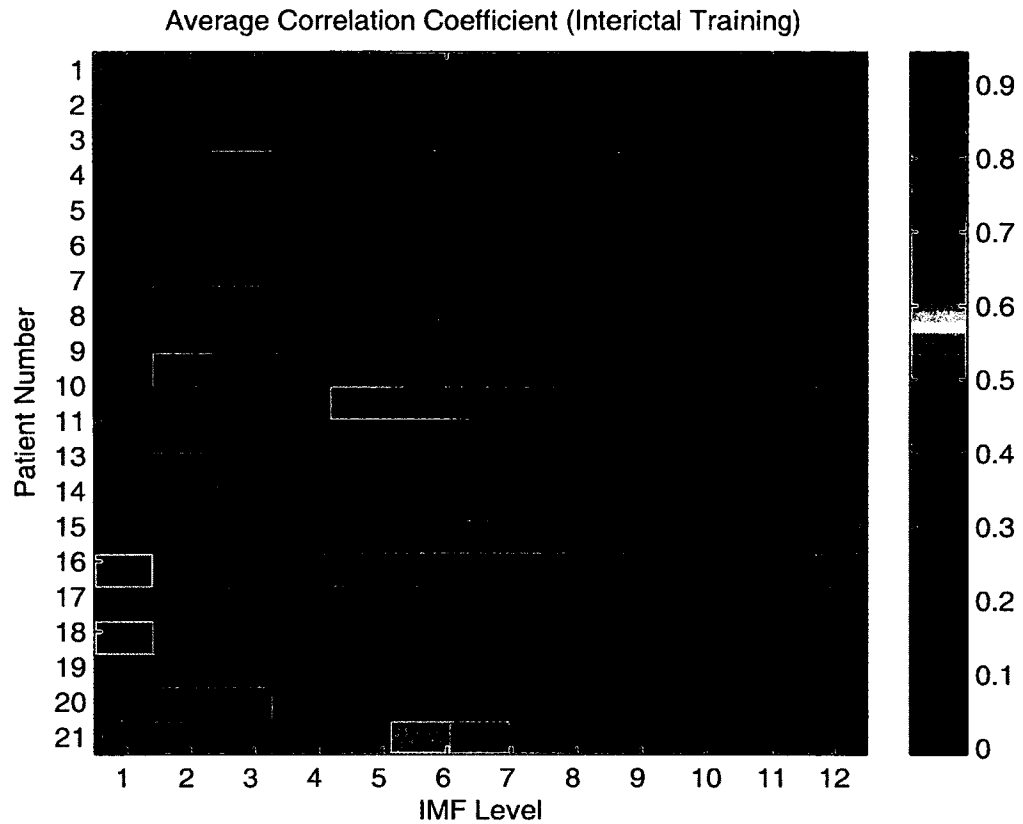


Figure A.9: Average correlation coefficient indicating statistical information for correlation coefficient measure of interictal training data. The image map shows each patient's average (across the 15 channel pairs) of correlation coefficient at each IMF level.

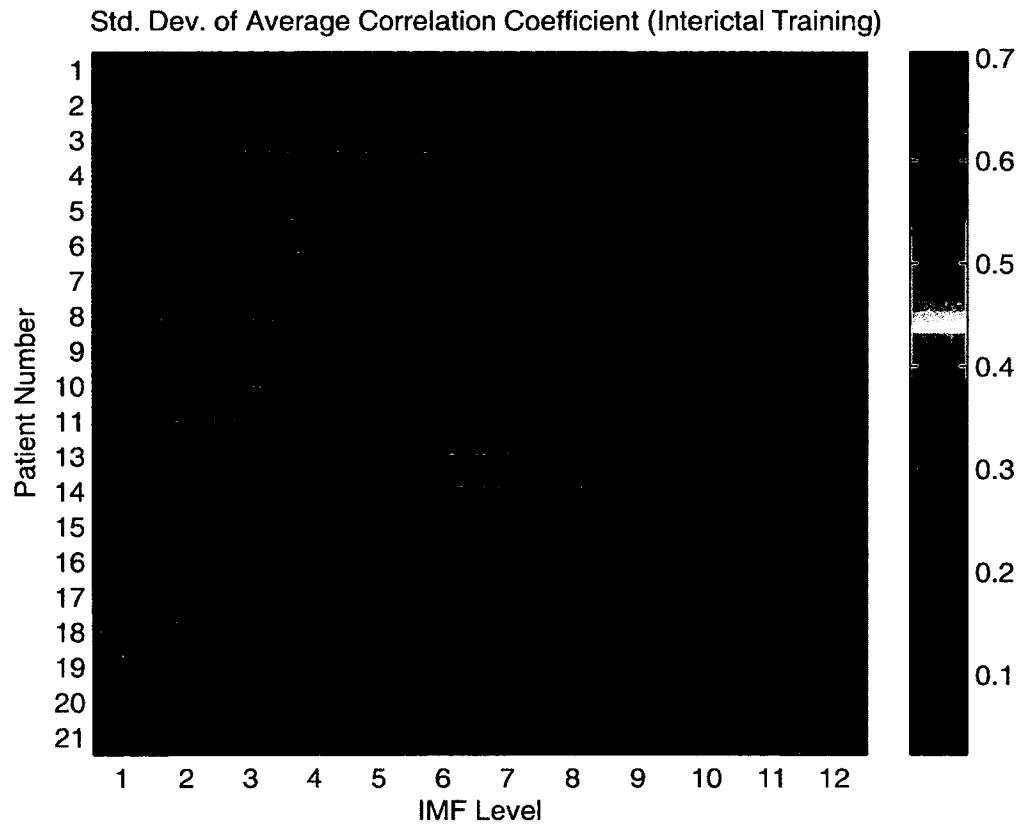


Figure A.10: Standard deviation of average correlation coefficient indicating statistical information for correlation coefficient measure of interictal training data. The image map shows each patient's average (across the 15 channel pairs) of correlation coefficient at each IMF level.

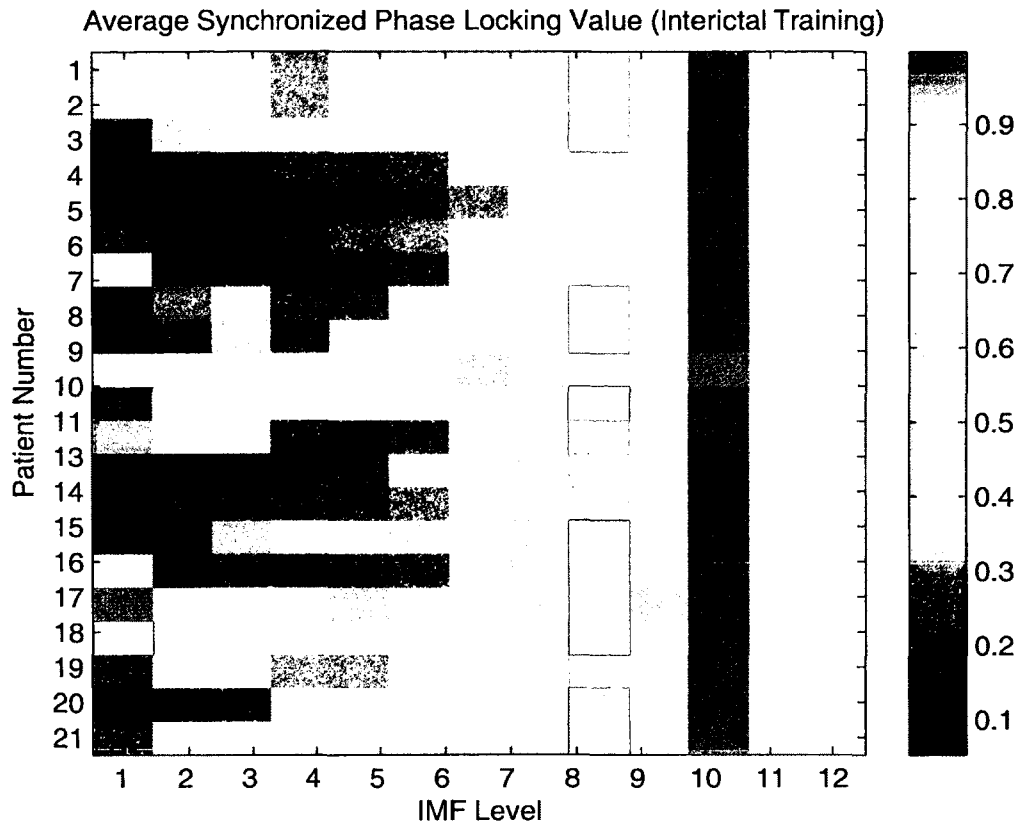


Figure A.11: Average synchronized phase locking value indicating statistical information for synchronized phase locking value measure of interictal training data. The image map shows each patient's average (across the 15 channel pairs) of synchronized phase locking value at each IMF level.

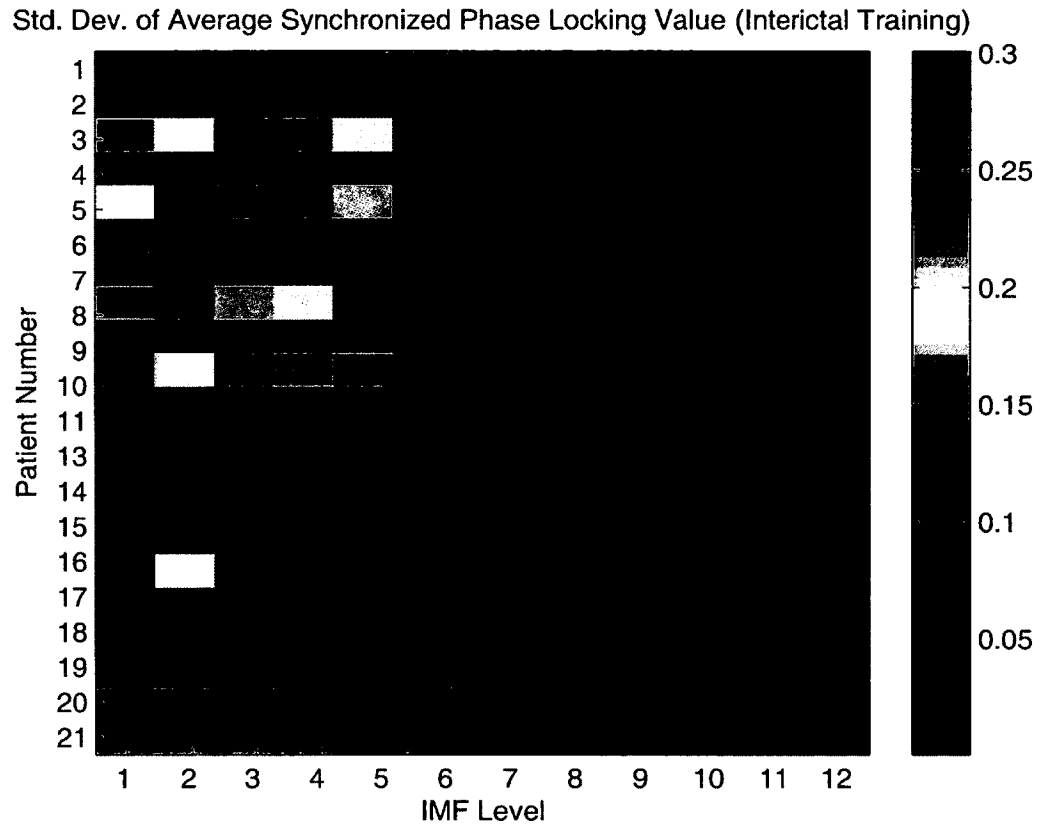


Figure A.12: Standard deviation of average synchronized phase locking value indicating statistical information for synchronized phase locking value measure of interictal training data. The image map shows each patient's average (across the 15 channel pairs) of synchronized phase locking value at each IMF level.

APPENDIX B

IMF-Coh STATISTICAL THRESHOLD TESTING CONNECTIVITY PLOTS

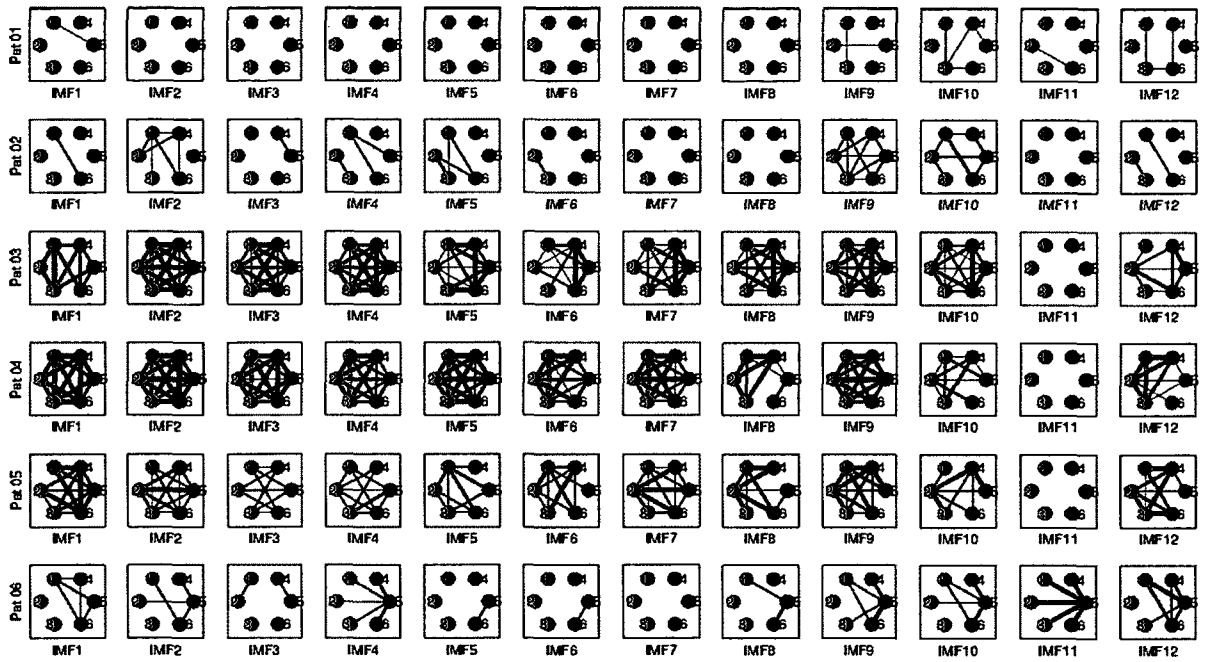


Figure B.1: IMF-Coh connectivity plots for statistical threshold testing (Patients 1 to 6). IMF-Coh connectivity plots of channel pairs for Patients 1 through 6 show correct detection of periictal dynamics for statistical threshold testing. Channels 1-3 (red nodes) are identified as focal electrodes, while channels 4-6 (blue nodes) are extrafocal electrodes. The line width is proportional to the true positive (TP) rate. Information regarding anticipation time is not included in the plots.

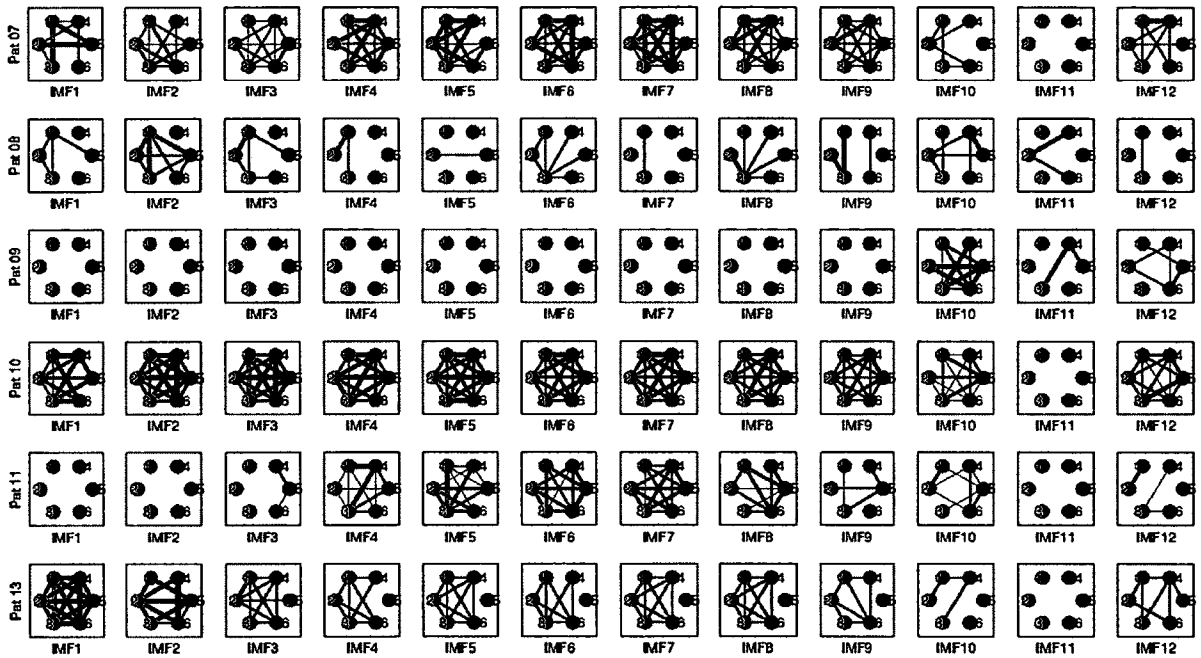


Figure B.2: IMF-Coh connectivity plots for statistical threshold testing (Patients 7 to 13). IMF-Coh connectivity plots of channel pairs for Patients 7 through 13 show correct detection of periictal dynamics for statistical threshold testing. Channels 1-3 (red nodes) are identified as focal electrodes, while channels 4-6 (blue nodes) are extrafocal electrodes. The line width is proportional to the true positive (TP) rate. Information regarding anticipation time is not included in the plots.

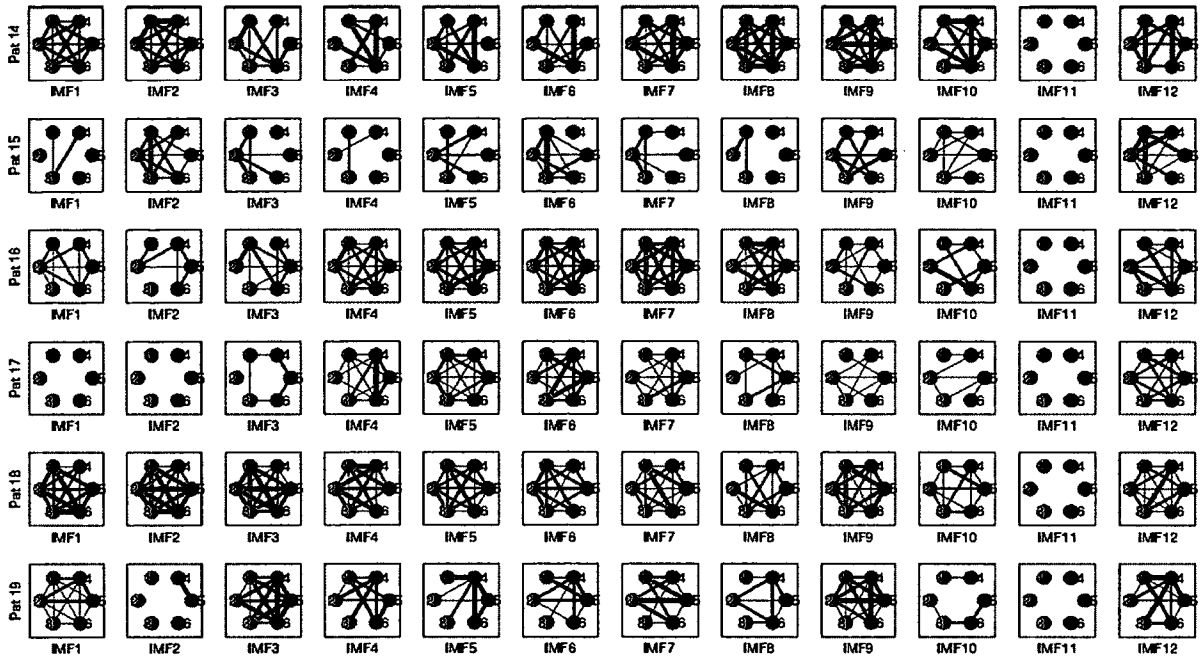


Figure B.3: IMF-Coh connectivity plots for statistical threshold testing (Patients 14 to 19). IMF-Coh connectivity plots of channel pairs for Patients 14 through 19 show correct detection of perictal dynamics for statistical threshold testing. Channels 1-3 (red nodes) are identified as focal electrodes, while channels 4-6 (blue nodes) are extrafocal electrodes. The line width is proportional to the true positive (TP) rate. Information regarding anticipation time is not included in the plots.

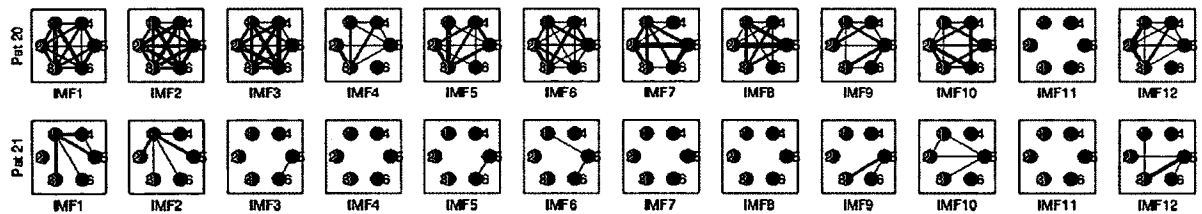


Figure B.4: IMF-Coh connectivity plots for statistical threshold testing (Patients 20 to 21). IMF-Coh connectivity plots of channel pairs for Patients 20 through 21 show correct detection of perictal dynamics for statistical threshold testing. Channels 1-3 (red nodes) are identified as focal electrodes, while channels 4-6 (blue nodes) are extrafocal electrodes. The line width is proportional to the true positive (TP) rate. Information regarding anticipation time is not included in the plots.

APPENDIX C

IMF-Coh_{max} STATISTICAL THRESHOLD TESTING CONNECTIVITY PLOTS

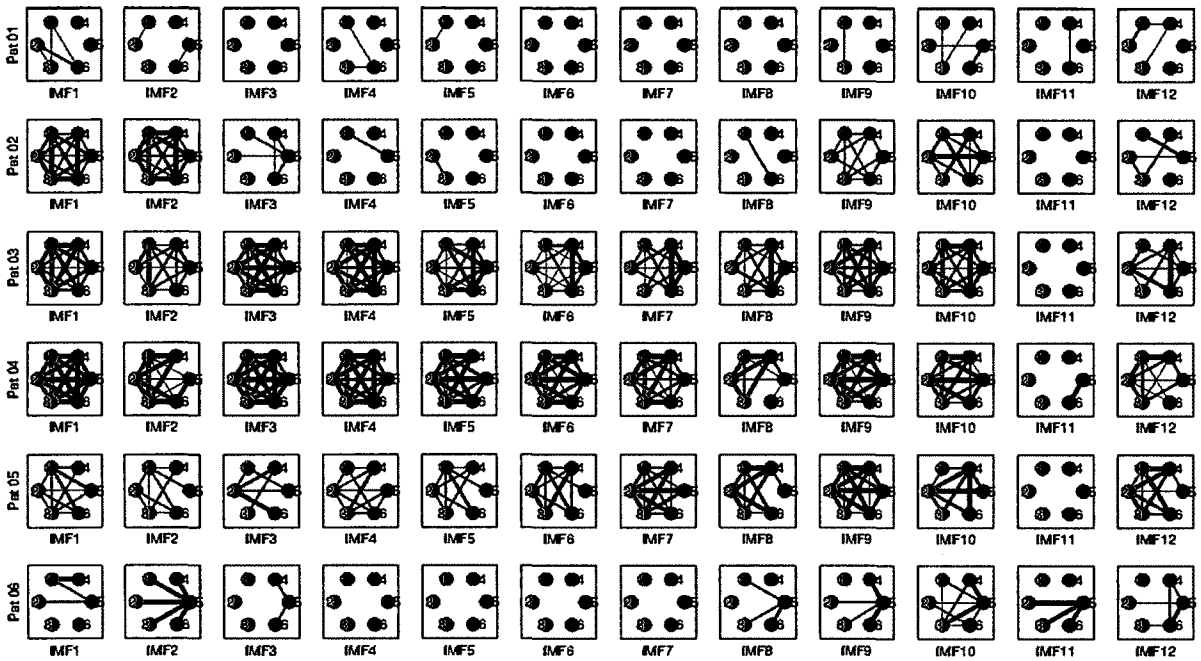


Figure C.1: IMF- Coh_{max} connectivity plots for statistical threshold testing (Patients 1 to 6). IMF- Coh_{max} connectivity plots of channel pairs for Patients 1 through 6 show correct detection of periictal dynamics for statistical threshold testing. Channels 1-3 (red nodes) are identified as focal electrodes, while channels 4-6 (blue nodes) are extrafocal electrodes. The line width is proportional to the true positive (TP) rate. Information regarding anticipation time is not included in the plots.

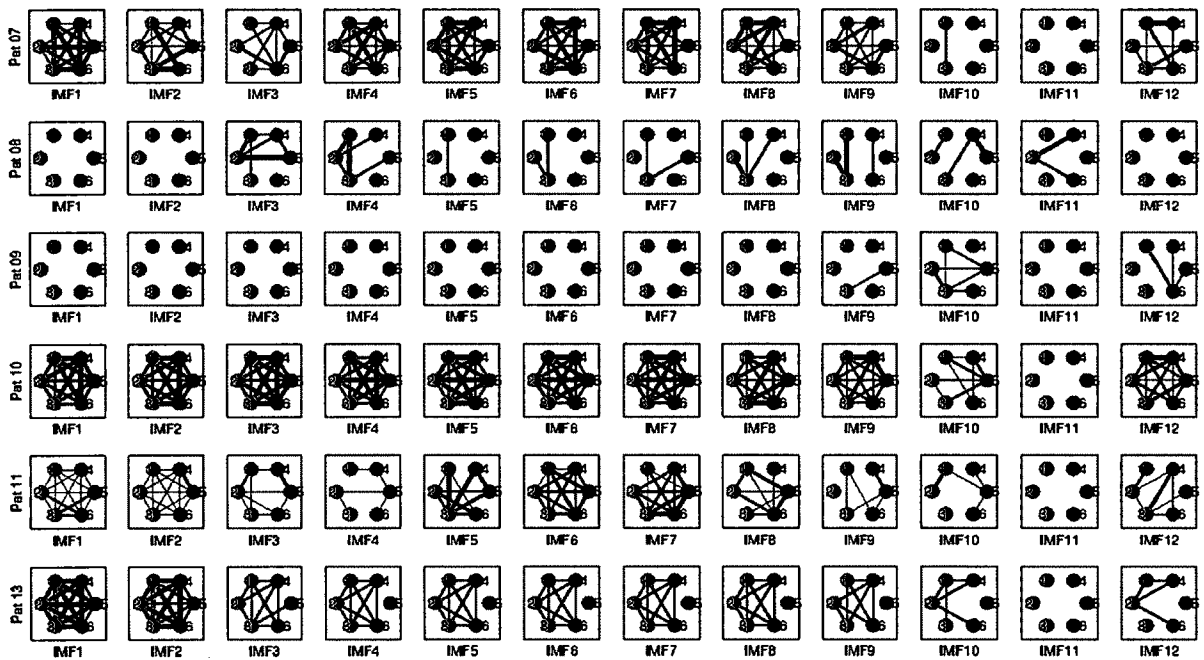


Figure C.2: IMF- Coh_{max} connectivity plots for statistical threshold testing (Patients 7 to 13). IMF- Coh_{max} connectivity plots of channel pairs for Patients 7 through 13 show correct detection of periictal dynamics for statistical threshold testing. Channels 1-3 (red nodes) are identified as focal electrodes, while channels 4-6 (blue nodes) are extrafocal electrodes. The line width is proportional to the true positive (TP) rate. Information regarding anticipation time is not included in the plots.

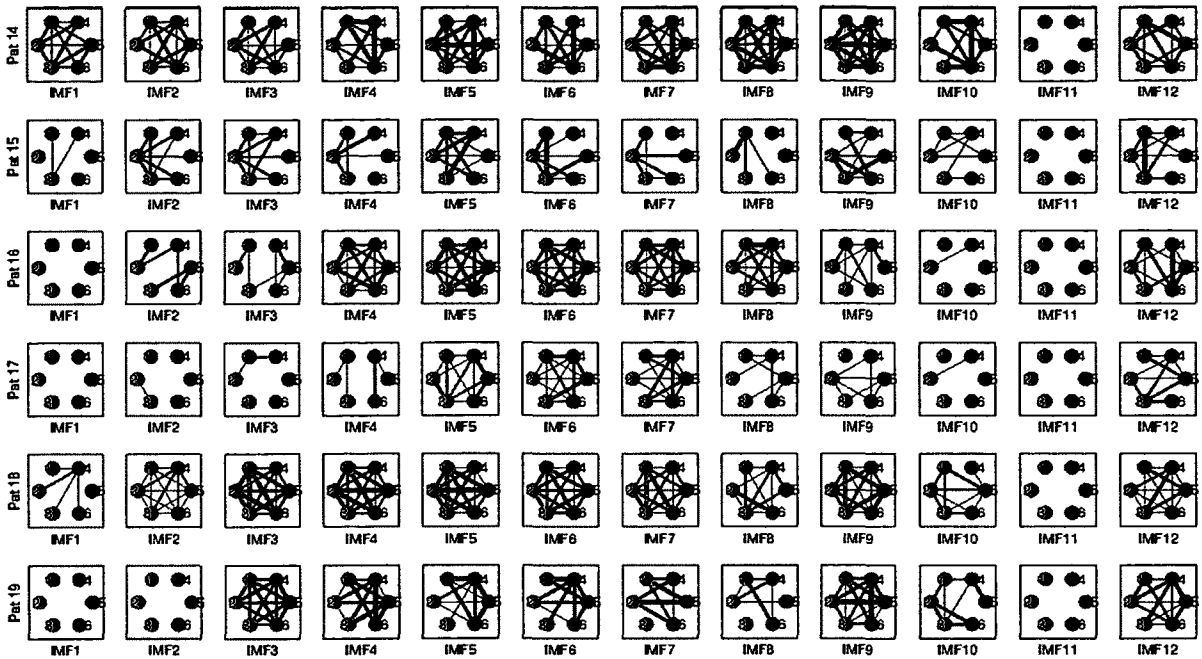


Figure C.3: IMF-Coh_{max} connectivity plots for statistical threshold testing (Patients 14 to 19). IMF-Coh_{max} connectivity plots of channel pairs for Patients 14 through 19 show correct detection of periictal dynamics for statistical threshold testing. Channels 1-3 (red nodes) are identified as focal electrodes, while channels 4-6 (blue nodes) are extrafocal electrodes. The line width is proportional to the true positive (TP) rate. Information regarding anticipation time is not included in the plots.

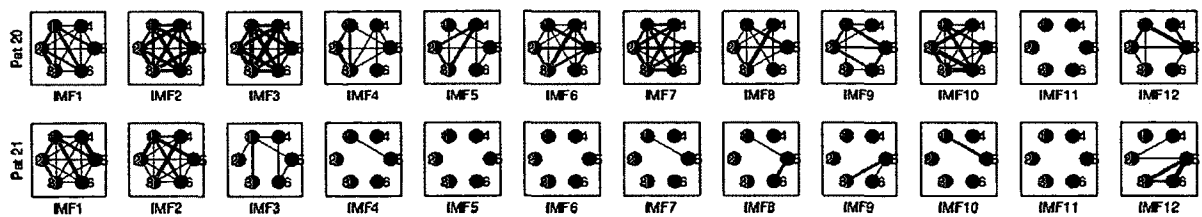


Figure C.4: IMF-Coh_{max} connectivity plots for statistical threshold testing (Patients 20 to 21). IMF-Coh_{max} connectivity plots of channel pairs for Patients 20 through 21 show correct detection of periictal dynamics for statistical threshold testing. Channels 1-3 (red nodes) are identified as focal electrodes, while channels 4-6 (blue nodes) are extrafocal electrodes. The line width is proportional to the true positive (TP) rate. Information regarding anticipation time is not included in the plots.

APPENDIX D

IMF-CCoef STATISTICAL THRESHOLD TESTING CONNECTIVITY PLOTS

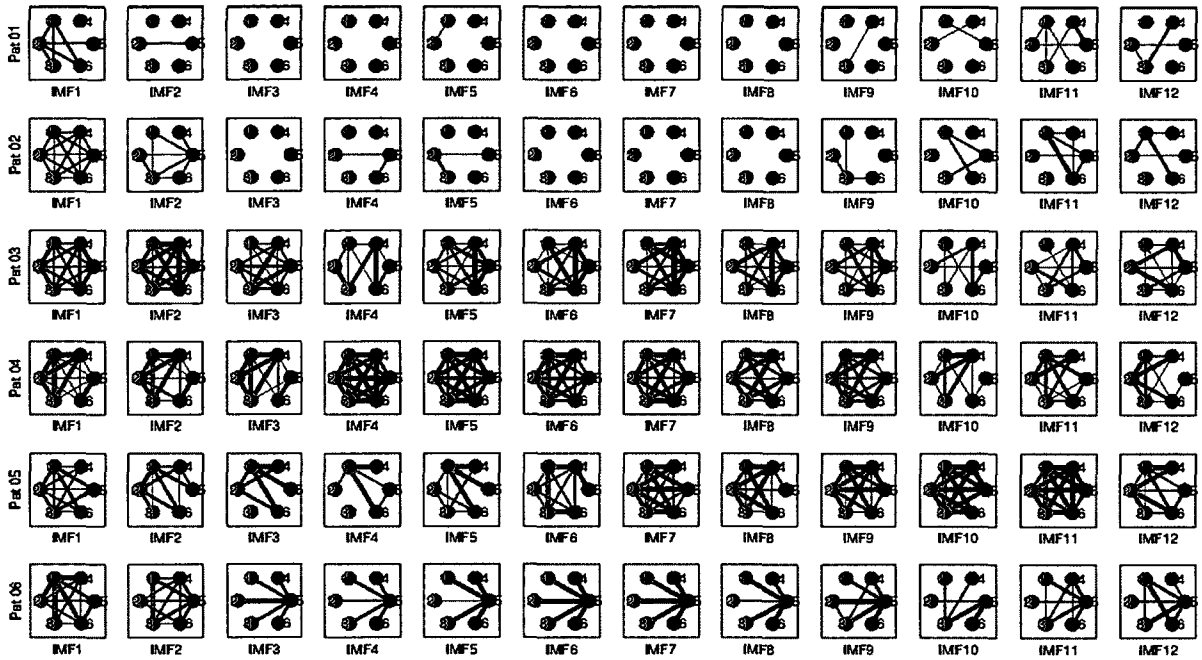


Figure D.1: IMF-CCoef connectivity plots for statistical threshold testing (Patients 1 to 6). IMF-CCoef connectivity plots of channel pairs for Patients 1 through 6 show correct detection of perictal dynamics for statistical threshold testing. Channels 1-3 (red nodes) are identified as focal electrodes, while channels 4-6 (blue nodes) are extrafocal electrodes. The line width is proportional to the true positive (TP) rate. Information regarding anticipation time is not included in the plots.

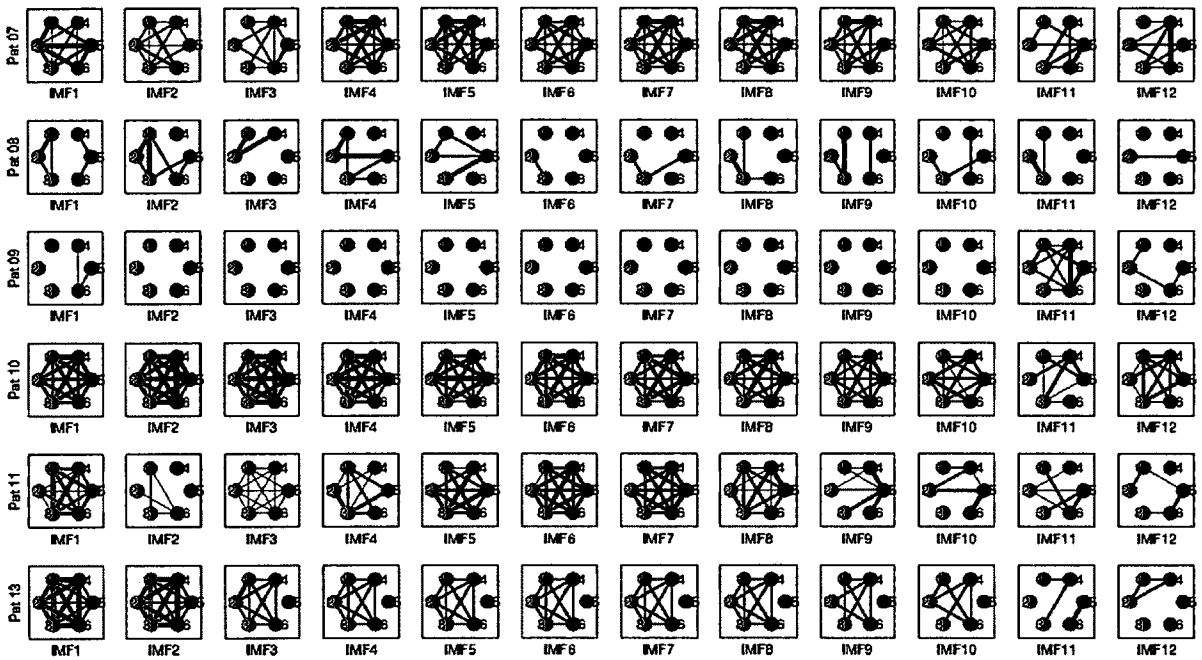


Figure D.2: IMF-CCoef connectivity plots for statistical threshold testing (Patients 7 to 13). IMF-CCoef connectivity plots of channel pairs for Patients 7 through 13 show correct detection of perictal dynamics for statistical threshold testing. Channels 1-3 (red nodes) are identified as focal electrodes, while channels 4-6 (blue nodes) are extrafocal electrodes. The line width is proportional to the true positive (TP) rate. Information regarding anticipation time is not included in the plots.

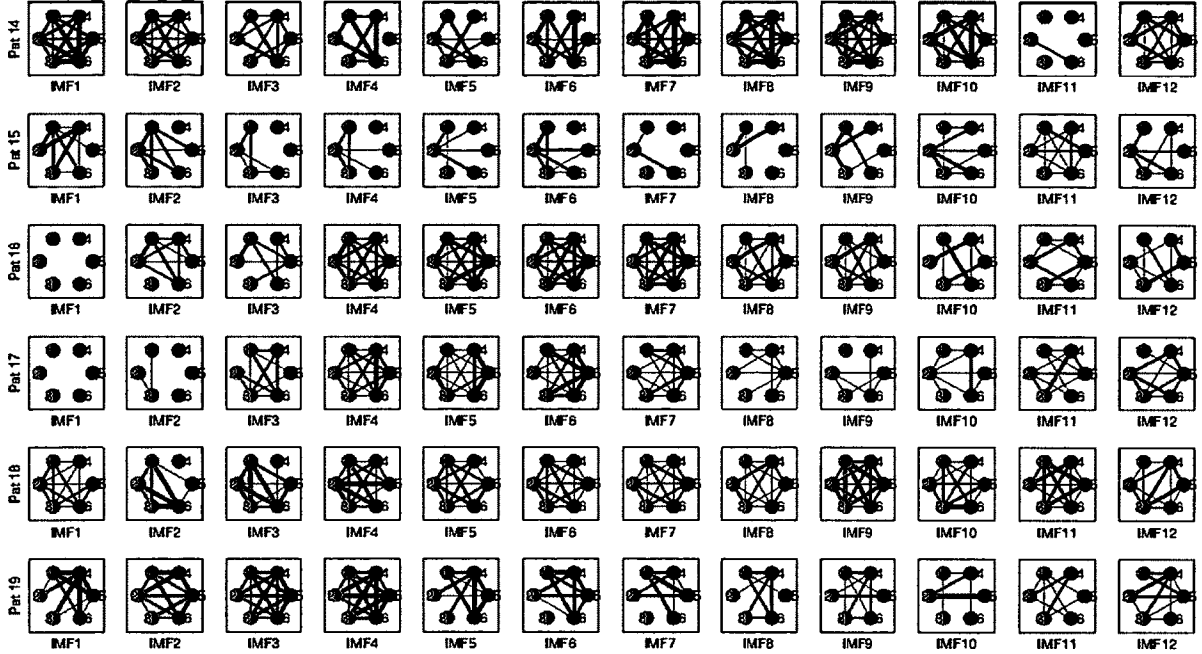


Figure D.3: IMF-CCoef connectivity plots for statistical threshold testing (Patients 14 to 19). IMF-CCoef connectivity plots of channel pairs for Patients 14 through 19 show correct detection of periictal dynamics for statistical threshold testing. Channels 1-3 (red nodes) are identified as focal electrodes, while channels 4-6 (blue nodes) are extrafocal electrodes. The line width is proportional to the true positive (TP) rate. Information regarding anticipation time is not included in the plots.

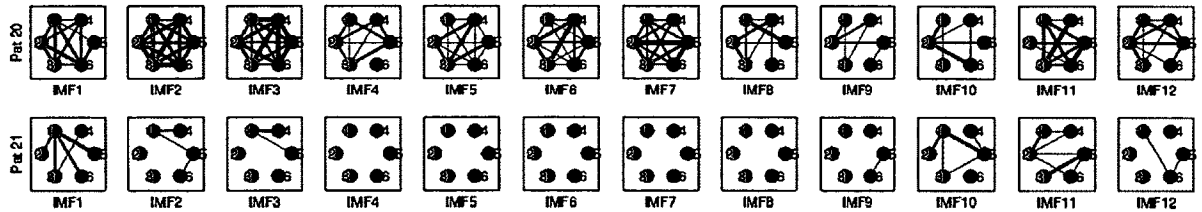


Figure D.4: IMF-CCoef connectivity plots for statistical threshold testing (Patients 20 to 21). IMF-CCoef connectivity plots of channel pairs for Patients 20 through 21 show correct detection of periictal dynamics for statistical threshold testing. Channels 1-3 (red nodes) are identified as focal electrodes, while channels 4-6 (blue nodes) are extrafocal electrodes. The line width is proportional to the true positive (TP) rate. Information regarding anticipation time is not included in the plots.

APPENDIX E

IMF-SPLV STATISTICAL THRESHOLD TESTING CONNECTIVITY PLOTS

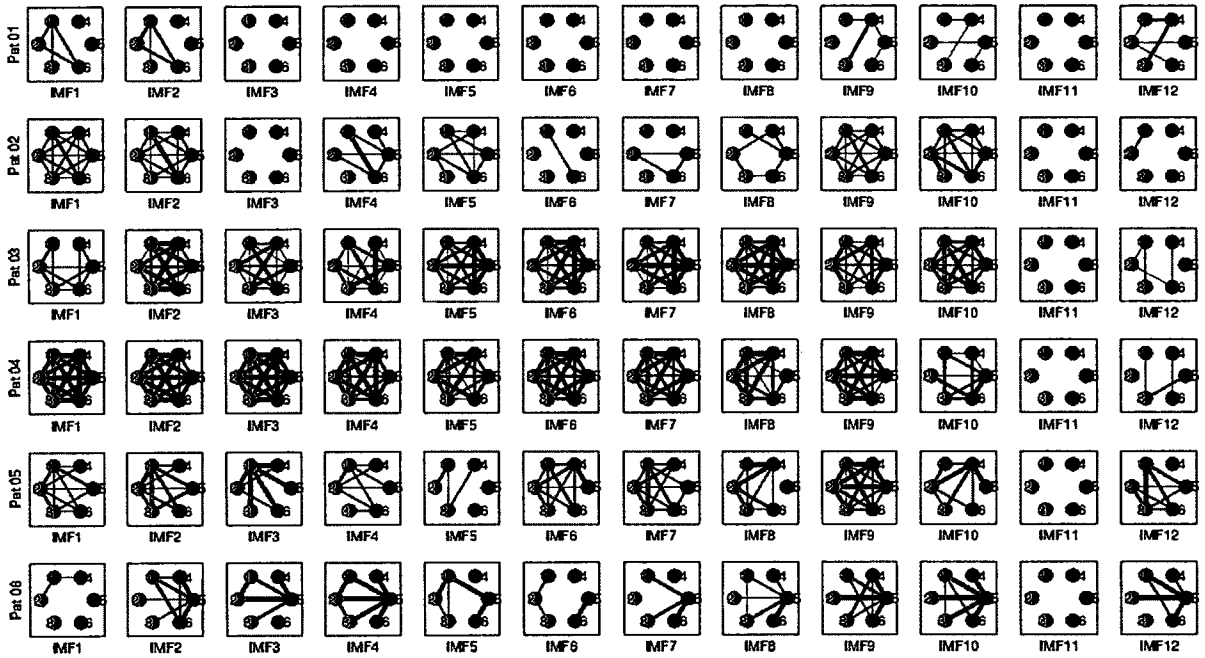


Figure E.1: IMF-SPLV connectivity plots for statistical threshold testing (Patients 1 to 6). IMF-SPLV connectivity plots of channel pairs for Patients 1 through 6 show correct detection of periictal dynamics for statistical threshold testing. Channels 1-3 (red nodes) are identified as focal electrodes, while channels 4-6 (blue nodes) are extrafocal electrodes. The line width is proportional to the true positive (TP) rate. Information regarding anticipation time is not included in the plots.

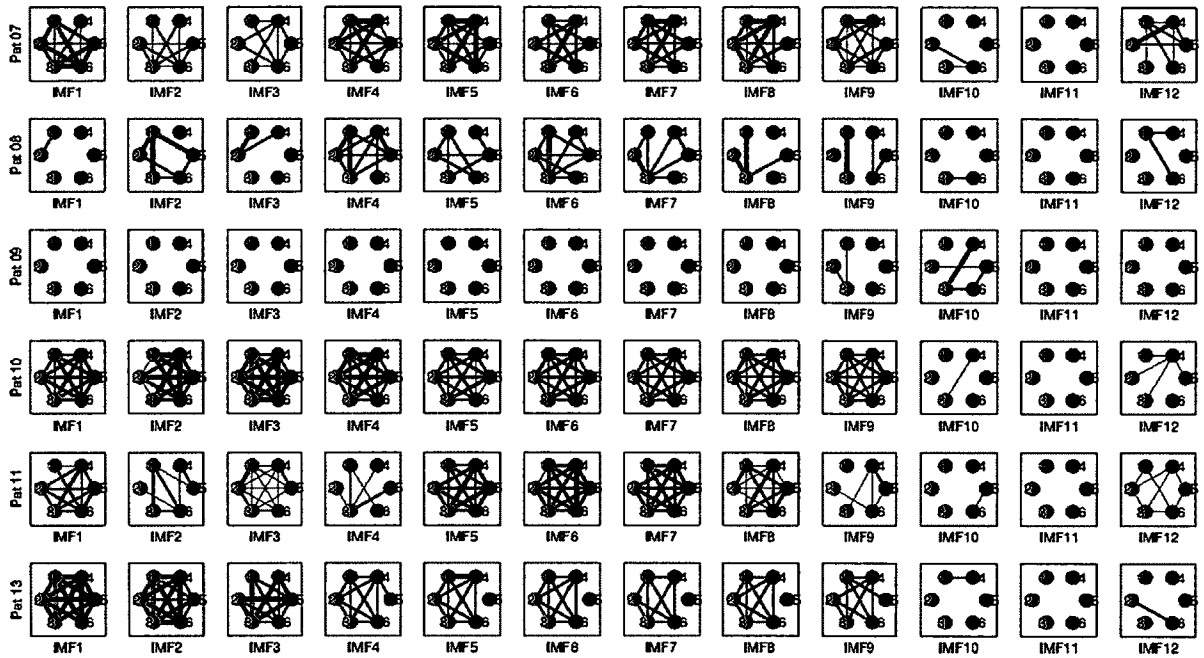


Figure E.2: IMF-SPLV connectivity plots for statistical threshold testing (Patients 7 to 13). IMF-SPLV connectivity plots of channel pairs for Patients 7 through 13 show correct detection of periictal dynamics for statistical threshold testing. Channels 1-3 (red nodes) are identified as focal electrodes, while channels 4-6 (blue nodes) are extrafocal electrodes. The line width is proportional to the true positive (TP) rate. Information regarding anticipation time is not included in the plots.

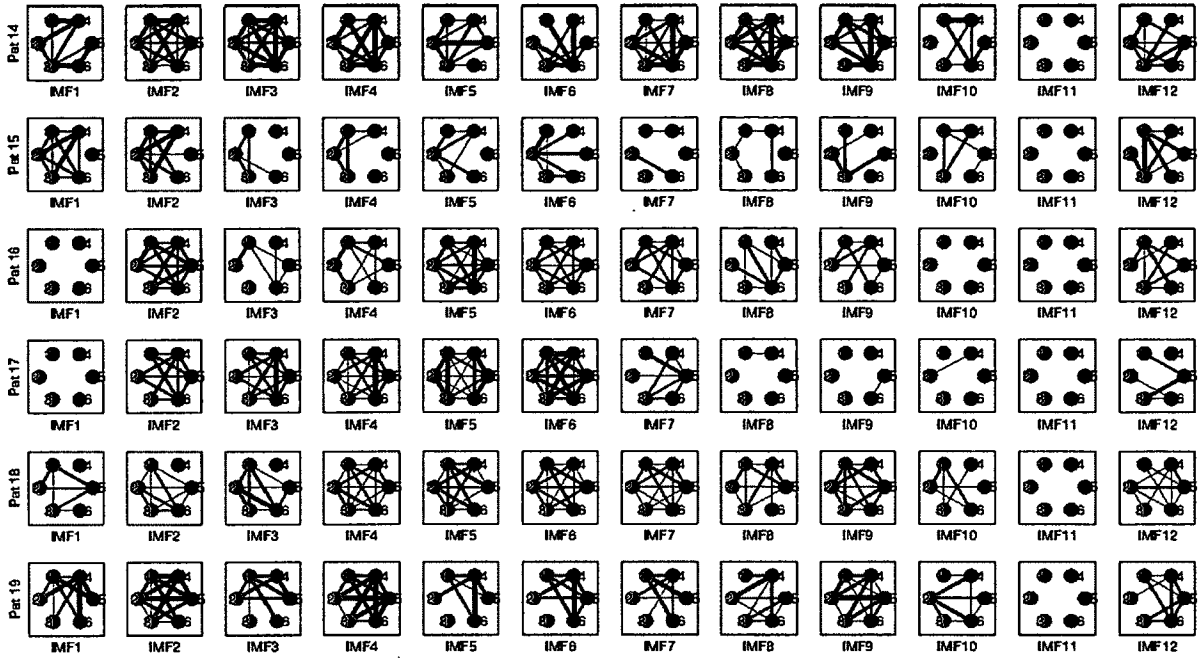


Figure E.3: IMF-SPLV connectivity plots for statistical threshold testing (Patients 14 to 19). IMF-SPLV connectivity plots of channel pairs for Patients 14 through 19 show correct detection of periictal dynamics for statistical threshold testing. Channels 1-3 (red nodes) are identified as focal electrodes, while channels 4-6 (blue nodes) are extrafocal electrodes. The line width is proportional to the true positive (TP) rate. Information regarding anticipation time is not included in the plots.

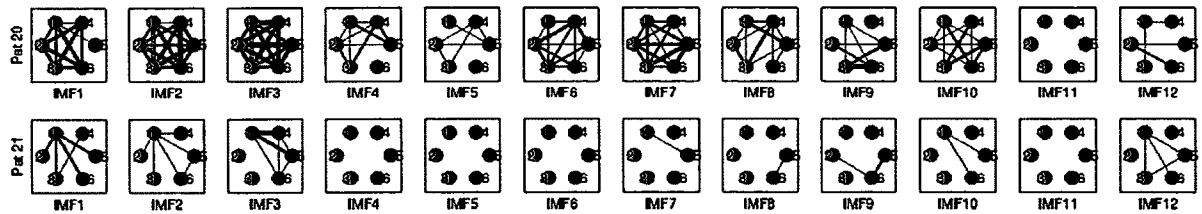


Figure E.4: IMF-SPLV connectivity plots for statistical threshold testing (Patients 20 to 21). IMF-SPLV connectivity plots of channel pairs for Patients 20 through 21 show correct detection of periictal dynamics for statistical threshold testing. Channels 1-3 (red nodes) are identified as focal electrodes, while channels 4-6 (blue nodes) are extrafocal electrodes. The line width is proportional to the true positive (TP) rate. Information regarding anticipation time is not included in the plots.

APPENDIX F

IMF-XCor STATISTICAL THRESHOLD TESTING CONNECTIVITY PLOTS

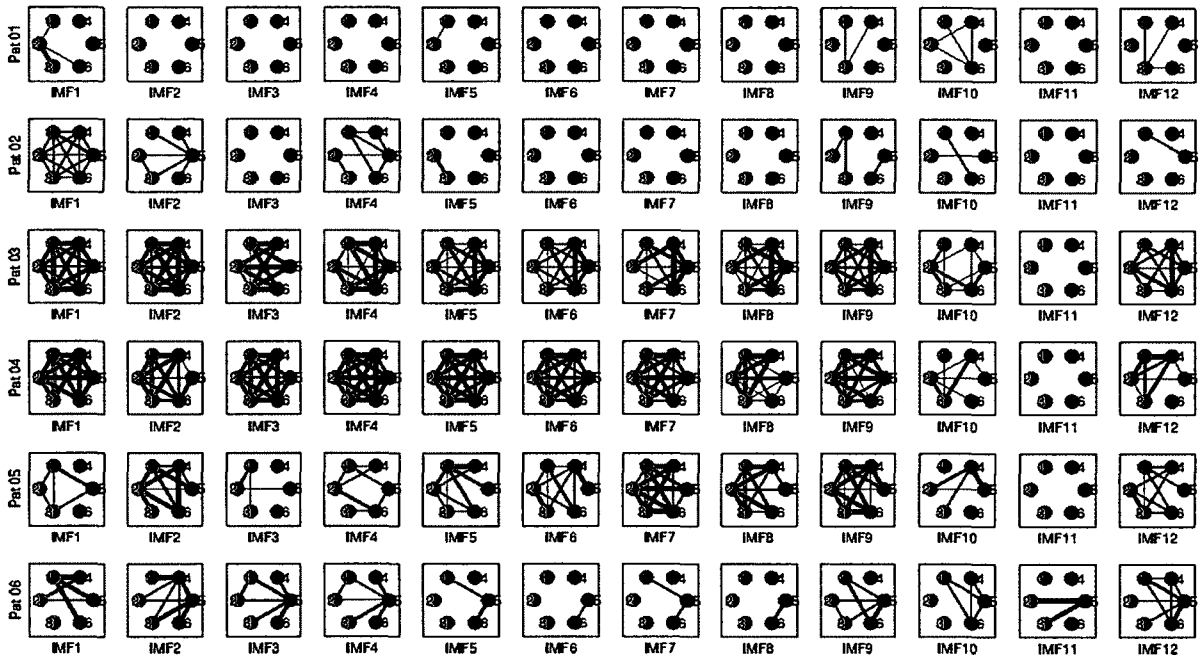


Figure F.1: IMF-XCor connectivity plots for statistical threshold testing (Patients 1 to 6). IMF-XCor connectivity plots of channel pairs for Patients 1 through 6 show correct detection of periictal dynamics for statistical threshold testing. Channels 1-3 (red nodes) are identified as focal electrodes, while channels 4-6 (blue nodes) are extrafocal electrodes. The line width is proportional to the true positive (TP) rate. Information regarding anticipation time is not included in the plots.

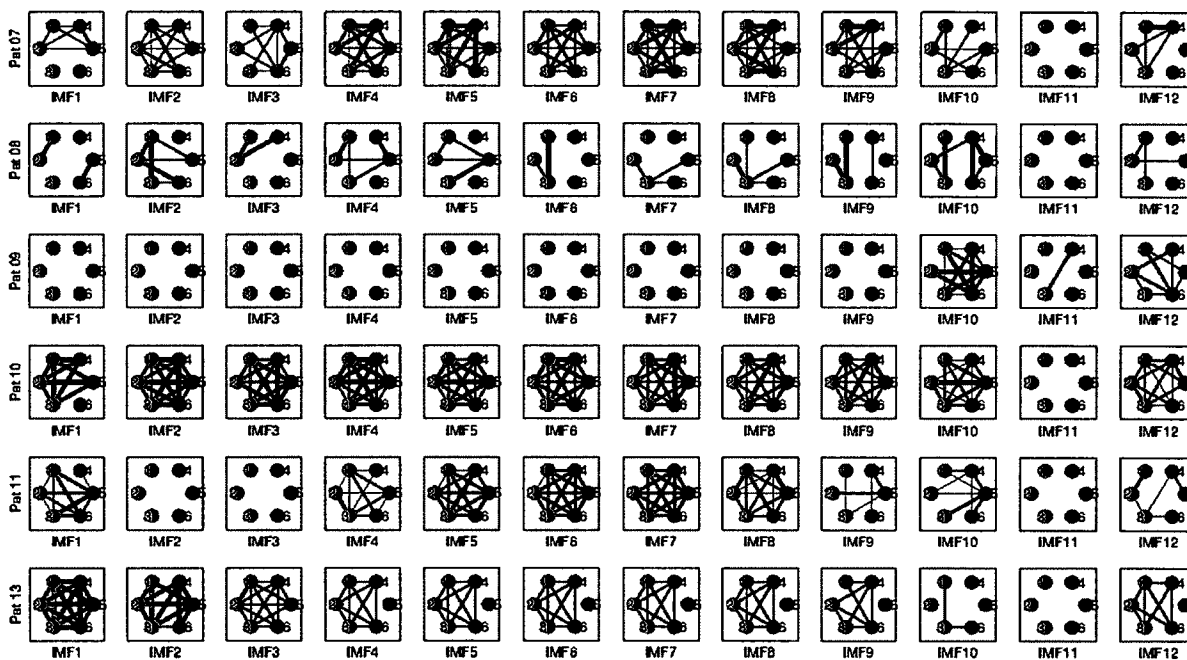


Figure F.2: IMF-XCor connectivity plots for statistical threshold testing (Patients 7 to 13). IMF-XCor connectivity plots of channel pairs for Patients 7 through 13 show correct detection of perictal dynamics for statistical threshold testing. Channels 1-3 (red nodes) are identified as focal electrodes, while channels 4-6 (blue nodes) are extrafocal electrodes. The line width is proportional to the true positive (TP) rate. Information regarding anticipation time is not included in the plots.

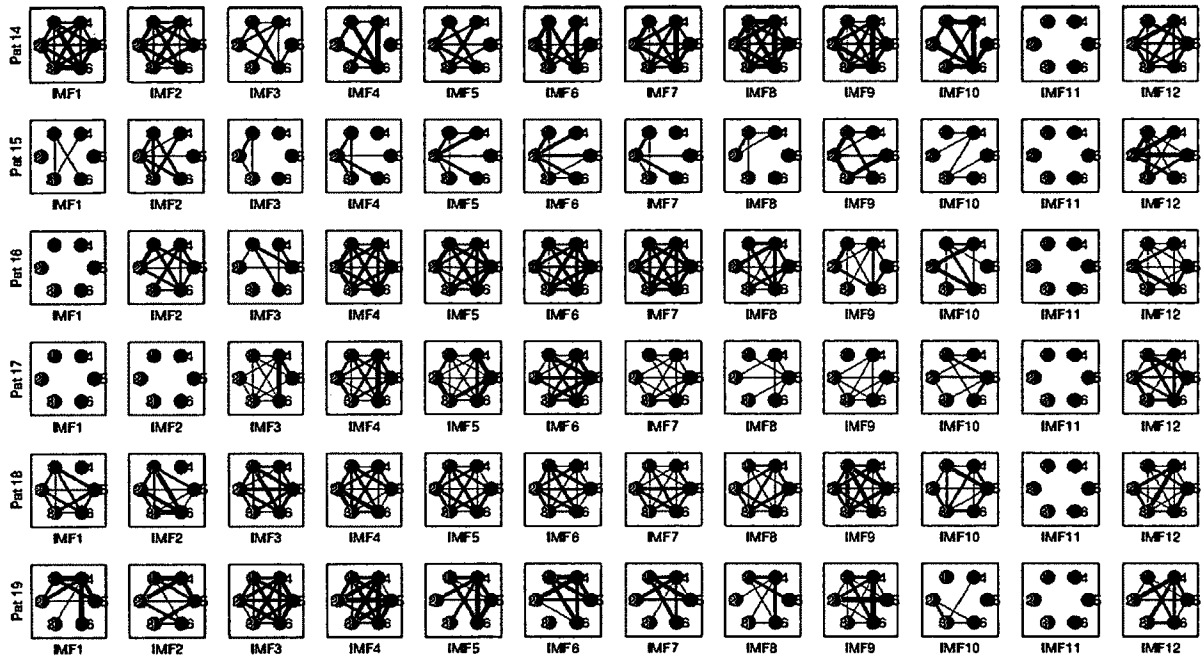


Figure F.3: IMF-XCor connectivity plots for statistical threshold testing (Patients 14 to 19). IMF-XCor connectivity plots of channel pairs for Patients 14 through 19 show correct detection of perictal dynamics for statistical threshold testing. Channels 1-3 (red nodes) are identified as focal electrodes, while channels 4-6 (blue nodes) are extrafocal electrodes. The line width is proportional to the true positive (TP) rate. Information regarding anticipation time is not included in the plots.

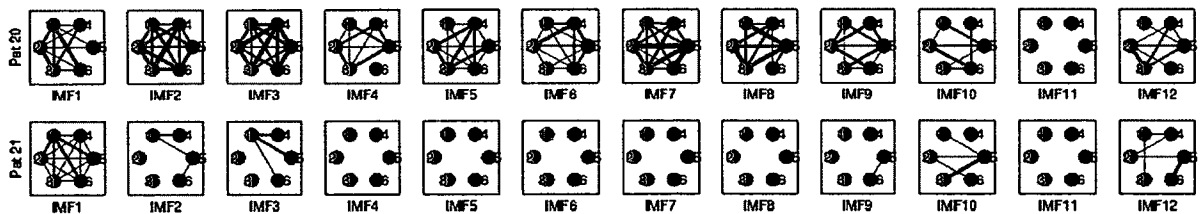


Figure F.4: IMF-XCor connectivity plots for statistical threshold testing (Patients 20 to 21). IMF-XCor connectivity plots of channel pairs for Patients 20 through 21 show correct detection of perictal dynamics for statistical threshold testing. Channels 1-3 (red nodes) are identified as focal electrodes, while channels 4-6 (blue nodes) are extrafocal electrodes. The line width is proportional to the true positive (TP) rate. Information regarding anticipation time is not included in the plots.

APPENDIX G

IMF-XCor_{max} STATISTICAL THRESHOLD TESTING CONNECTIVITY PLOTS

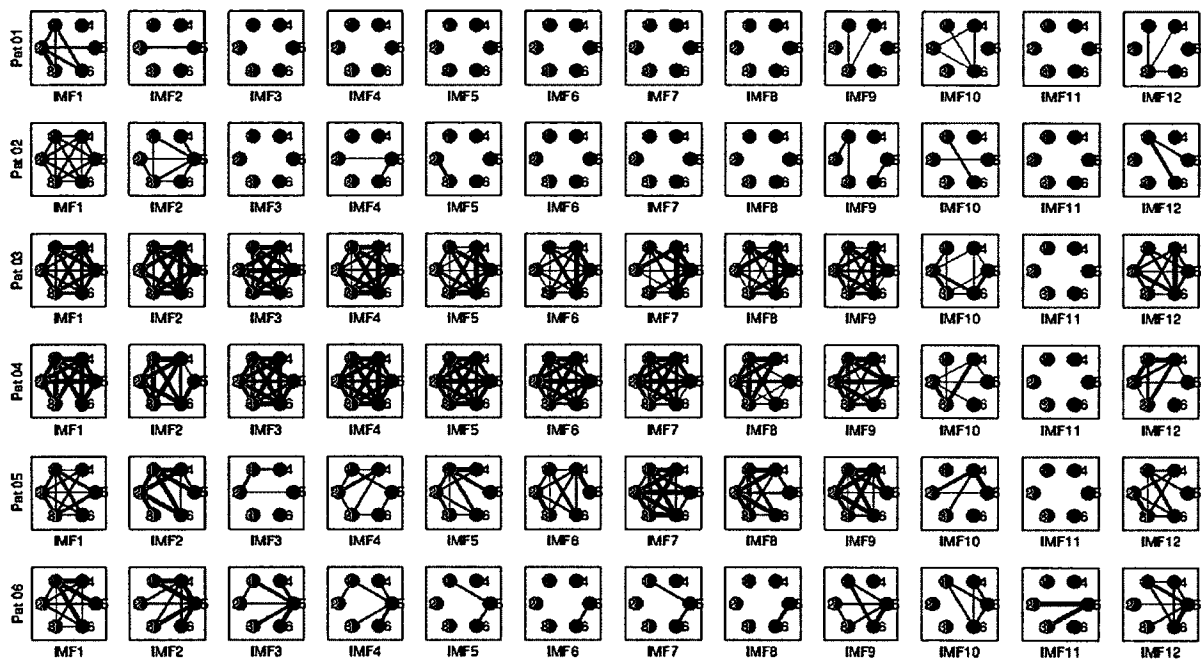


Figure G.1: IMF- $XCor_{max}$ connectivity plots for statistical threshold testing (Patients 1 to 6). IMF- $XCor_{max}$ connectivity plots of channel pairs for Patients 1 through 6 show correct detection of periictal dynamics for statistical threshold testing. Channels 1-3 (red nodes) are identified as focal electrodes, while channels 4-6 (blue nodes) are extrafocal electrodes. The line width is proportional to the true positive (TP) rate. Information regarding anticipation time is not included in the plots.

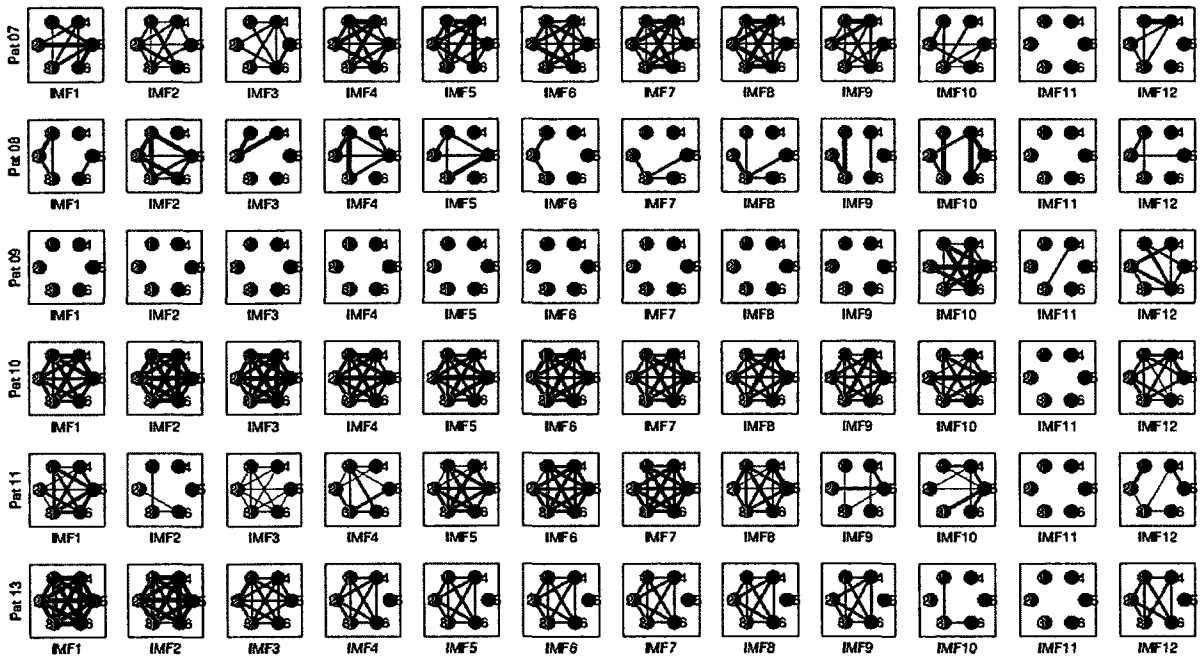


Figure G.2: IMF- $XCor_{max}$ connectivity plots for statistical threshold testing (Patients 7 to 13). IMF- $XCor_{max}$ connectivity plots of channel pairs for Patients 7 through 13 show correct detection of periictal dynamics for statistical threshold testing. Channels 1-3 (red nodes) are identified as focal electrodes, while channels 4-6 (blue nodes) are extrafocal electrodes. The line width is proportional to the true positive (TP) rate. Information regarding anticipation time is not included in the plots.

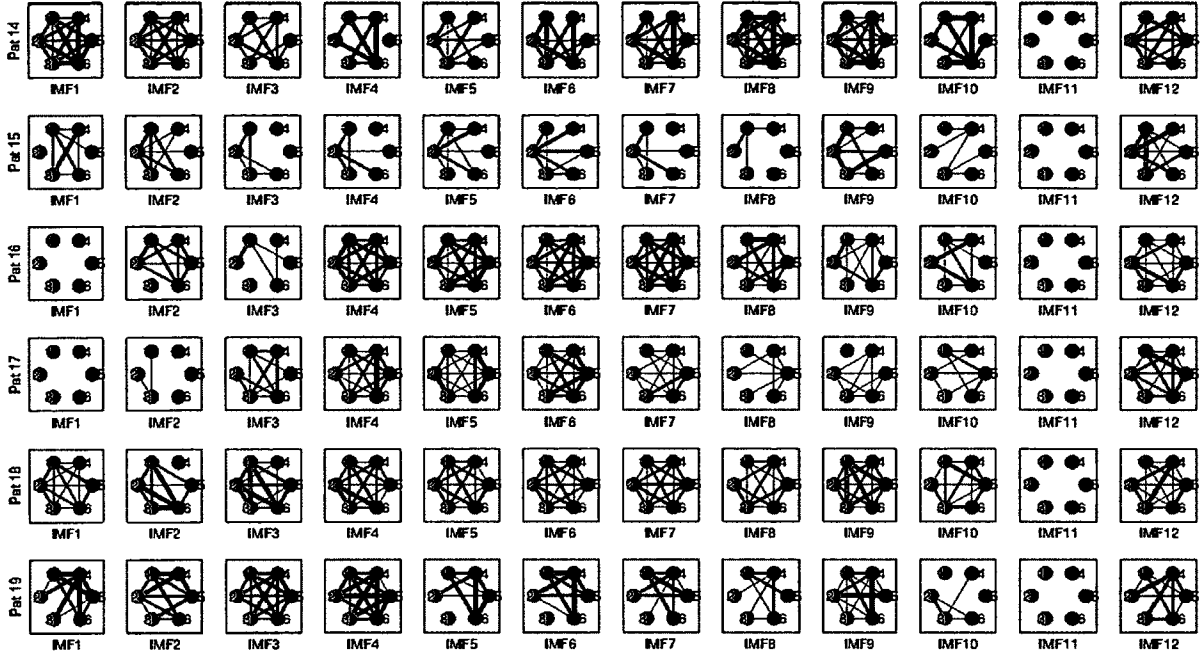


Figure G.3: IMF- $XCor_{max}$ connectivity plots for statistical threshold testing (Patients 14 to 19). IMF- $XCor_{max}$ connectivity plots of channel pairs for Patients 14 through 19 show correct detection of periictal dynamics for statistical threshold testing. Channels 1-3 (red nodes) are identified as focal electrodes, while channels 4-6 (blue nodes) are extrafocal electrodes. The line width is proportional to the true positive (TP) rate. Information regarding anticipation time is not included in the plots.

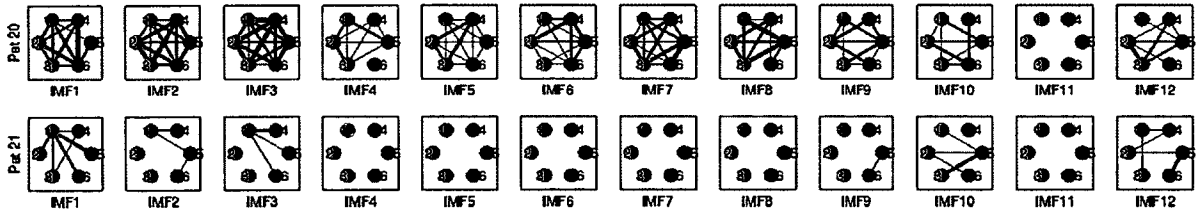


Figure G.4: IMF- $XCor_{max}$ connectivity plots for statistical threshold testing (Patients 20 to 21). IMF- $XCor_{max}$ connectivity plots of channel pairs for Patients 20 through 21 show correct detection of periictal dynamics for statistical threshold testing. Channels 1-3 (red nodes) are identified as focal electrodes, while channels 4-6 (blue nodes) are extrafocal electrodes. The line width is proportional to the true positive (TP) rate. Information regarding anticipation time is not included in the plots.

APPENDIX H

MATLAB CODE

The following are sample code listings representing a portion of the MATLAB code used in this study. Some code was developed by the author of this dissertation, while some code was obtained from other sources. Included sample listings of MATLAB code in Appendix H are as follows:

- coh_ch_viz.m
- eemd.m
- feat_caselist2.m
- freiburg.m
- freiburg_dataprep.m
- full_emd_coh_func.m
- mcoh.m
- patSelectinfo.m

H.1 coh_ch_viz.m

```

% COH.CH.VIZ
% This program performs analysis for Freiburg database eeg recordings in
% search of separable features using EEMD. Data is first run thru
% eemd_analyze.m, then eemd_coh.m, giving a *_coh.mat file that has
% coherence values between pairs of channels for each of the EEMD IMF's.
% This coherence data is partitioned and used to find an average and
% standard deviation appropriate for interictal activity. The ictal (and
% some interictal) data is tested against the identified statistics in
% order to determine seizure anticipation times and false positives.
%
% *****
% Daniel Moller
% PhD Program Graduate Student in Biomedical Engineering
% Louisiana Tech University
% dwm027@latech.edu
% -----
% Author: Daniel Moller
% Program: coh_ch_viz.m          Version: 1.0.00
% Original Date: 3/21/11
%
% Function calls:
% none
%
% Function called by:
% none
%
% Revision History (include version, programmer, date and description)
% =====
% 1.0.0 (Orig) D. Moller 3/21/11
%
% Notes
% *****
% *****

%% Clear workspace and close open figures
clear all; clc; close all; warning off;
[comp,pathname] = chkcomp;
pathname_data = '1Research\SRC_DATA\Freiburg_Data\mat\ '
tic

%% Enter data to be analyzed
avgwin = 20;
plotpats = 6;
twindow = 16;
modestart = 1; modeend = 6;
std_start = 2; std_step = 0.5; std_end = 5;
thresh = std_start:std_step:std_end;
% patSelect{1} = '003';

% ALL H & NC
patSelect = {'001' '002' '003' '004' '005' '006' '007' '008' '009' ...
            '010' '011' '013' '014' '015' '016' '017' '018' '019'...
            '020' '021'}; %'012'

% % % Hippocampal/Neocortical (H/NC)
% patSelect = {'014' '015'};

% Hippocampal (H)
% patSelect = {'002' '004' '006' '007' '010' '013' '016'}; %'012'

% % Neocortical (NC)
% patSelect = {'001' '003' '005' '008' '009' '011' '017' '018' '019' '020' '021'};

```

```

scrsz = get(0,'ScreenSize');
% pxv = 1; pyv = 1; pxdv = 700; pydv = 1500;
pxv = 0.0; pyv = 0.0; pxdv = 0.4; pydv = 1.6;

figure('Units','Normalized','Position',[pxv pyv pxdv pydv])
spno = 0;
for patno = 1:length(patSelect)
    %% clear repeated data
    clear xls fpr fp maii_train maii_test masz_test ii_test linewidthdat
    clear mno sz_test
    %% Get data from saved files
    patId{1} = patSelect{patno};
    [fnames] = patSelectinfo(patId,twindow);
    [nr,nc] = size(fnames);
    numfiles = 0;
    noii = 0;
    nosz = 0;

    %% Load data and prepare
    % -compute avgwin-pt moving average
    % -keep track of number of files for each type
    % -interictal training: 1st half (30min) of each interictal file
    % -interictal testing: 2nd half (30min) of each interictal file
    % -seizure testing: preictal/ictal/postictal
    for i = 1:nr
        for j = 1:nc
            if isempty(findstr(fnames{i,j},'?')) && ~isempty(fnames{i,j})
                load(fnames{i,j},'cohpair','tvcpair');
                [imfs, epochs] = size(cohpair(1).coh);
                [dummy,tvcpairno] = size(cohpair);
                numfiles = numfiles+1;
                switch i
                    case 1
                        noii = noii+1;
                        for pairno = 1:tvcpairno
                            for k = 1:imfs
                                for j = avgwin:floor(epochs/2)
                                    maii_train(noii,pairno,k,j) = ...
                                        mean(cohpair(pairno).coh(k,j-(avgwin-1):j))←
                                        ;
                                end
                            end
                            for k = 1:imfs
                                for j = avgwin+floor(epochs/2)+1:epochs
                                    maii_test(noii,pairno,k,j-floor(epochs/2)) = ←
                                    ...
                                    mean(cohpair(pairno).coh(k,j-(avgwin-1):j))←
                                    ;
                                end
                            end
                        end
                    case 2
                        nosz = nosz+1;
                        for pairno = 1:tvcpairno
                            for k = 1:imfs
                                for j = avgwin:epochs
                                    masz_test(nosz,pairno,k,j) = ...
                                        mean(cohpair(pairno).coh(k,j-(avgwin-1):j))←
                                        ;
                                end
                            end
                        end
                    end
                end
                clear cohpair tvcpair
            end
        end
    end
end
end

```

```

%% Interictal Training
% -find average & stdev
clear nofiles tvcpairno imfs epochs
[nofiles , tvcpairno , imfs , epochs] = size(maii_train);
temp = [];
for j = 1:tvcpairno
    for k = 1:imfs
        for i = 1:nofiles
            epochstep = epochs-avgwin+1;
            temp(j,k,(i-1)*epochstep+1:i*epochstep) = ...
                maii_train(i,j,k,avgwin:epochs);
        end
        maii_trainfo(j,k,1) = mean(temp(j,k,:));
        maii_trainfo(j,k,2) = std(temp(j,k,:));
    end
end
maii_trainfo_perpat(patno, :, :, :) = maii_trainfo;

%% Interictal Testing
% - find False Positives
clear nofiles tvcpairno imfs epochs temp
[nofiles , tvcpairno , imfs , epochs] = size(maii_test);
for i = 1:nofiles
    for j = 1:tvcpairno
        for k = 1:imfs
            mno = 0;
            for m = std_start:std_step:std_end
                mno = mno+1;
                ii_test(i,j,k,mno,:) = zeros(1,epochs);
                ii_test(i,j,k,mno,...
                    find(maii_test(i,j,k,:) > ...
                        maii_trainfo(j,k,1)+m*maii_trainfo(j,k,2))) = 1;
            end
        end
    end
end

%% Compute FPR
clear nofiles tvcpairno imfs epochs
[nofiles , tvcpairno , imfs , nothresh , epochs] = size(ii_test);
for j = 1:tvcpairno
    for k = 1:imfs
        for m = 1:nothresh
            fp(j,k,m) = 0;
            for i = 1:nofiles
                for e = 1:epochs-1
                    if (ii_test(i,j,k,m,e+1)==1 && ii_test(i,j,k,m,e)==0)
                        fp(j,k,m) = fp(j,k,m)+1;
                    end
                end
            end
            fpr(j,k,m) = ...
                fp(j,k,m)/(nofiles*(epochs-(avgwin-1))*twindow/3600);
        end
    end
end

%% Identify Seizure data larger than II Average+StDev
clear nofiles tvcpairno imfs epochs
[nofiles , tvcpairno , imfs , epochs] = size(masz_test);
for i = 1:nofiles
    for j = 1:tvcpairno
        for k = 1:imfs
            mno = 0;
            for m = std_start:std_step:std_end
                mno = mno+1;

```

```

        sz_test(i,j,k,mno,:) = zeros(1,epochs);
        sz_test(i,j,k,mno,...
            find(masz_test(i,j,k,:) > ...
                maii_trainfo(j,k,1)+m*maii_trainfo(j,k,2))) = 1;
    end
end
end

%% Seizure Testing
% - find number of seizures detected
%   (most is 1 out of 1 for each seizure)
% - find horizon (anticipation) time in min for each seizure
% - find horizon time average & stdev
clear nofiles tvcpairno imfs epochs predictflag predicttime
[nofiles, tvcpairno, imfs, nothresh, epochs] = size(sz_test);
for k = 1:imfs
    for j = 1:tvcpairno
        for m = 1:nothresh
            for i = 1:nofiles
                predictflag(i) = 0;
                predicttime(i) = 0;
                for e = 1:epochs-1
                    if (sz_test(i,j,k,m,e+1)==1 && sz_test(i,j,k,m,e)==0 ...
                        && predictflag(i) == 0)
                        predictflag(i) = 1;
                        % presume all seizure files have 15min
                        % ictal/postictal regardless of total length
                        predicttime(i) = ...
                            (round(epochs-15*60/twindow)*twindow - ...
                                (e+1)*twindow)/60;
                        xls(k).sz(i).horizon(j,m) = ...
                            (round(epochs-15*60/twindow)*twindow - ...
                                (e+1)*twindow)/60;
                        %                               xls(k).sz(i).horizon(j,m) = ←
                            (3600-(e+1)*twindow)/60;
                    end
                end
            end
            xls(k).szdet(j,m) = sum(predictflag(:));
            xls(k).horizon_avg(j,m) = sum(predicttime)/xls(k).szdet(j,m);
            xls(k).horizon_std(j,m) = std(predicttime(find(predictflag(:)==1))←
                ;
            xlspat(patno).xls(k).szdet(j,m)=xls(k).szdet(j,m);
            xlspat(patno).xls(k).horizon_avg(j,m)=xls(k).horizon_avg(j,m);
            xlspat(patno).xls(k).horizon_std(j,m)=xls(k).horizon_std(j,m);
            xlspat(patno).nosz=nofiles;
            xlspat(patno).xls(k).sz(j,m).sztest=squeeze(sz_test(:,j,k,m,:));
        end
    end
end

%% Output channel visualization

% set up locations of channel points for graph
ch(1,:) = [cos(deg2rad(120)) sin(deg2rad(120))];
ch(2,:) = [cos(deg2rad(180)) sin(deg2rad(180))];
ch(3,:) = [cos(deg2rad(240)) sin(deg2rad(240))];
ch(4,:) = [cos(deg2rad(60)) sin(deg2rad(60))];
ch(5,:) = [cos(deg2rad(0)) sin(deg2rad(0))];
ch(6,:) = [cos(deg2rad(300)) sin(deg2rad(300))];

infokus = [1 2 3];
outfokus = [4 5 6];
% nosubplots = 4*(modeend-modestart+1)
for k = 1:imfs
    if k >= modestart && k <= modeend
        spno = spno+1;
    end
end

```



```

save('xlspat\coh_xlspat.mat','xlspat');

%% %% Interictal Testing - Output FPR to Excel
% patId = patSelect{1}
% runinfo1 = datestr(now,'yymmdd');
% runinfo2 = datestr(now,'HHMM');
% runinfo = strcat(runinfo1,'-',runinfo2);
%
% fnameexcel = [patId '_results_' num2str(twindow) '_' runinfo];
% % tvcpairorder = [1 2 6 3 4 5 7 8 9 10 11 12 13 14 15];
% tvcpair = [1 2; 1 3; 1 4; 1 5; 1 6; 2 3; 2 4; 2 5; 2 6; 3 4; 3 5; 3 6;...
% 4 5; 4 6; 5 6];
% for k = 1:imfs
%     sheet = ['IMF' num2str(k)];
%     headname = {'False Positive Rate of Interictal Test Data: IMF' num2str(k)};
%     for j = 1:tvcpairno
%         for m = 1:nothresh
%             xls(k).fpr(j,m) = fpr(j,k,m);
%         end
%     end
%     xlswrite(fnameexcel,headname,sheet,'A1');
%     xlswrite(fnameexcel,{'Multiples of StDev (from II testing data)'},...
%         sheet,'C2');
%     xlswrite(fnameexcel,thresh,sheet,'C3');
%     xlswrite(fnameexcel,{'CHA' 'CHB'},sheet,'A3');
%     xlswrite(fnameexcel,tvcpair,sheet,'A4');
%     xlswrite(fnameexcel,xls(k).fpr,sheet,'C4');
%     if rem(k,2)==0
%         fprintf('FPR: Mode %i complete at %5.2f\n',k,toc)
%     end
% end

%% %% Seizure Testing - Output to Excel
% for k = 1:imfs
%     sheet = ['IMF' num2str(k)];
%     headname = ...
%         {'MEAN Horizon Time (min) of Seizure Testing Data: IMF' ...
%         num2str(k)};
%     for j = 1:length(tvcpairorder)
%         for m = 1:nothresh
%             xls(k).(tvcpairorder(j),m) = fpr(tvcpairorder(j),k,m);
%         end
%     end
%     xlswrite(fnameexcel,headname,sheet,'A20');
%     xlswrite(fnameexcel,{'Multiples of StDev (from II testing data)'},...
%         sheet,'C21');
%     xlswrite(fnameexcel,thresh,sheet,'C22');
%     xlswrite(fnameexcel,{'CHA' 'CHB'},sheet,'A22');
%     xlswrite(fnameexcel,tvcpair,sheet,'A23');
%     xlswrite(fnameexcel,xls(k).horizon_avg,sheet,'C23');
%
%     headname = ...
%         {'# of Seizures Detected out of' blanks(1) num2str(nofiles)...
%         ': IMF' num2str(k)};
%     xlswrite(fnameexcel,headname,sheet,'A40');
%     xlswrite(fnameexcel,{'Multiples of StDev (from II testing data)'},...
%         sheet,'C41');
%     xlswrite(fnameexcel,thresh,sheet,'C42');
%     xlswrite(fnameexcel,{'CHA' 'CHB'},sheet,'A42');
%     xlswrite(fnameexcel,tvcpair,sheet,'A43');
%     xlswrite(fnameexcel,xls(k).szdet,sheet,'C43');
%
%     headname = ...
%         {'STDEV Horizon Time (min) of Seizure Testing Data: IMF' ...
%         num2str(k)};
%     xlswrite(fnameexcel,headname,sheet,'A60');
%     xlswrite(fnameexcel,{'Multiples of StDev (from II testing data)'},...

```



```
%      sheet, 'C61');
%      xlswrite(fnameexcel, thresh, sheet, 'C62');
%      xlswrite(fnameexcel, {'CHA' 'CHB'}, sheet, 'A62');
%      xlswrite(fnameexcel, tucpair, sheet, 'A63');
%      xlswrite(fnameexcel, xls(k).horizon_std, sheet, 'C63');
%
%      if rem(k,2)==0
%          fprintf('HORIZON: Mode %i complete at %5.2f\n', k, toc)
%      end
% end
%
% save(fnameexcel, 'xls', 'ii_test', 'sz_test')
%
```

H.2 eemd.m

```

% This is an EMD/EEMD program
%
% function allmode=eemd(Y,Nstd,NE)
%
% INPUT:
%   Y: Inputted data;
%   Nstd: ratio of the standard deviation of the added noise and that of Y;
%   NE: Ensemble number for the EEMD
% OUTPUT:
%   A matrix of N*(m+1) matrix, where N is the length of the input
%   data Y, and m=fix(log2(N))-1. Column 1 is the original data, columns 2, 3, ←
%   ...
%   m are the IMFs from high to low frequency, and column (m+1) is the
%   residual (over all trend).
%
% NOTE:
%   It should be noted that when Nstd is set to zero and NE is set to 1, the
%   program degenerates to a EMD program.
%
% References can be found in the "Reference" section.
%
% The code is prepared by Zhaohua Wu. For questions, please read the "Q&A" section ←
%   or
%   contact
%   zhww@cola.iges.org
%
function allmode=eemd(Y,Nstd,NE)
xsize=length(Y);
dd=1:1:xsize;
Ystd=std(Y);
Y=Y/Ystd;

TNM=fix(log2(xsize))-1;
TNM2=TNM+2;
for kk=1:1:TNM2,
    for ii=1:1:xsize,
        allmode(ii, kk)=0.0;
    end
end

for iii=1:1:NE,
    for i=1:1:xsize,
        temp=randn(1,1)*Nstd;
        X1(i)=Y(i)+temp;
    end

    for jj=1:1:xsize,
        mode(jj, 1) = Y(jj);
    end

    xorigin = X1;
    xend = xorigin;

    nmode = 1;
    while nmode <= TNM,
        xstart = xend;
        iter = 1;

        while iter <= 10,
            [spmax, spmin, flag]=extrema(xstart);
            upper= spline(spmax(:,1),spmax(:,2),dd);
            lower= spline(spmin(:,1),spmin(:,2),dd);
            mean_ul = (upper + lower)/2;

```

```
        xstart = xstart - mean_ul;
        iter = iter + 1;
    end
    xend = xend - xstart;

    nmode=nmode+1;

    for jj=1:1:xsize ,
        mode(jj ,nmode) = xstart(jj);
    end
end

for jj=1:1:xsize ,
    mode(jj ,nmode+1)=xend(jj);
end

allmode=allmode+mode;

end

allmode=allmode/NE;
allmode=allmode*Ystd;
```

H.3 feat_caselist2.m

```

function [caselist] = feat_caselist2(ttSet,Fs,iistart,iistop,iinewname)
% FEAT_CASELIST -
% This program uses patId to supply case-specific information to the hmm
% code.
%
% *****
% Daniel Moller
% PhD Program Graduate Student in Biomedical Engineering
% Louisiana Tech University
% dwm027@latech.edu
% -----
% Author: Daniel Moller
% Program: hmm_caselist.m           Version: 1.0.00
% Original Date: 7/14/10
%
% Function calls:
%
% Function called by:
%
% Revision History (include version, programmer, date and description)
% =====
% 1.0.00 <orig>   D. Moller   7/14/10
%   copied from hmm_freiburg.m (v1.0.01)
%
% Notes
% *****
% For documentation purposes, copy the pathnames and filenames for which
% the channel data is associated from the bsidevam.m file.
% *****
caselist = struct('pname',[],'fnameext',[],'fullname',[],'tstart',[],...
    'tstop',[],'szon',[],'szoff',[]);

[comp,pathx] = chkcomp;
if strcmp(comp,'ddzmrover')
    pname = 'C:\Users\Daniel Moller\LA_Tech\MatlabWork\';
elseif strcmp(comp,'cal01')
    pname = 'X:\MatlabWork\';
end
xlspt = [pname '1Research\SRC_DATA\Freiburg_Data\freiburg_info.xlsx'];
pname = [pname '1Research\src_DATA\Freiburg_Data\mat\'];

%% Create list of seizure names
mmm = 1;
for m = 1:21
    if m<10; temp = ['00' num2str(m)]; else; temp = ['0' num2str(m)]; end
    for mm = 1:5
        temp2 = [temp '_' num2str(mm)];
        listofszfiles{mmm} = temp2;
        mmm = mmm+1;
    end
end

%% Identify start and end times
for i = 1:length(ttSet)
    patId = ttSet{i};
    switch patId
        case listofszfiles
            d = dir([pname patId(1:3) '_s*']);
            j = 1;
            [num,txt]=xlsread(xlspt,['pat' patId(1:3)],'A3:F7');
            fileflag = 0;
            szno = str2num(patId(length(patId)))
            while (j <= length(d) && fileflag == 0)
                clear fnames
    
```

```

load([pname d(j).name], 'fnames')
load([pname d(j).name], 'CH01')
if length(CH01)/256/3600 ~= length(fnames)
    disp('Watch out for file length!')
end
for k = 1:length(fnames)
    if strcmp(txt(szno,:), fnames{k}(1:length(fnames{k})-6))
        tstart = round(num(szno,1)/Fs)+(k-2)*3600
        if tstart < 0
            tstartoverlap = abs(tstart); tstart = 0;
        else
            tstartoverlap = 0;
        end
        tstop = round(num(szno,1)/Fs)+(k-1)*3600+900
        tstop = tstart+4500;
        if tstop > length(CH01)/256
            tstop = length(CH01)/256
        end
        szon = 3600 - tstartoverlap;
        szoff = szon + round(num(szno,5));
        fnameext = d(j).name;
        fullname = strcat(pname, fnameext);
        fileflag = 1;
    end
end
j = j+1;
end
if fileflag == 0
    error(['No seizure data for ' blanks(1) patId '!'])
end
otherwise
    fprintf('This is nonseizure, interictal data\n')
    fnameext = patId(1:5);
    fullname = strcat(pname, fnameext);
    tstart = 3600*iistart; tstop = 3600*iistop;
    szon = 1; szoff = 1;
    d = dir([pname patId(1:3) '-']);
end

caselist(i).pname = pname;
caselist(i).fnameext = fnameext;
caselist(i).fullname = fullname;
caselist(i).tstart = tstart;
caselist(i).tstop = tstop;
caselist(i).szon = szon;
caselist(i).szoff = szoff;
end

```

H.4 freiburg.m

```

%% FREIBURG -
% This program prepares the Freiburg data for submission to the EVAM
% program.
%
% *****
% Daniel Moller
% PhD Candidate, Biomedical Engineering
% Louisiana Tech University
% dwm027@latech.edu
% -----
% Author: Daniel Moller
% Program: freiburg.m
% Original Date: 4/14/09
%
% Function calls:
% none
%
% Function called by:
%
%
% Revision History (include version, programmer, date and description)
% =====
% 1.0.00 (Orig) D. Moller 4/14/09
% Use Freiburg Data to run on EVAM
% 1.0.01 D. Moller 4/1/10
% added more seizures to list
% 1.0.02 D. Moller 5/4/10
% included interictal blocks
%
% Notes
% *****
% *****

clear all
close all

%% Set up Filenames & Choose Patient/Blocks/other
runinfo1 = datestr(now, 'yymmdd');
runinfo2 = datestr(now, 'HHMM');
runinfo = strcat(runinfo1, '-', runinfo2);
% enter <patient ID>-<seizure number> as text
patIdcell{1} = '004_a';
% patIdcell{2} = '016_2';
% patIdcell{3} = '016_3';
% patIdcell{4} = '016_4';
% patIdcell{5} = '016_5';

pname = 'X:\MatlabWork\1Research\SRC.DATA\Freiburg_Data\mat';
Fs = 256;

%% Load the Data
for i = 1:length(patIdcell)
    patId = patIdcell{i}
    switch patId
        case '018_1' % Patient 018 - seizure 1
            % blockNo: number of *.asc blocks needed to have 60min preictal and
            % 15min ictal/postictal
            blockNo = 2;
            freiPath = 'X:\MatlabWork\1Research\SRC.DATA\Freiburg_Data\pat018';
            freiPath1a = [freiPath '\pat018Iktal\020207aa-0010-1.asc'];
            freiPath1b = [freiPath '\pat018Iktal\020207aa-0011-1.asc'];
            freiPath2a = [freiPath '\pat018Iktal\020207aa-0010-2.asc'];
            freiPath2b = [freiPath '\pat018Iktal\020207aa-0011-2.asc'];
    end
end

```



```

freiPath3a = [freiPath '\pat016Iktal\010823ab_0082_3.asc'];
freiPath3b = [freiPath '\pat016Iktal\010823ab_0083_3.asc'];
freiPath4a = [freiPath '\pat016Iktal\010823ab_0082_4.asc'];
freiPath4b = [freiPath '\pat016Iktal\010823ab_0083_4.asc'];
freiPath5a = [freiPath '\pat016Iktal\010823ab_0082_5.asc'];
freiPath5b = [freiPath '\pat016Iktal\010823ab_0083_5.asc'];
freiPath6a = [freiPath '\pat016Iktal\010823ab_0082_6.asc'];
freiPath6b = [freiPath '\pat016Iktal\010823ab_0083_6.asc'];

case '016_a' % patient 016 - interictal + sz 1
blockNo = 7;
freiPath = 'X:\MatlabWork\1Research\SRCDATA\Freiburg_Data\pat016';

freiPath1a = [freiPath '\pat016Iktal\010823ab_0007_1.asc'];
freiPath1b = [freiPath '\pat016Iktal\010823ab_0008_1.asc'];
freiPath1c = [freiPath '\pat016Iktal\010823ab_0009_1.asc'];
freiPath1d = [freiPath '\pat016Interiktal\010823ab_0010_1.asc'];
freiPath1e = [freiPath '\pat016Interiktal\010823ab_0011_1.asc'];
freiPath1f = [freiPath '\pat016Interiktal\010823ab_0012_1.asc'];
freiPath1g = [freiPath '\pat016Interiktal\010823ab_0013_1.asc'];

freiPath2a = [freiPath '\pat016Iktal\010823ab_0007_2.asc'];
freiPath2b = [freiPath '\pat016Iktal\010823ab_0008_2.asc'];
freiPath2c = [freiPath '\pat016Iktal\010823ab_0009_2.asc'];
freiPath2d = [freiPath '\pat016Interiktal\010823ab_0010_2.asc'];
freiPath2e = [freiPath '\pat016Interiktal\010823ab_0011_2.asc'];
freiPath2f = [freiPath '\pat016Interiktal\010823ab_0012_2.asc'];
freiPath2g = [freiPath '\pat016Interiktal\010823ab_0013_2.asc'];

freiPath3a = [freiPath '\pat016Iktal\010823ab_0007_3.asc'];
freiPath3b = [freiPath '\pat016Iktal\010823ab_0008_3.asc'];
freiPath3c = [freiPath '\pat016Iktal\010823ab_0009_3.asc'];
freiPath3d = [freiPath '\pat016Interiktal\010823ab_0010_3.asc'];
freiPath3e = [freiPath '\pat016Interiktal\010823ab_0011_3.asc'];
freiPath3f = [freiPath '\pat016Interiktal\010823ab_0012_3.asc'];
freiPath3g = [freiPath '\pat016Interiktal\010823ab_0013_3.asc'];

freiPath4a = [freiPath '\pat016Iktal\010823ab_0007_4.asc'];
freiPath4b = [freiPath '\pat016Iktal\010823ab_0008_4.asc'];
freiPath4c = [freiPath '\pat016Iktal\010823ab_0009_4.asc'];
freiPath4d = [freiPath '\pat016Interiktal\010823ab_0010_4.asc'];
freiPath4e = [freiPath '\pat016Interiktal\010823ab_0011_4.asc'];
freiPath4f = [freiPath '\pat016Interiktal\010823ab_0012_4.asc'];
freiPath4g = [freiPath '\pat016Interiktal\010823ab_0013_4.asc'];

freiPath5a = [freiPath '\pat016Iktal\010823ab_0007_5.asc'];
freiPath5b = [freiPath '\pat016Iktal\010823ab_0008_5.asc'];
freiPath5c = [freiPath '\pat016Iktal\010823ab_0009_5.asc'];
freiPath5d = [freiPath '\pat016Interiktal\010823ab_0010_5.asc'];
freiPath5e = [freiPath '\pat016Interiktal\010823ab_0011_5.asc'];
freiPath5f = [freiPath '\pat016Interiktal\010823ab_0012_5.asc'];
freiPath5g = [freiPath '\pat016Interiktal\010823ab_0013_5.asc'];

freiPath6a = [freiPath '\pat016Iktal\010823ab_0007_6.asc'];
freiPath6b = [freiPath '\pat016Iktal\010823ab_0008_6.asc'];
freiPath6c = [freiPath '\pat016Iktal\010823ab_0009_6.asc'];
freiPath6d = [freiPath '\pat016Interiktal\010823ab_0010_6.asc'];
freiPath6e = [freiPath '\pat016Interiktal\010823ab_0011_6.asc'];
freiPath6f = [freiPath '\pat016Interiktal\010823ab_0012_6.asc'];
freiPath6g = [freiPath '\pat016Interiktal\010823ab_0013_6.asc'];

case '016_b' % patient 016 - ictal: seizure 2 ,+1 hour
blockNo = 2;
freiPath = 'X:\MatlabWork\1Research\SRCDATA\Freiburg_Data\pat016';

freiPath1a = [freiPath '\pat016Iktal\010823ab_0026_1.asc'];
freiPath1b = [freiPath '\pat016Iktal\010823ab_0027_1.asc'];

```

```

freiPath2a = [freiPath '\pat016Iktal\010823ab-0026-2.asc'];
freiPath2b = [freiPath '\pat016Iktal\010823ab-0027-2.asc'];

freiPath3a = [freiPath '\pat016Iktal\010823ab-0026-3.asc'];
freiPath3b = [freiPath '\pat016Iktal\010823ab-0027-3.asc'];

freiPath4a = [freiPath '\pat016Iktal\010823ab-0026-4.asc'];
freiPath4b = [freiPath '\pat016Iktal\010823ab-0027-4.asc'];

freiPath5a = [freiPath '\pat016Iktal\010823ab-0026-5.asc'];
freiPath5b = [freiPath '\pat016Iktal\010823ab-0027-5.asc'];

freiPath6a = [freiPath '\pat016Iktal\010823ab-0026-6.asc'];
freiPath6b = [freiPath '\pat016Iktal\010823ab-0027-6.asc'];

case '016_c' % patient 016 - ictal: seizure 3, +2 hours
blockNo = 3;
freiPath = 'X:\MatlabWork\1Research\SRC_DATA\Freiburg_Data\pat016';

freiPath1a = [freiPath '\pat016Iktal\010823ab-0040-1.asc'];
freiPath1b = [freiPath '\pat016Iktal\010823ab-0041-1.asc'];
freiPath1c = [freiPath '\pat016Iktal\010823ab-0042-1.asc'];

freiPath2a = [freiPath '\pat016Iktal\010823ab-0040-2.asc'];
freiPath2b = [freiPath '\pat016Iktal\010823ab-0041-2.asc'];
freiPath2c = [freiPath '\pat016Iktal\010823ab-0042-2.asc'];

freiPath3a = [freiPath '\pat016Iktal\010823ab-0040-3.asc'];
freiPath3b = [freiPath '\pat016Iktal\010823ab-0041-3.asc'];
freiPath3c = [freiPath '\pat016Iktal\010823ab-0042-3.asc'];

freiPath4a = [freiPath '\pat016Iktal\010823ab-0040-4.asc'];
freiPath4b = [freiPath '\pat016Iktal\010823ab-0041-4.asc'];
freiPath4c = [freiPath '\pat016Iktal\010823ab-0042-4.asc'];

freiPath5a = [freiPath '\pat016Iktal\010823ab-0040-5.asc'];
freiPath5b = [freiPath '\pat016Iktal\010823ab-0041-5.asc'];
freiPath5c = [freiPath '\pat016Iktal\010823ab-0042-5.asc'];

freiPath6a = [freiPath '\pat016Iktal\010823ab-0040-6.asc'];
freiPath6b = [freiPath '\pat016Iktal\010823ab-0041-6.asc'];
freiPath6c = [freiPath '\pat016Iktal\010823ab-0042-6.asc'];

case '016_d' % patient 016 - interictal
blockNo = 7;
freiPath = 'X:\MatlabWork\1Research\SRC_DATA\Freiburg_Data\pat016';

freiPath1a = [freiPath '\pat016Interiktal\010827aa-0010-1.asc'];
freiPath1b = [freiPath '\pat016Interiktal\010827aa-0011-1.asc'];
freiPath1c = [freiPath '\pat016Interiktal\010827aa-0012-1.asc'];
freiPath1d = [freiPath '\pat016Interiktal\010827aa-0013-1.asc'];
freiPath1e = [freiPath '\pat016Interiktal\010827aa-0014-1.asc'];
freiPath1f = [freiPath '\pat016Interiktal\010827aa-0015-1.asc'];
freiPath1g = [freiPath '\pat016Interiktal\010827aa-0016-1.asc'];

freiPath2a = [freiPath '\pat016Interiktal\010827aa-0010-2.asc'];
freiPath2b = [freiPath '\pat016Interiktal\010827aa-0011-2.asc'];
freiPath2c = [freiPath '\pat016Interiktal\010827aa-0012-2.asc'];
freiPath2d = [freiPath '\pat016Interiktal\010827aa-0013-2.asc'];
freiPath2e = [freiPath '\pat016Interiktal\010827aa-0014-2.asc'];
freiPath2f = [freiPath '\pat016Interiktal\010827aa-0015-2.asc'];
freiPath2g = [freiPath '\pat016Interiktal\010827aa-0016-2.asc'];

freiPath3a = [freiPath '\pat016Interiktal\010827aa-0010-3.asc'];
freiPath3b = [freiPath '\pat016Interiktal\010827aa-0011-3.asc'];
freiPath3c = [freiPath '\pat016Interiktal\010827aa-0012-3.asc'];
freiPath3d = [freiPath '\pat016Interiktal\010827aa-0013-3.asc'];
freiPath3e = [freiPath '\pat016Interiktal\010827aa-0014-3.asc'];

```

```

freiPath3f = [freiPath '\\pat016Interiktal\010827aa_0015_3.asc'];
freiPath3g = [freiPath '\\pat016Interiktal\010827aa_0016_3.asc'];

freiPath4a = [freiPath '\\pat016Interiktal\010827aa_0010_4.asc'];
freiPath4b = [freiPath '\\pat016Interiktal\010827aa_0011_4.asc'];
freiPath4c = [freiPath '\\pat016Interiktal\010827aa_0012_4.asc'];
freiPath4d = [freiPath '\\pat016Interiktal\010827aa_0013_4.asc'];
freiPath4e = [freiPath '\\pat016Interiktal\010827aa_0014_4.asc'];
freiPath4f = [freiPath '\\pat016Interiktal\010827aa_0015_4.asc'];
freiPath4g = [freiPath '\\pat016Interiktal\010827aa_0016_4.asc'];

freiPath5a = [freiPath '\\pat016Interiktal\010827aa_0010_5.asc'];
freiPath5b = [freiPath '\\pat016Interiktal\010827aa_0011_5.asc'];
freiPath5c = [freiPath '\\pat016Interiktal\010827aa_0012_5.asc'];
freiPath5d = [freiPath '\\pat016Interiktal\010827aa_0013_5.asc'];
freiPath5e = [freiPath '\\pat016Interiktal\010827aa_0014_5.asc'];
freiPath5f = [freiPath '\\pat016Interiktal\010827aa_0015_5.asc'];
freiPath5g = [freiPath '\\pat016Interiktal\010827aa_0016_5.asc'];

freiPath6a = [freiPath '\\pat016Interiktal\010827aa_0010_6.asc'];
freiPath6b = [freiPath '\\pat016Interiktal\010827aa_0011_6.asc'];
freiPath6c = [freiPath '\\pat016Interiktal\010827aa_0012_6.asc'];
freiPath6d = [freiPath '\\pat016Interiktal\010827aa_0013_6.asc'];
freiPath6e = [freiPath '\\pat016Interiktal\010827aa_0014_6.asc'];
freiPath6f = [freiPath '\\pat016Interiktal\010827aa_0015_6.asc'];
freiPath6g = [freiPath '\\pat016Interiktal\010827aa_0016_6.asc'];

case '016_e' % patient 016, sz 4
blockNo = 2;
freiPath = 'X:\MatlabWork\1Research\SRC_DATA\Freiburg_Data\pat016';

freiPath1a = [freiPath '\\pat016Iktal\010823ab_0047_1.asc'];
freiPath1b = [freiPath '\\pat016Iktal\010823ab_0048_1.asc'];

freiPath2a = [freiPath '\\pat016Iktal\010823ab_0047_2.asc'];
freiPath2b = [freiPath '\\pat016Iktal\010823ab_0048_2.asc'];

freiPath3a = [freiPath '\\pat016Iktal\010823ab_0047_3.asc'];
freiPath3b = [freiPath '\\pat016Iktal\010823ab_0048_3.asc'];

freiPath4a = [freiPath '\\pat016Iktal\010823ab_0047_4.asc'];
freiPath4b = [freiPath '\\pat016Iktal\010823ab_0048_4.asc'];

freiPath5a = [freiPath '\\pat016Iktal\010823ab_0047_5.asc'];
freiPath5b = [freiPath '\\pat016Iktal\010823ab_0048_5.asc'];

freiPath6a = [freiPath '\\pat016Iktal\010823ab_0047_6.asc'];
freiPath6b = [freiPath '\\pat016Iktal\010823ab_0048_6.asc'];

case '016_f' % patient 016, sz 4
blockNo = 2;
freiPath = 'X:\MatlabWork\1Research\SRC_DATA\Freiburg_Data\pat016';

freiPath1a = [freiPath '\\pat016Iktal\010823ab_0082_1.asc'];
freiPath1b = [freiPath '\\pat016Iktal\010823ab_0083_1.asc'];

freiPath2a = [freiPath '\\pat016Iktal\010823ab_0082_2.asc'];
freiPath2b = [freiPath '\\pat016Iktal\010823ab_0083_2.asc'];

freiPath3a = [freiPath '\\pat016Iktal\010823ab_0082_3.asc'];
freiPath3b = [freiPath '\\pat016Iktal\010823ab_0083_3.asc'];

freiPath4a = [freiPath '\\pat016Iktal\010823ab_0082_4.asc'];
freiPath4b = [freiPath '\\pat016Iktal\010823ab_0083_4.asc'];

freiPath5a = [freiPath '\\pat016Iktal\010823ab_0082_5.asc'];
freiPath5b = [freiPath '\\pat016Iktal\010823ab_0083_5.asc'];

```

```

freiPath6a = [freiPath '\pat016Iktal\010823ab_0082_6.asc'];
freiPath6b = [freiPath '\pat016Iktal\010823ab_0083_6.asc'];

% ***** PATIENT 004 *****
case '004_1' % Patient 004 - seizure 1
blockNo = 2;
freiPath = 'X:\MatlabWork\1Research\SRC.DATA\Freiburg_Data\pat004';
freiPath1a = [freiPath '\pat004Iktal\010525bb_0206_1.asc'];
freiPath1b = [freiPath '\pat004Iktal\010525bb_0207_1.asc'];

freiPath2a = [freiPath '\pat004Iktal\010525bb_0206_2.asc'];
freiPath2b = [freiPath '\pat004Iktal\010525bb_0207_2.asc'];

freiPath3a = [freiPath '\pat004Iktal\010525bb_0206_3.asc'];
freiPath3b = [freiPath '\pat004Iktal\010525bb_0207_3.asc'];

freiPath4a = [freiPath '\pat004Iktal\010525bb_0206_4.asc'];
freiPath4b = [freiPath '\pat004Iktal\010525bb_0207_4.asc'];

freiPath5a = [freiPath '\pat004Iktal\010525bb_0206_5.asc'];
freiPath5b = [freiPath '\pat004Iktal\010525bb_0207_5.asc'];

freiPath6a = [freiPath '\pat004Iktal\010525bb_0206_6.asc'];
freiPath6b = [freiPath '\pat004Iktal\010525bb_0207_6.asc'];

case '004_3' % Patient 004 - seizure 1
blockNo = 2;
freiPath = 'X:\MatlabWork\1Research\SRC.DATA\Freiburg_Data\pat004';
freiPath1a = [freiPath '\pat004Iktal\010525bb_0316_1.asc'];
freiPath1b = [freiPath '\pat004Iktal\010525bb_0317_1.asc'];

freiPath2a = [freiPath '\pat004Iktal\010525bb_0316_2.asc'];
freiPath2b = [freiPath '\pat004Iktal\010525bb_0317_2.asc'];

freiPath3a = [freiPath '\pat004Iktal\010525bb_0316_3.asc'];
freiPath3b = [freiPath '\pat004Iktal\010525bb_0317_3.asc'];

freiPath4a = [freiPath '\pat004Iktal\010525bb_0316_4.asc'];
freiPath4b = [freiPath '\pat004Iktal\010525bb_0317_4.asc'];

freiPath5a = [freiPath '\pat004Iktal\010525bb_0316_5.asc'];
freiPath5b = [freiPath '\pat004Iktal\010525bb_0317_5.asc'];

freiPath6a = [freiPath '\pat004Iktal\010525bb_0316_6.asc'];
freiPath6b = [freiPath '\pat004Iktal\010525bb_0317_6.asc'];

case '004_4' % Patient 004 - seizure 4
blockNo = 2;
freiPath = 'X:\MatlabWork\1Research\SRC.DATA\Freiburg_Data\pat004';
freiPath1a = [freiPath '\pat004Iktal\010525bb_0322_1.asc'];
freiPath1b = [freiPath '\pat004Iktal\010525bb_0323_1.asc'];

freiPath2a = [freiPath '\pat004Iktal\010525bb_0322_2.asc'];
freiPath2b = [freiPath '\pat004Iktal\010525bb_0323_2.asc'];

freiPath3a = [freiPath '\pat004Iktal\010525bb_0322_3.asc'];
freiPath3b = [freiPath '\pat004Iktal\010525bb_0323_3.asc'];

freiPath4a = [freiPath '\pat004Iktal\010525bb_0322_4.asc'];
freiPath4b = [freiPath '\pat004Iktal\010525bb_0323_4.asc'];

freiPath5a = [freiPath '\pat004Iktal\010525bb_0322_5.asc'];
freiPath5b = [freiPath '\pat004Iktal\010525bb_0323_5.asc'];

freiPath6a = [freiPath '\pat004Iktal\010525bb_0322_6.asc'];
freiPath6b = [freiPath '\pat004Iktal\010525bb_0323_6.asc'];

case '004_5' % Patient 004 - seizure 5

```

```

blockNo = 2;
freiPath = 'X:\MatlabWork\1 Research\SRC_DATA\Freiburg_Data\pat004';
freiPath1a = [freiPath '\pat004Iktal\010525bb_0327.1.asc'];
freiPath1b = [freiPath '\pat004Iktal\010525bb_0328.1.asc'];

freiPath2a = [freiPath '\pat004Iktal\010525bb_0327.2.asc'];
freiPath2b = [freiPath '\pat004Iktal\010525bb_0328.2.asc'];

freiPath3a = [freiPath '\pat004Iktal\010525bb_0327.3.asc'];
freiPath3b = [freiPath '\pat004Iktal\010525bb_0328.3.asc'];

freiPath4a = [freiPath '\pat004Iktal\010525bb_0327.4.asc'];
freiPath4b = [freiPath '\pat004Iktal\010525bb_0328.4.asc'];

freiPath5a = [freiPath '\pat004Iktal\010525bb_0327.5.asc'];
freiPath5b = [freiPath '\pat004Iktal\010525bb_0328.5.asc'];

freiPath6a = [freiPath '\pat004Iktal\010525bb_0327.6.asc'];
freiPath6b = [freiPath '\pat004Iktal\010525bb_0328.6.asc'];

case '004_a' % Patient 004 - 6 hours interictal
blockNo = 6;
freiPath = 'X:\MatlabWork\1 Research\SRC_DATA\Freiburg_Data\pat004';
freiPath1a = [freiPath '\pat004InterIktal\010516ba_0016.1.asc'];
freiPath1b = [freiPath '\pat004InterIktal\010516ba_0017.1.asc'];
freiPath1c = [freiPath '\pat004InterIktal\010516ba_0018.1.asc'];
freiPath1d = [freiPath '\pat004InterIktal\010516ba_0019.1.asc'];
freiPath1e = [freiPath '\pat004InterIktal\010516ba_0020.1.asc'];
freiPath1f = [freiPath '\pat004InterIktal\010516ba_0021.1.asc'];

freiPath2a = [freiPath '\pat004InterIktal\010516ba_0016.2.asc'];
freiPath2b = [freiPath '\pat004InterIktal\010516ba_0017.2.asc'];
freiPath2c = [freiPath '\pat004InterIktal\010516ba_0018.2.asc'];
freiPath2d = [freiPath '\pat004InterIktal\010516ba_0019.2.asc'];
freiPath2e = [freiPath '\pat004InterIktal\010516ba_0020.2.asc'];
freiPath2f = [freiPath '\pat004InterIktal\010516ba_0021.2.asc'];

freiPath3a = [freiPath '\pat004InterIktal\010516ba_0016.3.asc'];
freiPath3b = [freiPath '\pat004InterIktal\010516ba_0017.3.asc'];
freiPath3c = [freiPath '\pat004InterIktal\010516ba_0018.3.asc'];
freiPath3d = [freiPath '\pat004InterIktal\010516ba_0019.3.asc'];
freiPath3e = [freiPath '\pat004InterIktal\010516ba_0020.3.asc'];
freiPath3f = [freiPath '\pat004InterIktal\010516ba_0021.3.asc'];

freiPath4a = [freiPath '\pat004InterIktal\010516ba_0016.4.asc'];
freiPath4b = [freiPath '\pat004InterIktal\010516ba_0017.4.asc'];
freiPath4c = [freiPath '\pat004InterIktal\010516ba_0018.4.asc'];
freiPath4d = [freiPath '\pat004InterIktal\010516ba_0019.4.asc'];
freiPath4e = [freiPath '\pat004InterIktal\010516ba_0020.4.asc'];
freiPath4f = [freiPath '\pat004InterIktal\010516ba_0021.4.asc'];

freiPath5a = [freiPath '\pat004InterIktal\010516ba_0016.5.asc'];
freiPath5b = [freiPath '\pat004InterIktal\010516ba_0017.5.asc'];
freiPath5c = [freiPath '\pat004InterIktal\010516ba_0018.5.asc'];
freiPath5d = [freiPath '\pat004InterIktal\010516ba_0019.5.asc'];
freiPath5e = [freiPath '\pat004InterIktal\010516ba_0020.5.asc'];
freiPath5f = [freiPath '\pat004InterIktal\010516ba_0021.5.asc'];

freiPath6a = [freiPath '\pat004InterIktal\010516ba_0016.6.asc'];
freiPath6b = [freiPath '\pat004InterIktal\010516ba_0017.6.asc'];
freiPath6c = [freiPath '\pat004InterIktal\010516ba_0018.6.asc'];
freiPath6d = [freiPath '\pat004InterIktal\010516ba_0019.6.asc'];
freiPath6e = [freiPath '\pat004InterIktal\010516ba_0020.6.asc'];
freiPath6f = [freiPath '\pat004InterIktal\010516ba_0021.6.asc'];

% ***** PATIENT 012 *****
case '012_2' % Patient 012 - seizure 2

```

```

blockNo = 2;
freiPath = 'X:\MatlabWork\1Research\SRC.DATA\Freiburg_Data\pat012';
freiPath1a = [freiPath '\pat012Iktal\011211ea_0004.1.asc'];
freiPath1b = [freiPath '\pat012Iktal\011211ea_0005.1.asc'];

freiPath2a = [freiPath '\pat012Iktal\011211ea_0004.2.asc'];
freiPath2b = [freiPath '\pat012Iktal\011211ea_0005.2.asc'];

freiPath3a = [freiPath '\pat012Iktal\011211ea_0004.3.asc'];
freiPath3b = [freiPath '\pat012Iktal\011211ea_0005.3.asc'];

freiPath4a = [freiPath '\pat012Iktal\011211ea_0004.4.asc'];
freiPath4b = [freiPath '\pat012Iktal\011211ea_0005.4.asc'];

freiPath5a = [freiPath '\pat012Iktal\011211ea_0004.5.asc'];
freiPath5b = [freiPath '\pat012Iktal\011211ea_0005.5.asc'];

freiPath6a = [freiPath '\pat012Iktal\011211ea_0004.6.asc'];
freiPath6b = [freiPath '\pat012Iktal\011211ea_0005.6.asc'];

case '012_3' % Patient 012 - seizure 3
blockNo = 3;
freiPath = 'X:\MatlabWork\1Research\SRC.DATA\Freiburg_Data\pat012';
freiPath1a = [freiPath '\pat012Iktal\011211ea_0016.1.asc'];
freiPath1b = [freiPath '\pat012Iktal\011211ea_0017.1.asc'];
freiPath1c = [freiPath '\pat012Iktal\011211ea_0018.1.asc'];

freiPath2a = [freiPath '\pat012Iktal\011211ea_0016.2.asc'];
freiPath2b = [freiPath '\pat012Iktal\011211ea_0017.2.asc'];
freiPath2c = [freiPath '\pat012Iktal\011211ea_0018.2.asc'];

freiPath3a = [freiPath '\pat012Iktal\011211ea_0016.3.asc'];
freiPath3b = [freiPath '\pat012Iktal\011211ea_0017.3.asc'];
freiPath3c = [freiPath '\pat012Iktal\011211ea_0018.3.asc'];

freiPath4a = [freiPath '\pat012Iktal\011211ea_0016.4.asc'];
freiPath4b = [freiPath '\pat012Iktal\011211ea_0017.4.asc'];
freiPath4c = [freiPath '\pat012Iktal\011211ea_0018.4.asc'];

freiPath5a = [freiPath '\pat012Iktal\011211ea_0016.5.asc'];
freiPath5b = [freiPath '\pat012Iktal\011211ea_0017.5.asc'];
freiPath5c = [freiPath '\pat012Iktal\011211ea_0018.5.asc'];

freiPath6a = [freiPath '\pat012Iktal\011211ea_0016.6.asc'];
freiPath6b = [freiPath '\pat012Iktal\011211ea_0017.6.asc'];
freiPath6c = [freiPath '\pat012Iktal\011211ea_0018.6.asc'];

case '012_4' % Patient 012 - seizure 4
blockNo = 2;
freiPath = 'X:\MatlabWork\1Research\SRC.DATA\Freiburg_Data\pat012';
freiPath1a = [freiPath '\pat012Iktal\011211ea_0018.1.asc'];
freiPath1b = [freiPath '\pat012Iktal\011211ea_0019.1.asc'];

freiPath2a = [freiPath '\pat012Iktal\011211ea_0018.2.asc'];
freiPath2b = [freiPath '\pat012Iktal\011211ea_0019.2.asc'];

freiPath3a = [freiPath '\pat012Iktal\011211ea_0018.3.asc'];
freiPath3b = [freiPath '\pat012Iktal\011211ea_0019.3.asc'];

freiPath4a = [freiPath '\pat012Iktal\011211ea_0018.4.asc'];
freiPath4b = [freiPath '\pat012Iktal\011211ea_0019.4.asc'];

freiPath5a = [freiPath '\pat012Iktal\011211ea_0018.5.asc'];
freiPath5b = [freiPath '\pat012Iktal\011211ea_0019.5.asc'];

freiPath6a = [freiPath '\pat012Iktal\011211ea_0018.6.asc'];
freiPath6b = [freiPath '\pat012Iktal\011211ea_0019.6.asc'];

```

```

case '012_a' % Patient 012 -6 hours of interictal
    blockNo = 6;
    freiPath = 'X:\MatlabWork\1Research\SRC_DATA\Freiburg_Data\pat012';
    freiPath1a = [freiPath '\pat012InterIktal\011205ea_0021.1.asc'];
    freiPath1b = [freiPath '\pat012InterIktal\011205ea_0022.1.asc'];
    freiPath1c = [freiPath '\pat012InterIktal\011205ea_0023.1.asc'];
    freiPath1d = [freiPath '\pat012InterIktal\011205ea_0024.1.asc'];
    freiPath1e = [freiPath '\pat012InterIktal\011205ea_0025.1.asc'];
    freiPath1f = [freiPath '\pat012InterIktal\011205ea_0026.1.asc'];

    freiPath2a = [freiPath '\pat012InterIktal\011205ea_0021.2.asc'];
    freiPath2b = [freiPath '\pat012InterIktal\011205ea_0022.2.asc'];
    freiPath2c = [freiPath '\pat012InterIktal\011205ea_0023.2.asc'];
    freiPath2d = [freiPath '\pat012InterIktal\011205ea_0024.2.asc'];
    freiPath2e = [freiPath '\pat012InterIktal\011205ea_0025.2.asc'];
    freiPath2f = [freiPath '\pat012InterIktal\011205ea_0026.2.asc'];

    freiPath3a = [freiPath '\pat012InterIktal\011205ea_0021.3.asc'];
    freiPath3b = [freiPath '\pat012InterIktal\011205ea_0022.3.asc'];
    freiPath3c = [freiPath '\pat012InterIktal\011205ea_0023.3.asc'];
    freiPath3d = [freiPath '\pat012InterIktal\011205ea_0024.3.asc'];
    freiPath3e = [freiPath '\pat012InterIktal\011205ea_0025.3.asc'];
    freiPath3f = [freiPath '\pat012InterIktal\011205ea_0026.3.asc'];

    freiPath4a = [freiPath '\pat012InterIktal\011205ea_0021.4.asc'];
    freiPath4b = [freiPath '\pat012InterIktal\011205ea_0022.4.asc'];
    freiPath4c = [freiPath '\pat012InterIktal\011205ea_0023.4.asc'];
    freiPath4d = [freiPath '\pat012InterIktal\011205ea_0024.4.asc'];
    freiPath4e = [freiPath '\pat012InterIktal\011205ea_0025.4.asc'];
    freiPath4f = [freiPath '\pat012InterIktal\011205ea_0026.4.asc'];

    freiPath5a = [freiPath '\pat012InterIktal\011205ea_0021.5.asc'];
    freiPath5b = [freiPath '\pat012InterIktal\011205ea_0022.5.asc'];
    freiPath5c = [freiPath '\pat012InterIktal\011205ea_0023.5.asc'];
    freiPath5d = [freiPath '\pat012InterIktal\011205ea_0024.5.asc'];
    freiPath5e = [freiPath '\pat012InterIktal\011205ea_0025.5.asc'];
    freiPath5f = [freiPath '\pat012InterIktal\011205ea_0026.5.asc'];

    freiPath6a = [freiPath '\pat012InterIktal\011205ea_0021.6.asc'];
    freiPath6b = [freiPath '\pat012InterIktal\011205ea_0022.6.asc'];
    freiPath6c = [freiPath '\pat012InterIktal\011205ea_0023.6.asc'];
    freiPath6d = [freiPath '\pat012InterIktal\011205ea_0024.6.asc'];
    freiPath6e = [freiPath '\pat012InterIktal\011205ea_0025.6.asc'];
    freiPath6f = [freiPath '\pat012InterIktal\011205ea_0026.6.asc'];

```

```
end
```

```
CH01 = []; CH02 = []; CH03 = []; CH04 = []; CH05 = []; CH06 = [];
```

```
switch blockNo
```

```

    case 2
        data_a = load(freiPath1a);
        data_b = load(freiPath1b);
        CH01 = [data_a; data_b];
        clear data_a data_b
        data_a = load(freiPath2a);
        data_b = load(freiPath2b);
        CH02 = [data_a; data_b];
        clear data_a data_b
        data_a = load(freiPath3a);
        data_b = load(freiPath3b);
        CH03 = [data_a; data_b];
        clear data_a data_b
        data_a = load(freiPath4a);
        data_b = load(freiPath4b);
        CH04 = [data_a; data_b];
        clear data_a data_b

```

```

data_a = load(freiPath5a);
data_b = load(freiPath5b);
CH05 = [data_a; data_b];
clear data_a data_b
data_a = load(freiPath6a);
data_b = load(freiPath6b);
CH06 = [data_a; data_b];
clear data_a data_b

```

case 3

```

data_a = load(freiPath1a);
data_b = load(freiPath1b);
data_c = load(freiPath1c);
CH01 = [data_a; data_b; data_c];
clear data_a data_b data_c
data_a = load(freiPath2a);
data_b = load(freiPath2b);
data_c = load(freiPath2c);
CH02 = [data_a; data_b; data_c];
clear data_a data_b data_c
data_a = load(freiPath3a);
data_b = load(freiPath3b);
data_c = load(freiPath3c);
CH03 = [data_a; data_b; data_c];
clear data_a data_b data_c
data_a = load(freiPath4a);
data_b = load(freiPath4b);
data_c = load(freiPath4c);
CH04 = [data_a; data_b; data_c];
clear data_a data_b data_c
data_a = load(freiPath5a);
data_b = load(freiPath5b);
data_c = load(freiPath5c);
CH05 = [data_a; data_b; data_c];
clear data_a data_b data_c
data_a = load(freiPath6a);
data_b = load(freiPath6b);
data_c = load(freiPath6c);
CH06 = [data_a; data_b; data_c];
clear data_a data_b data_c

```

case 4

```

data_a = load(freiPath1a);
data_b = load(freiPath1b);
data_c = load(freiPath1c);
data_d = load(freiPath1d);
CH01 = [data_a; data_b; data_c; data_d];
clear data_a data_b data_c
data_a = load(freiPath2a);
data_b = load(freiPath2b);
data_c = load(freiPath2c);
data_d = load(freiPath2d);
CH02 = [data_a; data_b; data_c; data_d];
clear data_a data_b data_c
data_a = load(freiPath3a);
data_b = load(freiPath3b);
data_c = load(freiPath3c);
data_d = load(freiPath3d);
CH03 = [data_a; data_b; data_c; data_d];
clear data_a data_b data_c
data_a = load(freiPath4a);
data_b = load(freiPath4b);
data_c = load(freiPath4c);
data_d = load(freiPath4d);
CH04 = [data_a; data_b; data_c; data_d];
clear data_a data_b data_c
data_a = load(freiPath5a);
data_b = load(freiPath5b);

```



```

data_c = load(freiPath5c);
data_d = load(freiPath5d);
CH05 = [data_a; data_b; data_c; data_d];
clear data_a data_b data_c
data_a = load(freiPath6a);
data_b = load(freiPath6b);
data_c = load(freiPath6c);
data_d = load(freiPath6d);
CH06 = [data_a; data_b; data_c; data_d];
clear data_a data_b data_c

case 6
data_a = load(freiPath1a);
data_b = load(freiPath1b);
data_c = load(freiPath1c);
data_d = load(freiPath1d);
data_e = load(freiPath1e);
data_f = load(freiPath1f);
CH01 = [data_a; data_b; data_c; data_d; data_e; data_f];
clear data_a data_b data_c
data_a = load(freiPath2a);
data_b = load(freiPath2b);
data_c = load(freiPath2c);
data_d = load(freiPath2d);
data_e = load(freiPath2e);
data_f = load(freiPath2f);
CH02 = [data_a; data_b; data_c; data_d; data_e; data_f];
clear data_a data_b data_c
data_a = load(freiPath3a);
data_b = load(freiPath3b);
data_c = load(freiPath3c);
data_d = load(freiPath3d);
data_e = load(freiPath3e);
data_f = load(freiPath3f);
CH03 = [data_a; data_b; data_c; data_d; data_e; data_f];
clear data_a data_b data_c
data_a = load(freiPath4a);
data_b = load(freiPath4b);
data_c = load(freiPath4c);
data_d = load(freiPath4d);
data_e = load(freiPath4e);
data_f = load(freiPath4f);
CH04 = [data_a; data_b; data_c; data_d; data_e; data_f];
clear data_a data_b data_c
data_a = load(freiPath5a);
data_b = load(freiPath5b);
data_c = load(freiPath5c);
data_d = load(freiPath5d);
data_e = load(freiPath5e);
data_f = load(freiPath5f);
CH05 = [data_a; data_b; data_c; data_d; data_e; data_f];
clear data_a data_b data_c
data_a = load(freiPath6a);
data_b = load(freiPath6b);
data_c = load(freiPath6c);
data_d = load(freiPath6d);
data_e = load(freiPath6e);
data_f = load(freiPath6f);
CH06 = [data_a; data_b; data_c; data_d; data_e; data_f];
clear data_a data_b data_c

case 7
data_a = load(freiPath1a);
data_b = load(freiPath1b);
data_c = load(freiPath1c);
data_d = load(freiPath1d);
data_e = load(freiPath1e);
data_f = load(freiPath1f);

```

```

data_g = load(freiPath1g);
CH01 = [data_a; data_b; data_c; data_d; data_e; data_f; data_g];
clear data_a data_b data_c
data_a = load(freiPath2a);
data_b = load(freiPath2b);
data_c = load(freiPath2c);
data_d = load(freiPath2d);
data_e = load(freiPath2e);
data_f = load(freiPath2f);
data_g = load(freiPath2g);
CH02 = [data_a; data_b; data_c; data_d; data_e; data_f; data_g];
clear data_a data_b data_c
data_a = load(freiPath3a);
data_b = load(freiPath3b);
data_c = load(freiPath3c);
data_d = load(freiPath3d);
data_e = load(freiPath3e);
data_f = load(freiPath3f);
data_g = load(freiPath3g);
CH03 = [data_a; data_b; data_c; data_d; data_e; data_f; data_g];
clear data_a data_b data_c
data_a = load(freiPath4a);
data_b = load(freiPath4b);
data_c = load(freiPath4c);
data_d = load(freiPath4d);
data_e = load(freiPath4e);
data_f = load(freiPath4f);
data_g = load(freiPath4g);
CH04 = [data_a; data_b; data_c; data_d; data_e; data_f; data_g];
clear data_a data_b data_c
data_a = load(freiPath5a);
data_b = load(freiPath5b);
data_c = load(freiPath5c);
data_d = load(freiPath5d);
data_e = load(freiPath5e);
data_f = load(freiPath5f);
data_g = load(freiPath5g);
CH05 = [data_a; data_b; data_c; data_d; data_e; data_f; data_g];
clear data_a data_b data_c
data_a = load(freiPath6a);
data_b = load(freiPath6b);
data_c = load(freiPath6c);
data_d = load(freiPath6d);
data_e = load(freiPath6e);
data_f = load(freiPath6f);
data_g = load(freiPath6g);
CH06 = [data_a; data_b; data_c; data_d; data_e; data_f; data_g];
clear data_a data_b data_c

end
%% Save assembled data
s = ['save' blanks(1) pname '\ ' patId '-' runinfo];
eval(s);
clear s

end

```

H.5 freiburg_dataprep.m

```

%% FREIBURG.DATAPREP -
% This program prepares the Freiburg data for submission to the EVAM
% program.
%
% *****
% Daniel Moller
% PhD Candidate, Biomedical Engineering
% Louisiana Tech University
% dwm027@latech.edu
% -----
% Author: Daniel Moller
% Program: freiburg.m           Version: 1.0.00
% Original Date: 2/8/11
%
% Function calls:
% none
%
% Function called by:
%
%
% Revision History (include version, programmer, date and description)
% =====
% 1.0.00 (Orig) D. Moller 2/8/11
% copied from freiburg.m
%
% Notes
% *****
% *****

clear all; close all

%% Set up Filenames & Choose Patient/Blocks/other
runinfo1 = datestr(now, 'yymmdd');
runinfo2 = datestr(now, 'HHMM');
runinfo = strcat(runinfo1, '-', runinfo2);
pname = 'X:\MatlabWork\1Research\SRC.DATA\Freiburg_Data\mat';
Fs = 256;

% enter <patient ID>-<seizure number> as text
% patIdcell{1} = '004-a';
% patIdcell{2} = '016-2';
% patIdcell{3} = '016-3';
% patIdcell{4} = '016-4';
% patIdcell{5} = '016-5';

[f_s] = fileselect;
[listing] = ls(f_s(1).pname);
[nofiles, dummy] = size(listing);
nofiles = nofiles - 2; % get rid of . and ..

for i = 1:6:nofiles
    for j = 0:5
        tempf{i+j} = listing(i+j+2,:);
    end
end

[patindex] = strfind(f_s(1).pname, 'pat');
patId = f_s(1).pname(patindex(1)+3:patindex(1)+5)

[eegindex] = strfind(f_s(1).pname, 'Inter');
if ~isempty(eegindex)
    eegtypeflag = 0;
else

```

```

    eegtypeflag = 1;
end
clear listing patindex eegindex
noch = 6;
maxblocks = 10;

for i = 1:noch:nofiles
    for j = 0:noch-1
        if ~strcmp(tempf{i}(1:length(tempf{i})-5),...
            tempf{i+j}(1:length(tempf{i+j})-5))
            error('data files missing')
        end
    end
end
if i == 1
    switch eegtypeflag
        case 0
            patId = [patId '_a']
        case 1
            sznum = 1;
            patId = [patId '_s' num2str(sznum)]
            sznum = sznum+1;
        end
    consecblocks = 1;
    fnames{consecblocks} = tempf{i};
    CH01 = []; CH02 = []; CH03 = [];
    CH04 = []; CH05 = []; CH06 = [];

else
    oldfile = ...
        str2num(tempf{i-noch}(length(tempf{i-noch})-9:length(tempf{i-noch})-6))←
        ;
    newfile = ...
        str2num(tempf{i}(length(tempf{i})-9:length(tempf{i})-6));
    if ((newfile-oldfile ~= 1) || ...
        ~strcmp(tempf{i-noch}(1:length(tempf{i-noch})-10),...
            tempf{i}(1:length(tempf{i})-10))) || ...
        consecblocks == maxblocks+1;
        savefile = [pname '\' patId];
        save(savefile, 'CH*', 'Fs', 'runinfo', 'patId', 'fnames');
        switch eegtypeflag
            case 0
                newletter = increment_letter(patId(length(patId)));
                patId = [patId(1:length(patId)-1) newletter]
            case 1
                patId = [patId(1:length(patId)-1) num2str(sznum)]
                sznum = sznum+1;
            end
        consecblocks = 1; clear fnames
        CH01 = []; CH02 = []; CH03 = [];
        CH04 = []; CH05 = []; CH06 = [];
    end
end
data_temp1 = load([f_s(1).pname tempf{i}]);
data_temp2 = load([f_s(1).pname tempf{i+1}]);
data_temp3 = load([f_s(1).pname tempf{i+2}]);
data_temp4 = load([f_s(1).pname tempf{i+3}]);
data_temp5 = load([f_s(1).pname tempf{i+4}]);
data_temp6 = load([f_s(1).pname tempf{i+5}]);

CH01 = [CH01; data_temp1];
CH02 = [CH02; data_temp2];
CH03 = [CH03; data_temp3];
CH04 = [CH04; data_temp4];
CH05 = [CH05; data_temp5];
CH06 = [CH06; data_temp6];
fnames{consecblocks} = tempf{i};
consecblocks = consecblocks+1;

```

```
if i+noch > nofiles
    savefile = [pname '\ ' patId];
    save(savefile, 'CH*', 'Fs', 'runinfo', 'patId', 'fnames');
end
end
```

H.6 full_emd_coh_func.m

```

function full_emd_coh_func(patId , iistart , iistop , iinewname)
%% FULLEEMD_COH_FUNCT -
% This program analyzes the Freiburg dataset in an automated fashion.
%
% *****
% Daniel Moller
% PhD Candidate, Biomedical Engineering
% Louisiana Tech University
% dwm027@latech.edu
% -----
% Author: Daniel Moller
% Program: full_emd_coh.m           Version: 1.0.00
% Original Date: 2/15/11
%
% Function calls:
% none
%
% Function called by:
%
%
% Revision History (include version, programmer, date and description)
% =====
% 1.0.00 (Orig) D. Moller 2/15/11
%
% Notes
% *****
%
% *****
if nargin == 1
    iistart = 0; iistop = 0; iinewname = '';
end
disp(iinewname)

% Clear workspace and close open figures
clc; close all; warning off;
[comp,pathname] = chkcomp;
pathname_data = '1Research\SRC.DATA\Freiburg_Data\mat\ '
tic

dataSet{1} = patId

%% Set up Filenames & Choose Patient/Blocks/other
runinfo1 = datestr(now, 'yymmdd');
runinfo2 = datestr(now, 'HHMM');
runinfo = strcat(runinfo1, '-', runinfo2)
pname = 'X:\MatlabWork\1Research\SRC.DATA\Freiburg_Data\mat\';
Fs = 256;

%% Training Parameters
preprocessflag = 1;
emdflag = 1;
filtplan = '000'; % bandstop(49.5-50.5), lowpass(120), highpass(5)
twindow = 16;
noiselev = 0.1;
trials = 50;
% cov_type = 'full';
% pcaflag = 0;
% splvflag = 0;
% wavflag = 1; % obtains wavelet coefficients for signal data
% cohflag = 0; % obtains coherence values for signal data
% wavcohflag = 0; % obtains wavelet coherence values
% waverflag = 0;
% plotflag = 0; % plot (1) or don't plot (0)
% figflag = 0; % save figures as .fig (1), as .jpg (0)

```

```

% shuffle = 0;

%% Select data set: seizures & channels
% for naming reasons, order these with smallest patId and earliest szr
chan{1,1} = 'CH01';
chan{1,2} = 'CH02';
chan{1,3} = 'CH03';
chan{1,4} = 'CH04';
chan{1,5} = 'CH05';
chan{1,6} = 'CH06';

%% Modify order of training
% if shuffle == 1
%   r = rand(1, length(dataSet));
%   r = [r; 1:length(dataSet)];
%   r = r';
%   r = sortrows(r);
%   for i = 1:length(dataSet);
%       tempSet{i} = dataSet{r(i,2)};
%   end
%   r = r(:,2);
%   notrain = length(r);
%   dSet = tempSet;
%   clear shuffle tempSet
% else
%   nocases = length(dataSet);
%   r = [1:nocases]';
%   dSet = dataSet;
% end

nocases = length(dataSet);
r = [1:nocases]';
dSet = dataSet;

%% Timestamp
runinfo1 = datestr(now, 'yymmdd');
runinfo2 = datestr(now, 'HHMM');
runinfo = strcat(runinfo1, '-', runinfo2);

[caselist] = feat_caselist2(dataSet, Fs, iistart, iistop);

for szr = 1:nocases
    %% Load data
    chdata = [];
    [dummy, nochan] = size(chan);
    for k = 1:nochan
        %   patId = trainSet{r(szr)};
        channel = chan{r(szr), k};
        emdinput(szr, k, 1).channel = channel;
        load(caselist(szr).fullname, 'Fs')
        load(caselist(szr).fullname, channel)
        %   assignin('caller', channel, eval(channel))
        %   assignin('caller', 'chantext', ['clear(' '''' channel '''' ')'])
        %   tempchdata = evalin('caller', channel);
        %   evalin('caller', chantext)
        %   clear(channel);
        tempchdata = eval(channel);

        %   figure;
        %   subplot(1,2,1); plot(tempchdata); hold on; subplot(1,2,2); plot(CH01)
        % caselist(szr).tstart
        % caselist(szr).tstop
        %   whos
        %   pause
        %   chdata
        chdata(k,:) = ...
            [tempchdata(caselist(szr).tstart*Fs+1:caselist(szr).tstop*Fs)];
        clear tempchdata
    end
    tt=toc;
end

```

```

        fprintf('Loaded Channel %i at %5.1f minutes\n',k,tt/60);
    %     pause
end
fprintf('\n')
epochs = floor(length(chdata)/(Fs*twindow));

%% Preprocess Data
for k = 1:nochan
    for i = 1:epochs
        tempdata = chdata(k,(i-1)*(Fs*twindow)+1:i*(Fs*twindow));
        [emdininput(szr,k,i).ppdata] = preprocess_frei(tempdata,Fs,filtplan,1,1);
        clear tempdata
    end
    tt=toc;
    fprintf('Preprocessed Channel %i at %5.1f minutes\n',k,tt/60);
end
fprintf('\n')

%% EEMD
if emdflag == 1
    fprintf('STARTING EMD\n')
    for k = 1:nochan
        j = 1;
        for i = 1:epochs
            tempdata = emdininput(szr,k,i).ppdata;
            emdininput(szr,k,i).allmode = eemd(tempdata,noiselev, trials);
            clear tempdata;
            if rem(j,5)==0
                tt=toc;
                fprintf('  EMD CH %i, epoch %i @ %5.4f min\n',k,i,tt/60)
            end
            j = j+1;
        end
        tt=toc;
        fprintf('EMD Analysis of Channel %i complete at %5.4f minutes\n',k,tt←
            /60);
    end
end
end
for i = 1:length(dataSet)
    savename = [dataSet{i} '-'];
    if length(iinewname) ~= 0
        savename = [iinewname '-'];
    end
    %     for j = 1:length(chan)
    %         savename = [savename chan{j}];
    %     end
    savename = [savename 'CH1to6-'];
end
savename = [savename num2str(twindow) '.mat'];
save(savename,'emdininput','Fs','filtplan','twindow','runinfo')

%% Analyze Coherence
[dummy,nochan,epochs] = size(emdininput);
k=1;
for i = 1:nochan-1
    for j = i+1:nochan
        tvcpair(k,:) = [i j];
        k = k+1;
    end
end
[pairno,dummy] = size(tvcpair);
for i = 1:pairno
    for j = 1:epochs
        [dummy,modesplus1] = size(emdininput(1,1,1).allmode);
        nomodes = modesplus1 - 1;
        for m = 1:nomodes

```



```

        tempdata1 = ...
            emdinput(1, tvcpair(i,1), j).allmode(:, m+1);
        tempdata2 = ...
            emdinput(1, tvcpair(i,2), j).allmode(:, m+1);
%       [cohpair2(i).coh(m,j), freq(m,j)] = ...
%       mscohere(tempdata1, tempdata2, [], [], Fs);
        cohpair(i).coh(m,j) = ...
            mean(mscohere(tempdata1, tempdata2, [], [], Fs));
        cohpairstd(i).coh(m,j) = ...
            std(mscohere(tempdata1, tempdata2, [], [], Fs));
        clear tempdata1 tempdata2
    end
end
disp(i)
toc
end
% for i = 1:pairno
%     for j = 1:epochs
%         scftr = (length(cohpair(i).coh)-1)/(Fs/2);
%         for k = nextpow2(Fs)-1:-1:1
%             cohpair(i,m).cohdata(k,j) = ...
%                 mean(cohpair(i).coh((2^(k-1))*scftr+2:(2^k)*scftr+1,j));
%         end
%         cohpair(i).cohdata(1,j) = mean(cohpair(i).coh(1:scftr+1,j));
%     end
% end
savename = [savename(1:length(savename)-4) '_coh.mat'];

save(savename, 'cohpair', 'cohpairstd', 'tvcpair')

```

H.7 mcoh.m

```

function [mcohdat] = mcoh(fname, folder)
% mcoh -
% maximum coherence value
%
% *****
% Daniel Moller
% PhD Program Graduate Student in Biomedical Engineering
% Louisiana Tech University
% dwm027@latech.edu
% -----
% Author: Daniel Moller
% Program: mcoh.m          Version: 1.0.00
% Original Date: 7/18/10
%
% Function calls:
%
% Function called by:
%
% Revision History (include version, programmer, date and description)
% =====
% 1.0.00 <orig>    D. Moller    7/18/10
%
% Notes
% *****
% for j=1:2;
%     for i=2:13;
%         dat = emdinput(1,j,1).allmode(:,i);
%         x(j,:) = angle(hilbert(dat));
%         [fftfreq fftdata] = ssfft(dat,256);
%         figure; subplot(2,1,1);
%         plot(fftfreq, fftdata);
%         subplot(2,1,2);
%         plot(x(j,:));
%         clear fftfreq fftdata;
%     end
% end
% command line testing:
% close all; for j=1:2; for i=2:13; dat = emdinput(1,j,1).allmode(:,i); x(j,:) = ←
%     angle(hilbert(dat)); [fftfreq fftdata] = ssfft(dat,256); figure; subplot(2,1,1)←
%     ; plot(fftfreq, fftdata); subplot(2,1,2); plot(x(j,:)); clear fftfreq fftdata; ←
%     end; end
% for j = 1:15; for i = 20:length(mcohdat(j).mcoh(1,:)); mcohdat(j).avemcoh(:,i)= ←
%     mean(mcohdat(j).mcoh(:,i-19:i),2); end; end
% for j = 1:15; figure; for i = 1:12; subplot(6,2,i); title(['CH Pair Number:' ←
%     num2str(j)]); hold on; ylabel(['IMF' num2str(i)]); hold on; plot(mcohdat(j).←
%     avemcoh(i,:)); hold on; plot([225 225],[0 1], 'r');end;end
% *****
tic
Fs = 256;

if nargin == 1
    folder = '.';
end

if isempty(findstr(fname, '.mat'))
    savename = [folder '/' fname(1:length(fname)-4) '_mcoh.mat']
    fname = [folder '/' fname];
else
    savename = [folder '/' fname '_mcoh.mat']
    fname = [folder '/' fname '.mat'];
end

noimfs = 12;

load(fname, 'emdinput')

```

```

[dummy,nochan,epochs] = size(emdinput);
ind = 1;
for i = 1:nochan-1
    for j = i+1:nochan
        pairno(ind,1) = i;
        pairno(ind,2) = j;
        ind = ind+1;
    end
end
nopair = ind-1;

for j = 1:nopair
    for i = 1:noimfs
        for k = 1:epochs
            temp1 = emdinput(1,pairno(j,1),k).allmode(:,i+1);
            temp2 = emdinput(1,pairno(j,2),k).allmode(:,i+1);
            temp3 = mscohere(temp1,temp2,[],[],Fs);
            mcohdatt(j).mcoh(i,k) = ...
                max(abs(temp3));
            clear temp1 temp2 temp3
        end
    end
end
tt = toc;
% fprintf('Channel pair#:%i at time %5.2f\n',j,tt)
end

clear emdinput
save(savename,'mcohdatt');

```

H.8 patSelectinfo.m

```

%% FUNCTION for patSelectinfo
function [fnames] = patSelectinfo(patSelect , twindow , type);

if nargin == 2
    type = 'coh';
end

for i = 1:length(patSelect)
    patId = patSelect{i}
    % NOTE fnames{2,x} = seizure file
    %       fname{1,x} = interictal file
    switch patId
        case '001'
            if twindow == 16
                fnames{2,1} = '001_1-CH1to6-16-';
                fnames{2,2} = '001_2-CH1to6-16-';
                fnames{2,3} = '001_3-CH1to6-16-';
                fnames{2,4} = '001_4-CH1to6-16-';

                fnames{1,1} = '001_ii0to1-CH1to6-16-';
                fnames{1,2} = '001_ii1to2-CH1to6-16-';
                fnames{1,3} = '001_ii2to3-CH1to6-16-';
                fnames{1,4} = '001_ii3to4-CH1to6-16-';
                fnames{1,5} = '001_ii4to5-CH1to6-16-';
                fnames{1,6} = '001_ii5to6-CH1to6-16-';
            end
        case '002'
            if twindow == 16
                fnames{2,1} = '002_1-CH1to6-16-';
                fnames{2,2} = '002_2-CH1to6-16-';
                fnames{2,3} = '002_3-CH1to6-16-';

                fnames{1,1} = '002_ii0to1-CH1to6-16-';
                fnames{1,2} = '002_ii1to2-CH1to6-16-';
                fnames{1,3} = '002_ii2to3-CH1to6-16-';
                fnames{1,4} = '002_ii3to4-CH1to6-16-';
                fnames{1,5} = '002_ii4to5-CH1to6-16-';
                fnames{1,6} = '002_ii5to6-CH1to6-16-';
            end
        case '003'
            if twindow == 16
                fnames{2,1} = '003_1-CH1to6-16-';
                fnames{2,2} = '003_2-CH1to6-16-';
                fnames{2,3} = '003_3-CH1to6-16-';
                fnames{2,4} = '003_4-CH1to6-16-';
                fnames{2,5} = '003_5-CH1to6-16-';

                fnames{1,1} = '003_ii0to1-CH1to6-16-';
                fnames{1,2} = '003_ii1to2-CH1to6-16-';
                fnames{1,3} = '003_ii2to3-CH1to6-16-';
                fnames{1,4} = '003_ii3to4-CH1to6-16-';
                fnames{1,5} = '003_ii4to5-CH1to6-16-';
                fnames{1,6} = '003_ii5to6-CH1to6-16-';
            end
        case '004'
            if twindow == 16
                fnames{2,1} = '004_1-CH1to6-16-';
                fnames{2,2} = '004_2-CH1to6-16-';
                fnames{2,3} = '004_3-CH1to6-16-???';
                fnames{2,4} = '004_4-CH1to6-16-';
                fnames{2,5} = '004_5-CH1to6-16-';

                fnames{1,1} = '004_ii0to1-CH1to6-16-';
            end
    end
end

```

```

        fnames{1,2} = '004_ii1to2_CH1to6_16_';
        fnames{1,3} = '004_ii2to3_CH1to6_16_';
        fnames{1,4} = '004_ii3to4_CH1to6_16_';
        fnames{1,5} = '004_ii4to5_CH1to6_16_';
        fnames{1,6} = '004_ii5to6_CH1to6_16_';

        elseif twindow == 32
        end
    case '005'
        if twindow == 16
            fnames{2,1} = '005_1_CH1to6_16_';
            fnames{2,2} = '005_2_CH1to6_16_???';
            fnames{2,3} = '005_3_CH1to6_16_???';
            fnames{2,4} = '005_4_CH1to6_16_';
            fnames{2,5} = '005_5_CH1to6_16_';

            fnames{1,1} = '005_ii1to2_CH1to6_16_';
            fnames{1,2} = '005_ii2to3_CH1to6_16_';
            fnames{1,3} = '005_ii3to4_CH1to6_16_';
            fnames{1,4} = '005_ii4to5_CH1to6_16_';
            fnames{1,5} = '005_ii5to6_CH1to6_16_';
            fnames{1,6} = '005_ii6to7_CH1to6_16_';
        end
    case '006'
        if twindow == 16
            fnames{2,1} = '006_1_CH1to6_16_';
            fnames{2,2} = '006_2_CH1to6_16_';
            fnames{2,3} = '006_3_CH1to6_16_';
            fnames{2,4} = '006_4_CH1to6_16_???';
            fnames{2,5} = '006_5_CH1to6_16_???';

            fnames{1,1} = '006_ii0to1_CH1to6_16_';
            fnames{1,2} = '006_ii1to2_CH1to6_16_';
            fnames{1,3} = '006_ii2to3_CH1to6_16_';
            fnames{1,4} = '006_ii3to4_CH1to6_16_';
            fnames{1,5} = '006_ii4to5_CH1to6_16_';
            fnames{1,6} = '006_ii5to6_CH1to6_16_';
        end
    case '007'
        if twindow == 16
            fnames{2,1} = '007_1_CH1to6_16_';
            fnames{2,2} = '007_2_CH1to6_16_';
            fnames{2,3} = '007_3_CH1to6_16_';
            fnames{2,4} = '007_4_CH1to6_16_???';
            fnames{2,5} = '007_5_CH1to6_16_???';

            fnames{1,1} = '007_ii0to1_CH1to6_16_';
            fnames{1,2} = '007_ii1to2_CH1to6_16_';
            fnames{1,3} = '007_ii2to3_CH1to6_16_';
            fnames{1,4} = '007_ii3to4_CH1to6_16_';
            fnames{1,5} = '007_ii4to5_CH1to6_16_';
            fnames{1,6} = '007_ii5to6_CH1to6_16_';
        end
    case '008'
        if twindow == 16
            fnames{2,1} = '008_1_CH1to6_16_';
            fnames{2,2} = '008_2_CH1to6_16_';

            fnames{1,1} = '008_ii0to1_CH1to6_16_';
            fnames{1,2} = '008_ii1to2_CH1to6_16_';
            fnames{1,3} = '008_ii2to3_CH1to6_16_';
            fnames{1,4} = '008_ii3to4_CH1to6_16_';
            fnames{1,5} = '008_ii4to5_CH1to6_16_';
            fnames{1,6} = '008_ii5to6_CH1to6_16_';
        end
    case '009'

```

```

if twindow == 16
    fnames{2,1} = '009_1-CH1to6.16_';
    fnames{2,2} = '009_2-CH1to6.16_???';
    fnames{2,3} = '009_3-CH1to6.16_???';
    fnames{2,4} = '009_4-CH1to6.16_';
    fnames{2,5} = '009_5-CH1to6.16_';

    fnames{1,1} = '009_ii0to1-CH1to6.16_';
    fnames{1,2} = '009_ii1to2-CH1to6.16_';
    fnames{1,3} = '009_ii2to3-CH1to6.16_';
    fnames{1,4} = '009_ii3to4-CH1to6.16_';
    fnames{1,5} = '009_ii4to5-CH1to6.16_';
    fnames{1,6} = '009_ii5to6-CH1to6.16_';
end
case '010'
    if twindow == 16
        fnames{2,1} = '010_1-CH1to6.16_';
        fnames{2,2} = '010_2-CH1to6.16_???';
        fnames{2,3} = '010_3-CH1to6.16_';
        fnames{2,4} = '010_4-CH1to6.16_';
        fnames{2,5} = '010_5-CH1to6.16_';

        fnames{1,1} = '010_ii0to1-CH1to6.16_';
        fnames{1,2} = '010_ii1to2-CH1to6.16_';
        fnames{1,3} = '010_ii2to3-CH1to6.16_';
        fnames{1,4} = '010_ii3to4-CH1to6.16_';
        fnames{1,5} = '010_ii4to5-CH1to6.16_';
        fnames{1,6} = '010_ii5to6-CH1to6.16_';
    end
case '011'
    if twindow == 16
        fnames{2,1} = '011_1-CH1to6.16_';
        fnames{2,2} = '011_2-CH1to6.16_';
        fnames{2,3} = '011_3-CH1to6.16_';
        fnames{2,4} = '011_4-CH1to6.16_';

        fnames{1,1} = '011_ii0to1-CH1to6.16_';
        fnames{1,2} = '011_ii1to2-CH1to6.16_';
        fnames{1,3} = '011_ii2to3-CH1to6.16_';
        fnames{1,4} = '011_ii3to4-CH1to6.16_';
        fnames{1,5} = '011_ii4to5-CH1to6.16_';
        fnames{1,6} = '011_ii5to6-CH1to6.16_';
    end
case '012'
    if twindow == 16
        fnames{2,1} = '012_1-CH1to6.16_??????-????';
        fnames{2,2} = '012_2-CH1to6.16_110111-1945_';
        fnames{2,3} = '012_3-CH1to6.16_110112-0618_';
        fnames{2,4} = '012_4-CH1to6.16_110112-1655_';

        fnames{1,1} = '012_a0to1-CH1to6.16_110111-1112_';
        fnames{1,2} = '012_a1to2-CH1to6.16_110124-2156_';
        fnames{1,3} = '012_a2to3-CH1to6.16_110125-0636_';
        fnames{1,4} = '012_a3to4-CH1to6.16_110125-1714_';
        fnames{1,5} = '012_a4to5-CH1to6.16_110126-0158_';
        fnames{1,6} = '012_a5to6-CH1to6.16_110126-2116_';
    end
elseif twindow == 32
end
case '013'
    if twindow == 16
        fnames{2,1} = '013_1-CH1to6.16_';
        fnames{2,2} = '013_2-CH1to6.16_';
        fnames{2,3} = '013_3-CH1to6.16_???';
        fnames{2,4} = '013_4-CH1to6.16_???';
    end

```

```

        fnames{2,5} = '013.5-CH1to6.16-???';

        fnames{1,1} = '013.ii0to1-CH1to6.16-';
        fnames{1,2} = '013.ii1to2-CH1to6.16-';
        fnames{1,3} = '013.ii2to3-CH1to6.16-';
        fnames{1,4} = '013.ii3to4-CH1to6.16-';
        fnames{1,5} = '013.ii4to5-CH1to6.16-';
        fnames{1,6} = '013.ii5to6-CH1to6.16-';
    end
case '014'
    if twindow == 16
        fnames{2,1} = '014.1-CH1to6.16-';
        fnames{2,2} = '014.2-CH1to6.16-';
        fnames{2,3} = '014.3-CH1to6.16-';
        fnames{2,4} = '014.4-CH1to6.16-???';
        fnames{2,5} = '014.5-CH1to6.16-???';

        fnames{1,1} = '014.ii0to1-CH1to6.16-';
        fnames{1,2} = '014.ii1to2-CH1to6.16-';
        fnames{1,3} = '014.ii2to3-CH1to6.16-';
        fnames{1,4} = '014.ii3to4-CH1to6.16-';
        fnames{1,5} = '014.ii4to5-CH1to6.16-';
        fnames{1,6} = '014.ii5to6-CH1to6.16-';
    end
case '015'
    if twindow == 16
        fnames{2,1} = '015.1-CH1to6.16-';
        fnames{2,2} = '015.2-CH1to6.16-';
        fnames{2,3} = '015.3-CH1to6.16-';
        fnames{2,4} = '015.4-CH1to6.16-';
        fnames{2,5} = '015.5-CH1to6.16-???';

        fnames{1,1} = '015.ii0to1-CH1to6.16-';
        fnames{1,2} = '015.ii1to2-CH1to6.16-';
        fnames{1,3} = '015.ii2to3-CH1to6.16-';
        fnames{1,4} = '015.ii3to4-CH1to6.16-';
        fnames{1,5} = '015.ii4to5-CH1to6.16-';
        fnames{1,6} = '015.ii5to6-CH1to6.16-';
    end
case '016'
    if twindow == 16
        fnames{2,1} = '016.1-CH1to6.16-';
        fnames{2,2} = '016.2-CH1to6.16-';
        fnames{2,3} = '016.3-CH1to6.16-';
        fnames{2,4} = '016.4-CH1to6.16-';
        fnames{2,5} = '016.5-CH1to6.16-';

        fnames{1,1} = '016.ii0to1-CH1to6.16-';
        fnames{1,2} = '016.ii1to2-CH1to6.16-';
        fnames{1,3} = '016.ii2to3-CH1to6.16-';
        fnames{1,4} = '016.ii3to4-CH1to6.16-';
        fnames{1,5} = '016.ii4to5-CH1to6.16-';
        fnames{1,6} = '016.ii5to6-CH1to6.16-';

    elseif twindow == 32
        fnames{2,1} = '016.1-CH1to6.32-??????-????';
        fnames{2,2} = '016.2-CH1to6.32.110107-1347-';
        fnames{2,3} = '016.3-CH1to6.32-??????-????';
        fnames{2,4} = '016.4-CH1to6.32.110105-2311-';
        fnames{2,5} = '016.5-CH1to6.32.110106-0934-';
        fnames{1,1} = '016.d0to1-CH1to6.32.110106-2021-';
        fnames{1,2} = '016.d1to2-CH1to6.32.110106-2021-';
    end
case '017'
    if twindow == 16
        fnames{2,1} = '017.1-CH1to6.16-';
        fnames{2,2} = '017.2-CH1to6.16-';
        fnames{2,3} = '017.3-CH1to6.16-';

```

```

fnames{2,4} = '017_4-CH1to6.16-';
fnames{2,5} = '017_5-CH1to6.16-';

fnames{1,1} = '017_ii0to1-CH1to6.16-';
fnames{1,2} = '017_ii1to2-CH1to6.16-';
fnames{1,3} = '017_ii2to3-CH1to6.16-';
fnames{1,4} = '017_ii3to4-CH1to6.16-';
fnames{1,5} = '017_ii4to5-CH1to6.16-';
fnames{1,6} = '017_ii5to6-CH1to6.16-';
end
case '018'
if twindow == 16
fnames{2,1} = '018_1-CH1to6.16-';
fnames{2,2} = '018_2-CH1to6.16-';
fnames{2,3} = '018_3-CH1to6.16-';
fnames{2,4} = '018_4-CH1to6.16-';
fnames{2,5} = '018_5-CH1to6.16-';

fnames{1,1} = '018_ii0to1-CH1to6.16-';
fnames{1,2} = '018_ii1to2-CH1to6.16-';
fnames{1,3} = '018_ii2to3-CH1to6.16-';
fnames{1,4} = '018_ii3to4-CH1to6.16-';
fnames{1,5} = '018_ii4to5-CH1to6.16-';
fnames{1,6} = '018_ii5to6-CH1to6.16-';
end
case '019'
if twindow == 16
fnames{2,1} = '019_1-CH1to6.16-';
fnames{2,2} = '019_2-CH1to6.16-';
fnames{2,3} = '019_3-CH1to6.16-';
fnames{2,4} = '019_4-CH1to6.16-';
fnames{2,5} = '019_5-CH1to6.16-???';

fnames{1,1} = '019_ii0to1-CH1to6.16-';
fnames{1,2} = '019_ii1to2-CH1to6.16-';
fnames{1,3} = '019_ii2to3-CH1to6.16-';
fnames{1,4} = '019_ii3to4-CH1to6.16-';
fnames{1,5} = '019_ii4to5-CH1to6.16-';
fnames{1,6} = '019_ii5to6-CH1to6.16-';
end
case '020'
if twindow == 16
fnames{2,1} = '020_1-CH1to6.16-';
fnames{2,2} = '020_2-CH1to6.16-';
fnames{2,3} = '020_3-CH1to6.16-';
fnames{2,4} = '020_4-CH1to6.16-';
fnames{2,5} = '020_5-CH1to6.16-';

fnames{1,1} = '020_ii0to1-CH1to6.16-';
fnames{1,2} = '020_ii1to2-CH1to6.16-';
fnames{1,3} = '020_ii2to3-CH1to6.16-';
fnames{1,4} = '020_ii3to4-CH1to6.16-';
fnames{1,5} = '020_ii4to5-CH1to6.16-';
fnames{1,6} = '020_ii5to6-CH1to6.16-';
end
case '021'
if twindow == 16
fnames{2,1} = '021_1-CH1to6.16-';
fnames{2,2} = '021_2-CH1to6.16-';
fnames{2,3} = '021_3-CH1to6.16-???';
fnames{2,4} = '021_4-CH1to6.16-';
fnames{2,5} = '021_5-CH1to6.16-';

fnames{1,1} = '021_ii0to1-CH1to6.16-';
fnames{1,2} = '021_ii1to2-CH1to6.16-';
fnames{1,3} = '021_ii2to3-CH1to6.16-';
fnames{1,4} = '021_ii3to4-CH1to6.16-';
fnames{1,5} = '021_ii4to5-CH1to6.16-';

```



```

        fnames{1,6} = '021_ii5to6-CH1to6-16-';
    end

    end

end
[nr,nc] = size(fnames);
for i = 1:nr
    for j = 1:nc
        switch type
            case 'coh'
                if ~isempty(fnames{i,j})
                    fnames{i,j} = [fnames{i,j} 'coh.mat'];
                end
            case 'mcoh'
                if ~isempty(fnames{i,j})
                    fnames{i,j} = [fnames{i,j} 'mcoh.mat'];
                end
            case 'splv'
                if ~isempty(fnames{i,j})
                    fnames{i,j} = [fnames{i,j} 'splv.mat'];
                end
            case 'xcor'
                if ~isempty(fnames{i,j})
                    fnames{i,j} = [fnames{i,j} 'xcor.mat'];
                end
            case 'mxcr'
                if ~isempty(fnames{i,j})
                    fnames{i,j} = [fnames{i,j} 'mxcr.mat'];
                end
            case 'corc'
                if ~isempty(fnames{i,j})
                    fnames{i,j} = [fnames{i,j} 'corc.mat'];
                end
            end
        end
    end
end
end
end

```

REFERENCES

- [1] J. F. Annegers. *The epidemiology in epilepsy*. The Treatment of Epilepsy: Principle and Practice. Williams and Wilkins, Baltimore, 1996.
- [2] Global Campaign against Epilepsy, International Bureau of Epilepsy, and International League against Epilepsy. *Atlas: Epilepsy Care in the World*. Programme for Neurological Diseases and Neuroscience, Department of Mental Health and Substance Abuse, World Health Organization, Geneva, 2005.
- [3] C. E. Elger and D. Schmidt. Modern management of epilepsy: A practical approach. *Epilepsy & Behavior*, 12(4):501–539, 2008.
- [4] A. Schulze-Bonhage and S. Haut. Premonitory features and seizure self-prediction: artifact or real? *Epilepsy Research*, 97(3):231–235, 2011.
- [5] J. Hughes, O. Devinsky, E. Feldmann, and E. Bromfield. Premonitory symptoms in epilepsy. *Seizure*, 2(3):201–203, 1993.
- [6] P. Rajna, B. Clemens, E. Csibri, E. Dobos, A. Geregely, M. Gottschal, I. Gyorgy, A. Horvath, F. Horvath, L. Mezofi, I. Velkey, J. Veres, and E. Wagner. Hungarian multicentre epidemiologic study of the warning and initial symptoms (prodrome, aura) of epileptic seizures. *Seizure*, 6(5):361–368, 1997.
- [7] A. Schulze-Bonhage, C. Kurth, A. Carius, B. J. Steinhoff, and T. Mayer. Seizure anticipation by patients with focal and generalized epilepsy: a multicentre assessment of premonitory symptoms. *Epilepsy Research*, 70(1):83–88, 2006.
- [8] L. Tebartz van Elst, G. Baker, and M. Kerr. The psychosocial impact of epilepsy in older people. *Epilepsy & Behavior*, 15(2 Suppl 1):S17–S19, 2009.
- [9] J. Santhouse, C. Carrier, S. Arya, H. Fowler, and S. Duncan. A comparison of self-reported quality of life between patients with epilepsy and neurocardiogenic syncope. *Epilepsia*, 48(5):1019–1022, 2007.
- [10] O. C. Cockerell. The mortality of epilepsy. *Current Opinion in Neurology*, 9(2): 93–96, 1996.
- [11] D. Buck, G. A. Baker, A. Jacoby, D. F. Smith, and D. W. Chadwick. Patients' experiences of injury as a result of epilepsy. *Epilepsia*, 38(4):439–444, 1997.

- [12] R. Quintas, A. Raggi, A. M. Giovannetti, M. Pagani, C. Sabariego, A. Cieza, and M. Leonardi. Psychosocial difficulties in people with epilepsy: a systematic review of literature from 2005 until 2010. *Epilepsy & Behavior*, 25(1):60–67, 2012.
- [13] A. Wilensky. History of focal epilepsy and criteria for medical intractability. *Neurosurgery clinics of North America*, 4(2):193–198, 1993.
- [14] D. Buck, A. Jacoby, G. A. Baker, and D. W. Chadwick. Factors influencing compliance with antiepileptic drug regimes. *Seizure*, 6(2):87–93, 1997.
- [15] D. W. Loring and K. J. Meador. Cognitive side effects of antiepileptic drugs in children. *Neurology*, 62(6):872–877, 2004.
- [16] H. Jokeit, G. Kramer, and A. Ebner. Do antiepileptic drugs accelerate forgetting? *Epilepsy & Behavior*, 6(3):430–432, 2005.
- [17] B. Gomer, K. Wagner, L. Frings, J. Saar, A. Carius, M. Harle, B. J. Steinhoff, and A. Schulze-Bonhage. The influence of antiepileptic drugs on cognition: a comparison of levetiracetam with topiramate. *Epilepsy & Behavior*, 10(3):486–494, 2007.
- [18] L. Frings, K. Wagner, T. Maiwald, A. Carius, A. Schinkel, C. Lehmann, and A. Schulze-Bonhage. Early detection of behavioral side effects of antiepileptic treatment using handheld computers. *Epilepsy & Behavior*, 13(2):402–406, 2008.
- [19] G. Vingerhoets. Cognitive effects of seizures. *Seizure*, 15(4):221–226, 2006.
- [20] K. Jin-Sook, A. Kondratyev, Y. Tomita, and K. Gale. Neurodevelopmental impact of antiepileptic drugs and seizures in the immature brain. *Epilepsia*, 48(1):19–26, 2007.
- [21] P. Bittigau, M. Sifringer, and C. Ikonomidou. Antiepileptic drugs and apoptosis in the developing brain. *Annals of the New York Academy of Sciences*, 993:103–114; discussion 123–124, 2003.
- [22] M. Nei, M. O’Connor, J. Liporace, and M. R. Sperling. Refractory generalized seizures: Response to corpus callosotomy and vagal nerve stimulation. *Epilepsia*, 47(1):115–122, 2006.
- [23] J. V. Murphy and A. Patil. Stimulation of the nervous system for the management of seizures: Current and future developments. *CNS Drugs*, 17(2):101–115, 2003.

- [24] S. A. Chkhenkeli, M. Sramka, G. S. Lortkipanidze, T. N. Rakviashvili, E. S. Bregvadze, G. E. Magalashvili, T. S. Gagoshidze, and I. S. Chkhenkeli. Electrophysiological effects and clinical results of direct brain stimulation for intractable epilepsy. *Clinical Neurology & Neurosurgery*, 106(4):318–329, 2004.
- [25] M. E. Lunde, E. K. Lee, and K. G. Rasmussen. Electroconvulsive therapy in patients with epilepsy. *Epilepsy & Behavior*, 9(2):355–359, 2006.
- [26] W. T. Regenold, D. Weintraub, and A. Taller. Electroconvulsive therapy for epilepsy and major depression. *American Journal of Geriatric Psychiatry*, 6(2):180–183, 1998.
- [27] F. Mormann, R. G. Andrzejak, C. E. Elger, and K. Lehnertz. Seizure prediction: the long and winding road. *Brain*, 130(Pt 2):314–333, 2007.
- [28] M. Winterhalder, T. Maiwald, H. U. Voss, R. Aschenbrenner-Scheibe, J. Timmer, and A. Schulze-Bonhage. The seizure prediction characteristic: a general framework to assess and compare seizure prediction methods. *Epilepsy & Behavior*, 4(3):318–325, 2003.
- [29] F. Lopes Da Silva, W. Blanes, S. N. Kalitzin, J. Parra, P. Suffczynski, and D. N. Velis. Epilepsies as dynamical diseases of brain systems: Basic models of the transition between normal and epileptic activity. *Epilepsia*, 44(Suppl 12):72–83, 2003.
- [30] S. Bialonski and K. Lehnertz. Identifying phase synchronization clusters in spatially extended dynamical systems. *Physical Review E - Statistical, Nonlinear, and Soft Matter Physics*, 74(5):051909, 2006.
- [31] A. Aarabi, F. Wallois, and R. Grebe. Does spatiotemporal synchronization of eeg change prior to absence seizures? *Brain Research*, 1188:207–221, 2008.
- [32] F. Amor, S. Baillet, V. Navarro, C. Adam, J. Martinerie, and M. Le Van Quyen. Cortical local and long-range synchronization interplay in human absence seizure initiation. *NeuroImage*, 45(3):950–962, 2009.
- [33] L. D. Iasemidis, S. Deng-Shan, J. C. Sackellares, P. M. Pardalos, and A. Prasad. Dynamical resetting of the human brain at epileptic seizures: application of nonlinear dynamics and global optimization techniques. *IEEE Transactions on Biomedical Engineering*, 51(3):493–506, 2004.
- [34] D. Gupta, C. J. James, and W. P. Gray. Phase synchronization with ica for epileptic seizure onset prediction in the long term eeg. In *Proceedings of the 4th IET International Conference on Advances in Medical, Signal and Information Processing (MEDSIP 2008)*, 1–4, 2008.

- [35] S. Sabesan, N. Chakravarthy, K. Tsakalis, P. Pardalos, and L. Iasemidis. Measuring resetting of brain dynamics at epileptic seizures: application of global optimization and spatial synchronization techniques. *Journal of Combinatorial Optimization*, 17(1):74–97, 2009.
- [36] S. Kalitzin, D. Velis, P. Suffczynski, J. Parra, and F. Lopes da Silva. Electrical brain-stimulation paradigm for estimating the seizure onset site and the time to ictal transition in temporal lobe epilepsy. *Clinical Neurophysiology*, 116(3):718–728, 2005.
- [37] P. Suffczynski, F. H. Lopes da Silva, J. Parra, D. N. Velis, B. M. Bouwman, C. M. van Rijn, P. van Hese, P. Boon, H. Khosravani, M. Derchansky, P. Carlen, and S. Kalitzin. Dynamics of epileptic phenomena determined from statistics of ictal transitions. *IEEE Transactions on Biomedical Engineering*, 53(3):524–532, 2006.
- [38] F. Mormann, T. Kreuz, C. Rieke, R. G. Andrzejak, A. Kraskov, P. David, C. E. Elger, and K. Lehnertz. On the predictability of epileptic seizures. *Clinical Neurophysiology*, 116(3):569–587, 2005.
- [39] M. Le Van Quyen, V. Navarro, J. Martinerie, M. Baulac, and F. J. Varela. Toward a neurodynamical understanding of ictogenesis. *Epilepsia*, 44(Suppl 12):30–43, 2003.
- [40] B. Litt and J. Echaz. Prediction of epileptic seizures. *Lancet Neurology*, 1(1):22–30, 2002.
- [41] L. D. Iasemidis. Seizure prediction and its applications. *Neurosurgery Clinics of North America*, 22(4):489–506, 2011.
- [42] K. Lehnertz. Seizure anticipation techniques: state of the art and future requirements. In *Proceedings of the 23rd Annual International Conference of the IEEE Engineering in Medicine and Biology Society (EMBC 2001)*, 4:4121–4123, 2001.
- [43] R. Aschenbrenner-Scheibe, T. Maiwald, M. Winterhalder, H. U. Voss, J. Timmer, and A. Schulze-Bonhage. How well can epileptic seizures be predicted? An evaluation of a nonlinear method. *Brain*, 126(12):2616–2626, 2003.
- [44] S. Sunderam, I. Osorio, and M. G. Frei. Epileptic seizures are temporally interdependent under certain conditions. *Epilepsy Research*, 76(2-3):77–84, 2007.

- [45] R. S. Delamont, P. O. Julu, and G. A. Jamal. Changes in a measure of cardiac vagal activity before and after epileptic seizures. *Epilepsy Research*, 35(2):87–94, 1999.
- [46] V. Novak, A. L. Reeves, P. Novak, P. A. Low, and F. W. Sharbrough. Time-frequency mapping of rr interval during complex partial seizures of temporal lobe origin. *Journal of the Autonomic Nervous System*, 77(23):195–202, 1999.
- [47] C. Baumgartner, W. Serles, F. Leutmezer, E. Patarraia, S. Aull, T. Czech, U. Pietrzyk, A. Relic, and I. Podreka. Preictal spect in temporal lobe epilepsy: Regional cerebral blood flow is increased prior to electroencephalography-seizure onset. *Journal of Nuclear Medicine*, 39(6):978–982, 1998.
- [48] P. D. Adelson, E. Nemoto, M. Scheuer, M. Painter, J. Morgan, and H. Yonas. Noninvasive continuous monitoring of cerebral oxygenation periictally using near-infrared spectroscopy: a preliminary report. *Epilepsia*, 40(11):1484–1489, 1999.
- [49] M. E. Weinand, L. P. Carter, W. F. El-Saadany, P. J. Sioutos, D. M. Labiner, and K. J. Oommen. Cerebral blood flow and temporal lobe epileptogenicity. *Neurosurgical Focus*, 1(5):E5, 1996.
- [50] J. A. French, P. D. Williamson, V. M. Thadani, T. M. Darcey, R. H. Mattson, S. S. Spencer, and D. D. Spencer. Characteristics of medial temporal lobe epilepsy: I. results of history and physical examination. *Annals of Neurology*, 34(6):774–780, 1993.
- [51] H. Osterhage, F. Mormann, M. U. Staniek, and K. Lehnertz. Measuring synchronization in the epileptic brain: A comparison of different approaches. *International Journal of Bifurcation and Chaos in Applied Sciences and Engineering*, 17(10):3539–3544, 2007.
- [52] G. Bettus, F. Wendling, M. Guye, L. Valton, J. Rgis, P. Chauvel, and F. Bartolomei. Enhanced eeg functional connectivity in mesial temporal lobe epilepsy. *Epilepsy Research*, 81(1):58–68, 2008.
- [53] C. A. Schevon, J. Cappell, R. Emerson, J. Isler, P. Grieve, R. Goodman, G. McKhann Jr, H. Weiner, W. Doyle, R. Kuzniecky, O. Devinsky, and F. Gilliam. Cortical abnormalities in epilepsy revealed by local eeg synchrony. *NeuroImage*, 35(1):140–148, 2007.
- [54] R. G. Andrzejak, F. Mormann, T. Kreuz, C. Rieke, A. Kraskov, C. E. Elger, and K. Lehnertz. Testing the null hypothesis of the nonexistence of a pre seizure state. *Physical Review E - Statistical, Nonlinear, and Soft Matter Physics*, 67(1 Pt 1):010901, 2003.

- [55] I. Osorio, M. Frei, and S. Wilkinson. Real-time automated detection and quantitative analysis of seizures and short-term prediction of clinical onset. *Epilepsia*, 39(6):615–627, 1998.
- [56] S. R. Haut, C. Swick, K. Freeman, and S. Spencer. Seizure clustering during epilepsy monitoring. *Epilepsia*, 43(7):711–5, 2002.
- [57] J. Bauer and W. Burr. Course of chronic focal epilepsy resistant to anticonvulsant treatment. *Seizure*, 10(4):239–246, 2001.
- [58] M. Winterhalder, B. Schelter, T. Maiwald, A. Brandt, A. Schad, A. Schulze-Bonhage, and J. Timmer. Spatio-temporal patient-individual assessment of synchronization changes for epileptic seizure prediction. *Clinical Neurophysiology*, 117(11):2399–2413, 2006.
- [59] T. Maiwald, M. Winterhalder, R. Aschenbrenner-Scheibe, H. U. Voss, A. Schulze-Bonhage, and J. Timmer. Comparison of three nonlinear seizure prediction methods by means of the seizure prediction characteristic. *Physica D: Nonlinear Phenomena*, 194(3-4):357–368, 2004.
- [60] F. Mormann, R. G. Andrzejak, T. Kreuz, C. Rieke, P. David, C. E. Elger, and K. Lehnertz. Automated detection of a pre-seizure state based on a decrease in synchronization in intracranial electroencephalogram recordings from epilepsy patients. *Physical Review E - Statistical, Nonlinear, and Soft Matter Physics*, 67(2 Pt 1):021912, 2003.
- [61] B. Schelter, M. Winterhalder, T. Maiwald, A. Brandt, A. Schad, J. Timmer, and A. Schulze-Bonhage. Do false predictions of seizures depend on the state of vigilance? a report from two seizure-prediction methods and proposed remedies. *Epilepsia*, 47(12):2058–2070, 2006.
- [62] B. Schelter, M. Winterhalder, T. Maiwald, A. Brandt, A. Schad, A. Schulze-Bonhage, and J. Timmer. Testing statistical significance of multivariate time series analysis techniques for epileptic seizure prediction. *Chaos*, 16(1):013108, 2006.
- [63] B. Schelter, M. Winterhalder, H. Feldwisch genannt Drentrup, J. Wohlmuth, J. Nawrath, A. Brandt, A. Schulze-Bonhage, and J. Timmer. Seizure prediction: the impact of long prediction horizons. *Epilepsy Research*, 73(2):213–217, 2007.
- [64] J. C. Sackellares, D. S. Shiao, J. C. Principe, M. C. Yang, L. K. Dance, W. Suharitdamrong, W. Chaovalitwongse, P. M. Pardalos, and L. D. Iasemidis. Predictability analysis for an automated seizure prediction algorithm. *Journal of Clinical Neurophysiology*, 23(6):509–520, 2006.

- [65] S. Wong, A. B. Gardner, A. M. Krieger, and B. Litt. A stochastic framework for evaluating seizure prediction algorithms using hidden markov models. *Journal of Neurophysiology*, 97(3):2525–2532, 2007.
- [66] R. G. Andrzejak, D. Chicharro, C. E. Elger, and F. Mormann. Seizure prediction: Any better than chance? *Clinical Neurophysiology*, 120(8):1465–1478, 2009.
- [67] K. Swartztrauber, S. Dewar, and J. Engel Jr. Patient attitudes about treatments for intractable epilepsy. *Epilepsy & Behavior*, 4(1):19–25, 2003.
- [68] Z. Rogowski, I. Gath, and E. Bental. On the prediction of epileptic seizures. *Biological Cybernetics*, 42(1):9–15, 1981.
- [69] H. Liyu, S. Qixin, C. Jingzhi, and H. Yuangui. Prediction of epileptic seizures using bispectrum analysis of electroencephalograms and artificial neural network. In *Proceedings of the 25th Annual International Conference of the IEEE Engineering in Medicine and Biology Society (EMBC 2003)*, 3:2947–2949, 2003.
- [70] B. Litt, R. Esteller, J. Echauz, M. D’Alessandro, R. Shor, T. Henry, P. Pennell, C. Epstein, R. Bakay, M. Dichter, and G. Vachtsevanos. Epileptic seizures may begin hours in advance of clinical onset: a report of five patients. *Neuron*, 30(1):51–64, 2001.
- [71] L. D. Iasemidis, D. S. Shiau, P. M. Pardalos, W. Chaovalitwongse, K. Narayanan, A. Prasad, K. Tsakalis, P. R. Carney, and J. C. Sackellares. Long-term prospective on-line real-time seizure prediction. *Clinical Neurophysiology*, 116(3):532–544, 2005.
- [72] K. Lehnertz and C. E. Elger. Neuronal complexity loss in temporal lobe epilepsy: effects of carbamazepine on the dynamics of the epileptogenic focus. *Electroencephalography and Clinical Neurophysiology*, 103(3):376–380, 1997.
- [73] R. B. Duckrow and T. K. Tcheng. Daily variation in an intracranial eeg feature in humans detected by a responsive neurostimulator system. *Epilepsia*, 48(8):1614–1620, 2007.
- [74] A. Katz, D. A. Marks, G. McCarthy, and S. S. Spencer. Does interictal spiking change prior to seizures? *Electroencephalography and Clinical Neurophysiology*, 79(2):153–156, 1991.
- [75] W. Penfield and H. H. Jasper. *Epilepsy and the functional anatomy of the human brain*. Little, Boston, 1st edition, 1954.

- [76] G. K. Bergey and P. J. Franaszczuk. Epileptic seizures are characterized by changing signal complexity. *Clinical Neurophysiology*, 112(2):241–249, 2001.
- [77] S. J. Schiff, T. Sauer, R. Kumar, and S. L. Weinstein. Neuronal spatiotemporal pattern discrimination: the dynamical evolution of seizures. *Neuroimage*, 28(4):1043–1055, 2005.
- [78] K. Schindler, C. E. Elger, and K. Lehnertz. Increasing synchronization may promote seizure termination: Evidence from status epilepticus. *Clinical Neurophysiology*, 118(9):1955–1968, 2007.
- [79] C. C. Jouny, B. Adamolekun, P. J. Franaszczuk, and G. K. Bergey. Intrinsic ictal dynamics at the seizure focus: Effects of secondary generalization revealed by complexity measures. *Epilepsia*, 48(2):297–304, 2007.
- [80] K. Gotz-Trabert, C. Hauck, K. Wagner, S. Fauser, and A. Schulze-Bonhage. Spread of ictal activity in focal epilepsy. *Epilepsia*, 49(9):1594–1601, 2008.
- [81] S. C. Ponten, L. Douw, F. Bartolomei, J. C. Reijneveld, and C. J. Stam. Indications for network regularization during absence seizures: Weighted and unweighted graph theoretical analyses. *Experimental Neurology*, 217(1):197–204, 2009.
- [82] T. Conlon, H. J. Ruskin, and M. Crane. Seizure characterisation using frequency-dependent multivariate dynamics. *Computers in Biology and Medicine*, 39(9):760–767, 2009.
- [83] F. Mormann, K. Lehnertz, P. David, and C. E. Elger. Mean phase coherence as a measure for phase synchronization and its application to the eeg of epilepsy patients. *Physica D: Nonlinear Phenomena*, 144(3):358–369, 2000.
- [84] F. Mormann, T. Kreuz, R. G. Andrzejak, P. David, K. Lehnertz, and C. E. Elger. Epileptic seizures are preceded by a decrease in synchronization. *Epilepsy Research*, 53(3):173–185, 2003.
- [85] P. Tass, M. G. Rosenblum, J. Weule, J. Kurths, A. Pikovsky, J. Volkmann, A. Schnitzler, and H. J. Freund. Detection of n:m phase locking from noisy data: Application to magnetoencephalography. *Physical Review Letters*, 81(15):3291–3294, 1998.
- [86] P. W. Mirowski, L. Yann, D. Madhavan, and R. Kuzniecky. Comparing svm and convolutional networks for epileptic seizure prediction from intracranial eeg. In *IEEE Workshop on Machine Learning for Signal Processing (MLSP 2008)*, 244–249, 2008.

- [87] P. Mirowski, D. Madhavan, Y. LeCun, and R. Kuzniecky. Classification of patterns of eeg synchronization for seizure prediction. *Clinical Neurophysiology*, 120(11):1927–1940, 2009.
- [88] M. H. Myers and R. Kozma. Seizure prediction through dynamic synchronization measures of neural populations. In *International Joint Conference on Neural Networks (IJCNN 2009)*, 2195–2201, 2009.
- [89] H. Feldwisch-Drentrup, B. Schelter, M. Jachan, J. Nawrath, J. Timmer, and A. Schulze-Bonhage. Joining the benefits: combining epileptic seizure prediction methods. *Epilepsia*, 51(8):1598–1606, 2010.
- [90] C. A. Teixeira, B. Direito, R. P. Costa, M. Valderrama, H. Feldwisch-Drentrup, S. Nikolopoulos, M. Le Van Quyen, B. Schelter, and A. Dourado. A computational environment for long-term multi-feature and multi-algorithm seizure prediction. In *Proceedings of the Annual International Conference of the IEEE Engineering in Medicine and Biology Society (EMBC 2010)*, 6341–6344, 2010.
- [91] S. Nesaei and S. Nesaei. Comparison of phase synchrony information flow in human eeg through wavelet phase synchronization analysis. In *Proceedings of the IEEE 10th International Conference on Signal Processing (ICSP 2010)*, 187–190, 2010.
- [92] C. C. B. Suarez, E. T. Fonoff, M. A. Munoz G, A. C. Godoi, G. Ballester, and F. J. Ramirez-Fernandez. Wavelet transform and cross-correlation as tools for seizure prediction. In *Proceedings of the Annual International Conference of the IEEE Engineering in Medicine and Biology Society (EMBC 2010)*, 4020–4023, 2010.
- [93] C. C. Jouny, P. J. Franaszczuk, and G. K. Bergey. Signal complexity and synchrony of epileptic seizures: is there an identifiable preictal period? *Clinical Neurophysiology*, 116(3):552–558, 2005.
- [94] K. K. Jerger, S. L. Weinstein, T. Sauer, and S. J. Schiff. Multivariate linear discrimination of seizures. *Clinical Neurophysiology*, 116(3):545–551, 2005.
- [95] E. O’Sullivan-Greene, I. Mareels, A. Burkitt, and L. Kulhmann. Observability issues in networked clocks with applications to epilepsy. In *Proceedings of the 48th IEEE Conference on Decision and Control held jointly with the 28th Chinese Control Conference (CDC/CCC 2009)*, 3527–3532, 2009.

- [96] E. O'Sullivan-Greene, I. Mareels, D. Freestone, L. Kulhmann, and A. Burkitt. A paradigm for epileptic seizure prediction using a coupled oscillator model of the brain. In *Proceedings of the Annual International Conference of the IEEE Engineering in Medicine and Biology Society (EMBC 2009)*, 6428–6431, 2009.
- [97] N. E. Huang, Z. Shen, S. R. Long, M. C. Wu, H. H. Shih, Q. Zheng, N.-C. Yen, C. C. Tung, and H. H. Liu. The empirical mode decomposition and the hilbert spectrum for nonlinear and non-stationary time series analysis. *Proceedings of the Royal Society of London. Series A: Mathematical, Physical and Engineering Sciences*, 454(1971):903–995, 1998.
- [98] A. K. Tafreshi, A. M. Nasrabadi, and A. H. Omidvarnia. Empirical mode decomposition in epileptic seizure prediction. In *Proceedings of the IEEE International Symposium on Signal Processing and Information Technology (ISSPIT 2008)*, 275–280, 2008.
- [99] Z. Tianqiao, H. Liyu, and T. Xuizi. Epileptic seizure prediction by using empirical mode decomposition and complexity analysis of single-channel scalp electroencephalogram. In *Proceedings of the 2nd International Conference on Biomedical Engineering and Informatics (BMEI 2009)*, 1–4, 2009.
- [100] L. Orosco, A. G. Correa, and E. Laciaar. Multiparametric detection of epileptic seizures using empirical mode decomposition of eeg records. In *Proceedings of the Annual International Conference of the IEEE Engineering in Medicine and Biology Society (EMBC 2010)*, 951–954, 2010.
- [101] R. Oweis and E. Abdulhay. Seizure classification in eeg signals utilizing hilbert-huang transform. *BioMedical Engineering OnLine*, 10:38, 2011.
- [102] Z. Wu and N. E. Huang. Ensemble empirical mode decomposition: a noise assisted data analysis method. *Advances in Adaptive Data Analysis*, 1(1):1–41, 2009.
- [103] P. Flandrin, G. Rilling, and P. Goncalves. Empirical mode decomposition as a filter bank. *IEEE Signal Processing Letters*, 11(2):112–114, 2004.
- [104] T. Netoff, P. Yun, and K. Parhi. Seizure prediction using cost-sensitive support vector machine. In *Proceedings of the Annual International Conference of the IEEE Engineering in Medicine and Biology Society (EMBC 2009)*, 3322–3325, 2009.
- [105] S. Talathi, D. Hwang, M. Spano, J. Simonotto, M. Furman, S. Myers, J. Winters, W. Ditto, and P. Carney. Non-parametric early seizure detection in an animal model of temporal lobe epilepsy. *Journal of Neural Engineering*, 5(1):85–98, 2008.

- [106] M. Le Van Quyen, J. Soss, V. Navarro, R. Robertson, M. Chavez, M. Baulac, and J. Martinerie. Preictal state identification by synchronization changes in long-term intracranial eeg recordings. *Clinical Neurophysiology*, 116(3):559–568, 2005.
- [107] H. P. Zaveri, R. B. Duckrow, N. C. de Lanerolle, and S. S. Spencer. Distinguishing subtypes of temporal lobe epilepsy with background hippocampal activity. *Epilepsia*, 42(6):725–730, 2001.
- [108] A. Schulze-Bonhage, F. Sales, K. Wagner, R. Teotonio, A. Carius, A. Schelle, and M. Ihle. Views of patients with epilepsy on seizure prediction devices. *Epilepsy & Behavior*, 18(4):388–396, 2010.

VITA

Daniel W. Moller obtained his B.S.E. in Biomedical Engineering from Tulane University in 1999. He worked for five years at a biomedical prototyping company in the Greater New Orleans area, primarily in research and development of machine perfusion for organ preservation. Following the aftermath of Hurricane Katrina, he obtained a position at Texas State Technical College Marshall teaching and developing a new Biomedical Equipment Technology program. He obtained his M.S. in 2010 and submits this dissertation as a requirement for the Ph.D. degree in Biomedical Engineering at Louisiana Tech University under the advisement of Alan W.L. Chiu, Ph.D. His dissertation research focused on synchronization measures for use in epileptic seizure anticipation. During his time at Louisiana Tech, he served as a National Science Foundation GK-12 Teaching Fellow and an instructor for the *Living with the Lab* project-driven freshman engineering program. He is currently a Visiting Assistant Professor in the College of Engineering and Science at Louisiana Tech University. His interests are machine learning, pattern recognition, signal processing and engineering education.